Dear Dr. Bengtson,

Thank you for submitting your manuscript “Lower oceanic δ13C during the Last Interglacial compared to the Holocene” to “Climate of the Past” and for your detailed reply to the two reviewers’ comments. Both reviewers were overall positive while recommending “major revisions”. Based on the review comments and your replies, I would like to invite you to resubmit a revised version of your manuscript taking the review comments into accounts. Please note that if you choose to resubmit, your revised version of the manuscript will be sent for a second round of reviews.

When reading the manuscript myself, I was wondering, why you place figures A1 and A2 in the appendix, as they to me are quite informative?
Fig 1: Please consider working on the layout of figure 1, as it should be possible to move the curves closer to each other. For all figures note that the text is written in a font that will likely make it difficult to read when the figures are reduced in size.

Kind regards,
Marit-Solveig Seidenkrantz

Dear Prof. Seidenkrantz,

Thank you for your invitation to resubmit the manuscript. Please see below our responses to the reviewers’ comments and the latexdiff file highlighting the manuscript revisions.

Additionally, we would like to thank you for your thoughts on our figures. We have reduced the spacing between the lines in Figure 1, increased the font sizing in all the figures, and included Figure S2 in the manuscript (Figure 3 in the revised version).

Kind regards,
Shannon Bengtson

Response to the Reviewers

Key:
Black= Reviewers’ comments
Blue= Authors’ responses
Green = Modified text in the manuscript

Reviewer #1:

We thank the Reviewer for their helpful comments. Please see below for the specific modifications to the manuscript and our response.

This paper describes a data compilation of benthic δ 13C data from the Last Interglacial (LIG), consisting of already publöished data. The authors compile material from two previous δ 13C compilations (Lisiecki and Stern 2016, Oliver et al 2010), and also add a few other cores. They compare their findings with benthic δ 13C from the mid-Holocene (HOL) and discuss 3 different hypothesis, which they suggest are the only possible ones to explain the

observed LIG-HOL offset. They conclude, that AMOC change was probably not the reason for their findings, but changes in the balance of weathering and sedimentation. The paper in principle covers a nice piece of work, however, I believe it is a bit loosely constrained at certain points and misses some of the already available / published literature. I suggest a major overhaul following replies and response to the points given below.

1. Definition of analysed data: Some data analysis covers the whole LIG, some 125-120 ka, some all available data including part of Termination II and of the glacial inception. Similarly for the HOL, with which they compare. This needs to be focused. Define your time interval, but also give reasons for your chosen definition. So far, it is said, that 125-120 ka and 7-4 ka are chosen because δ 13C is stable. Looking at figure 4c (Pacific in HOL), this does not seemed to be the case, here 5-2 ka is much more stable. Maybe use as has been done in Peterson et al. (2014) the late Holocene 6-0 ka. I also believe taking two time windows which are of the same length might be a valid idea. Furthermore, check on the definition of interglacials (Past Interglacials Working Group of PAGES, 2016) when the community thinks Termination I or II was over and when the last glacial inception started. Please discuss your choice based on such literature widely. Also: I believe somewhere it was written, that only data below 2500m water depth are analysed. Is this always the case? If not, please specify in each and every section, which water depth is considered, also add this information in the figure caption, if this info is not popping up from the figure itself.

We would like to thank the Reviewer for these suggestions. We agree that both the definition of the time periods selected and the explanation on why we decided on these definitions needed to be improved. The two periods were defined based on the following criteria: that data associated with glaciations/deglaciations are excluded, and that data from periods of known instability are avoided. Following the Reviewer's comment, we have now modified the Holocene period such that the lengths of the time periods considered during the LIG and the Holocene are the same. Based on this, we are now using the time period 7-2 ka BP for the Holocene. The LIG period used is still 125-120 ka BP. We are now providing the following explanation in the manuscript:

We then define the time periods within the LIG and the Holocene to perform our analyses. For the Holocene, as most of the available data is dated prior to 2 ka BP, we define the end of our Holocene time period as 2 ka BP. To capture as much of the Holocene data as possible, we include data back to 7 ka BP, ensuring that we do not include instability associated with the 8.2 kiloyear event (Alley et a., 2005; Thomas et al., 2007). This provides a time span of 5 ka of data that we will consider for our analysis of the Holocene.

For the LIG, we seek to avoid data associated with the end of the penultimate deglaciation, which is characterised by a benthic d13C increase in the Atlantic until ~128 ka BP (Govin et al., (2015); Menviel et al. (2019); Oliver et al. (2010), Fig. 4). In addition, a millennial-scale event has been identified in the North Atlantic between ~127 and 126 ka BP (Galaasen et al., 2014, Tzedakis et al., 2018). Considering the typical dating uncertainties associated with the LIG data (2 ka), we thus decide to start our LIG time period at 125 ka BP. To ensure that the two time periods are of same length (5 ka BP), we define the LIG period for our analysis to be 125-120 ka BP. We note that our definition should also avoid data associated with the glacial inception (Govin et al. (2015); Past Interglacial Working Group of PAGES, 2016). We verify that the LIG time period has sufficient data across the four selected regions, noting that the highest density of data falls within the 125-120 ka BP time period---particularly in the equatorial Atlantic and southeast Atlantic (Fig. 4b, c).

To test the impact of the time period studied during the LIG, we are now also comparing the results of the "early LIG", defined as the period 128 ka to 123 ka, and the "late LIG" (123 ka to 118 ka), compared to the results of the 125 to 120 ka time period. This comparison is now shown on a new figure (Figure 5). This figure shows that the results are not statistically different across the 3 LIG periods defined above. However, the spread in between the 1st and 3rd quartiles is much larger for the early LIG than the LIG, confirming that the time period principally used in this study is appropriate.

Our analysis is restricted to cores that were recovered from depths greater than 1,000 m. However, given the strong vertical d13C gradient due to oceanic circulation, we also split the cores by depth for some specific analyses. We have thus made changes throughout the text to ensure that this has been clarified at all points in the paper where a depth restriction has been placed on the visualisation and analysis:

L178-179: The average d13C anomaly between the LIG and Holocene periods for cores deeper than 2,500 m is consistent across the different regions despite their geographic separation

Table 2 caption: Regional breakdown of δ13C data for all depths during the Holocene (7–2 ka BP) and LIG (125–120 ka BP) averaged across the 1 ka timeslices.

Figure 5 caption: Comparison of volume-weighted δ13C for the Atlantic (red) and Pacific (blue) for the LIG and Holocene, calculated using the regions from Peterson et al. (2014) from data covering all depths...

2. You are missing one important review on simulating LIG vs HOL carbon cycle, which is Brovkin et al. (2016), which also deals with δ 13C. Discuss your potential explanations within the framework of that study, which contained results from different models, and which finds some explanations for the carbon cycle in the HOL, but not for the LIG. You might also note, that during the end of LIG / during glacial inception CO2 and sea level / land ice volume / temperature was decoupled on a multi-millennial timescale, which might indicate towards some processes that are important here (Barnola et al., 1987; Hasenclever et al., 2017; Köhler et al., 2018).

We apologise for not including Brovkin et al. 2016 in our review of the literature. We have now included extra information regarding the mechanisms that are presented in Brovkin et al. 2016.

For example, we have included the findings of the simulations in Brovkin et al. 2016 in references to aspects that need stronger constraint during the LIG in L48-51:

In particular, stronger constraints are needed on the extent of Greenland and Antarctic ice sheets, on ocean circulation and the global carbon cycle, including CaCO3 accumulation in shallow waters, and peat and permafrost carbon storage changes (Brovkin et al., 2016).

We have expanded L63-64 to include more details of different carbon stores on land:

Organic matter on land includes the terrestrial biosphere, as well as carbon stored in soils, such as in peats and permafrosts.

We have generalised L70-73 slightly to encompass other mechanisms that are discussed in Brovkin et al., 2016:

Thus, atmospheric δ13CO2 during the LIG (Fig. 1d) is influenced by the cycling of organic carbon within the ocean, changes in the amount of carbon stored in vegetation and soils, temperature-dependent air-sea flux fractionation (Lynch-Stieglitz et al., 1995; Zhang et al., 1995), and, on longer time scales, by interactions with the lithosphere (Tschumi et al., 2011).

We have also broken down the exchanges with the lithosphere further on L85-87 in line with the element discussed in Brovkin et al. 2016:

However, on longer time scales, exchanges with the lithosphere including volcanic outgassing (Hasenclever et al., 2017; Huybers and Langmuir 2009), CaCO3 burial in sediments and weathering, release of carbon from methane clathrates, and the net burial of organic carbon also influences the global mean d13C.

We have also rephrased significant portions of the discussion, including a paragraph where we explore the mechanisms presented in Brovkin et al. 2016 in more detail:

In addition, due to the warmer conditions at the LIG than during the Holocene, there could have been a release of methane clathrates which would have added isotopically light carbon (δ 13C: ~-47 ‰) to the ocean-atmosphere system. However, available evidence suggests that geological CH4 sources are rather small (Bock et al., 2017; Hmiel et al., 2020; Petrenko et al., 2017; 320 Saunois et al., 2020) making this explanation unlikely, although we cannot completely exclude the possibility that the geological CH4 source was larger at the LIG than the Holocene. Similarly, since the δ13C value of CO2 from volcanic outgassing is close to zero (Brovkin et al., 2016) and modelling suggests volcanic outgassing likely only had a minor impact on δ13CO2 (Roth and Joos, 2012), it is unlikely that volcanic outgassing of CO2 played a significant role in influencing the mean oceanic δ13C.

3. line 13: PI is NOT 0.7K cooler than the peak Holocene, this differences in Marcott et al 2013 compares peak Holocene with the Little Ice Age. The PI-peak-HOL difference is about 0.4K. The maximum Holocene peak is also not at 5 ka, but early, check the Marcott paper for details.

We apologise for the error. 0.7K has been changed to 0.4K and the time frame has been changed to 10-5 ka BP in L19 as suggested by Marcott et al (2013).

4. line 25: CO2 in the Holocene rose by maybe 18 ppm, but not by 28 ppm.

We have corrected this typo in L25. It now reads 18 p.p.m.

5. line 27: The details on CH4 need to condense.

L26-27 now read:

CH4 reached ~700 p.p.b and ~675 p.p.b during the LIG and the Holocene, respectively, and N2O peaked at ~267 p.p.b during both periods (Flückiger et al., 2002; Petit et al., 1999; Spahni et al., 2005).

6. line 28: The given warming on Greenland is for the NEEM site, not for the whole of Greeland. Please revise.

This line has been removed during the revision process.

7. line 38; SST record were 0.5K WARMER (not higher)

This has been changed to warmer.

8. All-in-all, the introduction on climate changes in the LIG needs some revision. Please focus on already existing stacks (which also have regional subdivions), that should also be plotted in Fig 1, e.g. Hoffman et al 2017, cited here.

We thank the Reviewer for their comments on the introduction. Based on the suggested changes to Fig. 1 (point #9), we have changed our exploration of LIG-Holocene temperature differences. Lines 32-44 now read:

Strong polar warming is supported by terrestrial and marine temperature reconstructions. A global analysis of SST records suggests that the mean surface ocean was 0.5±0.3◦C warmer during the LIG compared to 1870–1889 (Hoffman et al., 2017), similar to another global reconstruction estimate of 0.7±0.6◦C higher SSTs during the LIG compared to the late Holocene (McKay et al., 2011). However, there were differences in the timing of these SST peaks in different regions compared to the 1870–1889 mean: North Atlantic SST peaked at +0.6±0.5◦C at 125 ka BP (e.g. Fig. 1b) and Southern Hemisphere extratropical SSTs peaked at +1.1±0.5◦C at 129 ka BP (Hoffman et al., 2017). On land, proxy records from mid to high latitudes indicate higher temperatures during the LIG compared to PI, particularly in North America (Anderson et al., 2014; Axford et al., 2011; Montero-Serrano et al., 2011). Similarly, the EPICA DOME C record suggests that the highest Antarctic temperatures from the last 800 ka occurred during the LIG (Masson-Delmotte et al.,2010) (Fig. 1c).

9. Revise Figure 1: Consider using splines including uncertainites instead of single lines, e.g. CO2 from Köhler et al. (2017), temperature (should be SST) from Hoffman et al. (2017) and Marcott et al. (2013), atmospheric δ 13C from Eggleston et al. (2016), which also closes the gap at the onset of the Holocene (no data so far). In Eggleston et al. (2016); Köhler et al. (2017) the newest ice core age model AICC2012 is already included, which might not have been the case in the plotted data. Mark which time windows you analyse in this figure. If you do not use the suggested splines, please include data uncertainties in the plotting, and explain the chosen time series in more detail, e.g which age model, b is tempertature change in certain ice cores (which cores). Subfigure (c) would need a further motivation (why plotting a mediterranean SST here?). The legend is not useful, since all records are plotted on individual subfigures and explained in the caption.

Thank you for the suggestions on data to present in Figure 1. We have removed the redundant legend and are now more selective in the data that we present, with the subplots now showing the following (NB: subplots b and c have been swapped):

a) CO2 from Köhler et al. (2017) as suggested.
b) We were unable to find an SST stack that covers the same region during both the LIG and the Holocene. For this reason, we have chosen to use reconstructions from individual cores. However, we have now selected data from a region which is more relevant to our study, presenting two cores, one from the Iberian Margin, and the other from the North Atlantic.

c) We have now also provided the deuterium measurements from which surface air temperature was calculated.
d) For the Holocene, we have changed the atmospheric d13C to be the spline from the suggested reference (Eggleston et al., 2016). However, for the LIG we have decided to use the Monte Carlo average from Schneider et al. (2013) since the spline during the time period plotted (132-116 ka BP) from Eggleston et al. (2016) is only based on three data points.

The new figure caption reflects the changes in the data and now provides more details about the corresponding age models.

10. line 78: I do not understand how atmospheric δ 13C is influenced be the total amount of carbon in vegetation and soil, please expend.

Apologies, the sentence was misleading the way it was written. L70-73 now read:

Thus, atmospheric δ13CO2 during the LIG (Fig. 1d) is influenced by plant type, the cycling of organic carbon within the ocean, changes in the amount of carbon stored in vegetation and soils, temperature-dependent air-sea flux fractionation (Lynch-Stieglitz et al., 1995; Zhang et al., 1995), and, on longer time scales, by interactions with the lithosphere (Tschumi et al., 2011).

11. line 80: If you compare atmospheric δ 13C with modern values you need to include a sentence on the contribution of the 13C Suess effect. Either extend or rewrite to a comparison of the pre-Suess effect values.

Sorry, we meant to refer to PI and not to today. L73-74 now reads:

During PI, the mean surface DIC is thereby enriched by ~8.5 ‰ compared to the atmosphere due to fractionation during air-sea gas exchange (Menviel et al., 2015; Schmittner et al., 2013).

12. Introduction: I believe the subsections are not necessary here.

The subsection headings have now been removed.

13. line 123 and 133 (maybe elsewhere): Uncertainties are typically going symetrically in both direction, so “±” is not necessary. Also, please state, what these uncertainties are, is this 1σ?

The plus/minus signs in have been removed. The age model uncertainties are based on 2σ. We have added this clarification L115:

The estimated age model uncertainty (2σ) for this group of cores is 2 ka.

14. Table 1 and Fig 3: Please use error propagation and also include an uncertainty in the calculated anomaly Δδ 13C.

We have added the standard deviation in Δδ13C using error propagation to Table 1.

15. section 3.1. Use the same time window for analysis throughout, here 130-118 ka instead of 125-120 ka has been used.

We have adjusted the analysis in Section 3.1 to use the same time periods used elsewhere (125-120 ka BP, and 7-2 ka BP), and we have adjusted Fig. 1 accordingly.

16. lines 172ff. As said in #1, 7-4 ka is not a constant period. Please redefine.

The periods have been redefined as per our response to comment #1.

17. Fig 3: If I got it right these are only benthic forams from deep sedimemt cores from below 2500 m water depth, please say so. Revise the x-axis label: You have your mean times at full kiloyears, but the labels partly at half kiloyears.

We have revised the x-axis labels as per your comment.
The cores are indeed from depths below 2,500 m as written in the caption. We have added this clarification to the main text to improve clarity. L185-186 now reads:

Fig. 3 suggests that the difficulty in determining significance in this region for cores deeper than 2,500 m might be due to a singular...

18. line 192: It is not clear that the mentioned Fig A1 is from this paper, I thought it was from Peterson et al 2014.

We have modified the text in the main body and the figure caption to make this clearer. The text in the main body now reads:

We define our regional boundaries based on the regions described in (Peterson et al, 2014), however we only include the regions where there is enough data to justify an analysis. For all the data in each of these regions, we calculate a mean value by taking the direct averages of all data. We divide the ocean basins into eight regions (Table 4, shown in Fig. 2) and calculate the volume-weighted averages d13C for each of these regions.

This figure was also combined with figure 2. The figure caption now includes the following line:

Regional boundaries used to calculate the global volume-weighted mean δ13C (Sect. 3.2) are indicated by dotted black lines as defined in Peterson et al., (2014).

19. line 215, 222: 3 possible explanations. Maybe there are others which you did not think of so far (e.g. decoupling of CO2 with other climate records at the end of LIG, see #2). Also, you only in detail investigate AMOC changes, and briefly discuss the others. This should be a bit better balanced. I therefore suggest to move section 3.3 to the discussion, and also ask for some more thoughts on the alternative explanations.

We fully agree with the Reviewer that the discussion on land biosphere changes and on weathering-sediment fluxes belongs into the discussion section. These two issues are now discussed in section 4.

We also agree that the numbering of reasons for the difference may be misleading for some readers; we do not intend to exclude other explanations. We do not provide numbers anymore.

We consider the assessment of potential biases in our results and the tests presented in section 3.3 as an integral part of the result section and prefer to keep this text in section 3.3 We shortened the text on L229 to L230 to read:

Both the regional analysis of our new database and our volume-weighted estimate indicate that the global mean d13C was about 0.2 ‰ lower during the LIG than during the mid-Holocene. We further test the robustness of this result in the next section.

As far as other possible reasons are concerned, we now discuss explicitly the processes mentioned by Brovkin et al., 2016.

We now mention explicitly volcanic CO2 outgassing. We consider this to be an intrinsic part of the slow carbon cycle from the lithosphere (weathering, volcanic CO2 outgassing and sediment burial). We note that the impacts of volcanic outgassing on atmospheric d13C is simulated to be low (Roth, R., F. Joos, "Model limits on the role of volcanic carbon emissions in regulating glacial-interglacial CO2 variations", Earth and Planetary Science Letters, 329-330, 141-149,2012).

We also mention the possibility of CH4 release from clathrates. However, the available evidence suggests a small role for such a release (Bock et al., 2017; Hmiel et al., 2020; Petrenko et al., 2017; Saunois et al., 2020).

The discussion regarding volcanic outgassing and CH4 release from clathrates now reads:

In addition, due to the warmer conditions at the LIG than during the Holocene, there could have been a release of methane clathrates which would have added isotopically light carbon (δ 13C: ~-47 ‰) to the ocean-atmosphere system. However, available evidence suggests that geological CH4 sources are rather small (Bock et al., 2017; Hmiel et al., 2020; Petrenko et al., 2017; 320 Saunois et al., 2020) making this explanation unlikely, although we cannot completely exclude the possibility that the geological CH4 source was larger at the LIG than the Holocene. Similarly, since the δ 13C value of CO2 from volcanic outgassing is close to zero (Brovkin et al., 2016) and modelling suggests volcanic outgassing likely only had a minor impact on δ13CO2 (Roth and Joos, 2012), it is unlikely that volcanic outgassing of CO2 played a significant role in influencing the mean oceanic δ13C.

20. Fig 4: Again, revise your calculated offset in δ 13C based on a revised definition of time windows and include uncertainties in it.

The periods have been redefined as per our response to #1, and figure 6 (previously figure 4) modified accordingly. We have added the propagated sample standard deviations to the anomaly value in the figure.

21. Fig 5: I do not understand the backgorund shading which is labels as “reconstructed δ 13C. Reconstructed by what? Is this a model result or an interpolation.

We’re sorry that the figure caption was not clear. The caption has been revised to include the following line:

Background shading shows the reconstructed d13C using a quadratic statistical regression of the proxy data following the method described in Bengtson et al. (2019).

22. line 310: It could be that not only weathering and sedimentation but also volcanic CO2 might add to this mentioned imbalance.

Thank you for highlighting this factor. In light of your comment, we have added the following consideration to the discussion:

Similarly, since the d13C value of CO2 from volcanic outgassing is close to zero (Brovkin et al., 2016) and modelling suggests volcanic outgassing likely only had a minor impact on d13CO2 (Roth and Joos, 2012), it is unlikely that volcanic outgassing of CO2 played a significant role in influencing the mean oceanic d13C.

23. No data availability is given. Please upload your data base to a repository, e.g. PANGAEA.

The database has now been published. We have added the following link to the data availability section:

The data is published on Research Data Australia at DOI https://doi.org/10.26190/5efe841541f3b.

24. The SI reference list of cores should be contained in the main text.

The lists of cores for the LIG the Holocene have been inserted into the text (Table 1 and Table 2, respectively). The reference in the text at the end of L106 has been changed to:

The full core lists are provided in Tables 1 and 2 for the LIG and the Holocene, respectively.

Reviewer #2:

We thank Reviewer 2 for providing helpful comments on our manuscript. Please see below our responses to these comments.

The manuscript by Bengston et al. seeks to document the d13C of the LIG ocean for comparison to the mid-Holocene. Using published datasets, the authors calculate the average d13C for the LIG and Holocene and find that the LIG in certain areas was more 13C-depleted, by ~0.2 per mil. Given that atmospheric d13C was lower during the LIG, differences in air-sea gas exchange cannot be invoked to account for the oceanic discrepancy. Instead, the authors suggest the light LIG reflects a long-term imbalance between weathering and burial of carbon.

Strengths

The background section is a comprehensive review of the LIG literature that nicely summaries the keys aspects of LIG climate.

The authors assembled an impressive array of time series and evaluated potential biases associated with the averaging techniques. While it would always be useful to have more d13C data, especially in the volumetrically dominant Pacific, they make a compelling initial case that oceanic d13C in certain oceanic regions during the LIG was lighter than during the Holocene. The authors explicitly acknowledge the paucity of data in the Indian and Pacific Oceans, and work to address the issue by focusing on a few areas with relatively high

density of d13C records. In doing so, they are able to demonstrate, at least in certain regions, that there is a statistically different mean d13C during the LIG.

Weaknesses

The treatment of AMOC differences between the Holocene and LIG is underdeveloped. While there is evidence of short-term AMOC changes during the LIG that do not occur during the Holocene (e.g. Galassen et al., 2014), there are several other records from the North Atlantic that suggest the first half of the LIG had lower d13C values, which may reflect a weaker AMOC (see records summarized in Hodell et al., 2009, EPSL, 288, 10-19).

Thank you for drawing this to our attention. Please note that we have responded to this concern below when addressing the comment on our chosen time period within the LIG.

The age models used in the compilation are taken from published records. Given that most of the cores are from Lisiecki and Stern (2016), this shouldn't be a major issue because LS16 uses a consistent tuning method. However, the records in Oliver et al. (2010) and the other papers may use slightly different approaches. It would therefore be very useful to apply the methodology from LS16 to all of the cores in the presented compilation to eliminate potential age model biases. In lieu of such an effort, the authors could show how well the various d18O records during MIS 5d, 5e, and 6 align with the LS16 stack as evidence that age model offsets are not a major concern.

We thank the Reviewer for this comment. We have accordingly checked the d18O data from the other sources. There were indeed small dating offsets between some of the additional cores and the LS16 aligned data. We have adjusted these age models to align with the geographically closest LS16 stacks. We now provide a plot of the data before and after the adjustment in Fig S1. We have also updated our d13C analysis accordingly, noting that there were only small changes in our results due to the relatively small portion of the dataset that was affected. The following was added to the manuscript to L123:

In order to align all of the records, adjustments to the age models of cores from Oliver et al. (2010) and the four additional cores (CH69-K09, MD95-2042, MD03-2664 and ODP 1063) were made by aligning the d18O minima during the LIG to corresponding d18O minima of the nearest LS16 stack. The d18O data before and after the alignment is given in Fig. S1.

The other primary weakness is the limited number of records for the Pacific (18 LIG, 19 Holocene) and Indian Oceans (4 LIG, 7 Holocene). Given that the Pacific and Indian Oceans combined have ~3x the volume of the Atlantic, and therefore >3x the DIC, the paucity of data coverage in the Pacific and Indian Oceans is the greatest source of uncertainty for the mean oceanic d13C estimate. The addition of only a handful of Pacific records with slightly more positive d13C values could alter the conclusion that the mean oceanic d13C during the LIG was less than the Holocene.

Additionally, a non-trivial proportion of the Pacific records appear to come from relatively shallow locations, creating another source of potential bias. Here it would be useful to show not only the spatial coverage, as in Figure 1, but also a figure showing the depth coverage in zonal sections through the three major ocean basins. The authors address the depth dependency in Figure 3, where they calculate mean values based only those cores deeper than 2500 m. They also note that the volume weighted regional values are based on cores deeper than 1000 m. For the reader to get a better sense of the data coverage vs. depth,

however, it would be very helpful a figure with the zonal sections or a figure showing the eight regions used to estimate the regional values, with core locations superimposed.

We agree with the Reviewer that it would be a useful addition to the manuscript to have a figure of the data presented zonally. For this reason, we have added a new figure to manuscript (Fig. 3) and refer to this in L136:

The spatial distribution of the database for the Holocene and the LIG is shown in Fig. 2 and the depth distribution of each ocean basin is shown in Fig. 3.

We have added the following sentences to L216 and refer to Fig. 3:

We also note that the average depths of cores from the Pacific Ocean (LIG: 2,711 m, Holocene: 2,131 m) and Indian Ocean (LIG: 2,383 m, Holocene: 2,303 m) are shallower than that of the Atlantic Ocean (LIG: 3,531 m, Holocene: 3,157 m; Fig. 3). However, as the vertical gradient below 2,000 m depth in the Pacific Ocean is small (e.g. Eide et al., 2017), this might not significantly impact our results.

The other main weakness of the paper is the focus on the late LIG, which is motivated by the desire to avoid the lighter d13C observed in the early portion of many early LIG records. The authors note that their focus on the late LIG is to avoid low d13C values associated with the penultimate deglaciation, which is a reasonable consideration. However, many of these light d13C values occur well within MIS 5e as defined by the oxygen isotope stratigraphy in the associated cores (see for example the records in Hodell et al., 2009). Focusing on the late LIG for comparison to the Holocene makes sense for the mean d13C comparison, but it biases the Atlantic LIG records towards heavier d13C values, which therefore minimizes any differences in d13C that are related to AMOC variability. In other words, it is very likely that the authors are missing differences in the AMOC between the LIG and Holocene by focusing on the late LIG in the Atlantic d13C records.

Thank you for this suggestion. We have now added an analysis of d13C for a slightly earlier period (128-123 ka BP) to the new manuscript. Figure 5 shows the data distribution across 3 LIG time periods, as well as their median, first and third quartiles. Figure S2 compares the latitude-depth d13C distributions in the Atlantic basin during the early and late LIG. Figure 4 also shows the d13C time-evolution in the Northeast, Equatorial and southeast Atlantic from 130 to 118 ka. Our analysis suggests that there was indeed a difference in the volume weighted mean d13C between the early LIG (128-123 ka BP) and our time slice (125-120 ka BP), even though this difference is small (0.06 permil). We did not find a significant difference in NADW extent though additional studies are needed to fully resolve this. We would like to stress that we would not expect centennial-scale AMOC slowdown events to be detectable in this analysis because of age model uncertainties and the overall length of the time considered in this analysis (5 ka). We have added the following to the discussion L281:

A statistical reconstruction of the early LIG (128–123 ka BP) δ13C compared to our 125–120 ka BP reconstruction does not reveal a significant difference in either the NADW core depth or NADW extent as indicated by the meridional d13C gradients (Fig. S2). The volume weighted average d13C during the early LIG is 0.06 permil lighter than during the LIG period considered here (125-120 ka BP). Since both time slices (128–123 ka BP and 125–120 ka BP) are 5 ka averages and include dating uncertainties of ~2 ka, it is not possible to resolve potential centennial-scale oceanic circulation changes (e.g. Galaasen et al., 2014b; Tzedakiset al., 2018).

Additional points:

Title: As ‘interglacial’ is an adjective, please consider using instead ‘interglacial period’ or ‘interglacial interval’.

We have adjusted the title to be:

Lower oceanic d13C during the Last Interglacial Period compared to the Holocene

Figure 1: Given the issues associated with scaling dD to temperature, it would be helpful to use only dD for the y-axis here, with some explanation of how dD scales to temperature with modern spatial relationships. Alternatively, consider including dD on one of the y-axes so the reader understands the source of the temperature estimate. Please also include error estimates for the SST record so it is clear what part of the temperature signal is statistically meaningful. (On the positive side, the comparison of the LIG and Holocene on the same x and y axes is very useful for showing the clear difference in CO2 history between the two intervals.)

Thank you for the suggestion. We have added dD on a secondary y-axis along with the estimated temperature at this Antarctic site. We have also provided details on the age model and the method by which temperature was calculated from dD.

We have changed the SST data presented, now showing two cores, one from the Iberian Margin, and the other from the North Atlantic. The data from the North Atlantic is now presented with the standard deviation.

Figure 2: Please specify the confidence limit associated with the whiskers. Also note the statistical range noted by the colored boxes (box and whisker diagrams aren’t particularly common in the paleo literature).

We have added the following details to the figure caption (now Figure 5):

Lower end of the box indicates quartile 1 (Q1) and the upper end indicates quartile 3 (Q3). Orange vertical lines show the median and dotted vertical lines show the mean. The whiskers indicate the lower and upper fences of the data calculated as Q1-1.5*(Q3-Q1) and Q3+1.5*(Q3-Q1), respectively, and the clear circles are outliers.

Figure 3: Note that the choice of averaging interval for the LIG has a non-trivial influence on the mean d13C for the equatorial and SE Atlantic. Given that the chosen interval of 125-120 ka is somewhat arbitrary, it is necessary to more fully explore the sensitivity of the findings to the choice of time interval. For example, if the defined LIG interval were 124-120 ka, several light d13C points would be excluded, resulting in a higher mean LIG d13C. If the lighter points are excluded, like those earlier in the LIG, what is the resulting mean LIG d13C for the equatorial and SE Atlantic? Is it statistically different than the Holocene d13C?

Thank you for raising these questions. We have now included box plots (moved from Fig. 2 to a new Figure, now Figure 5) which explore the sensitivity of the anomaly to the LIG time period considered within 128 ka BP and 118 ka BP:

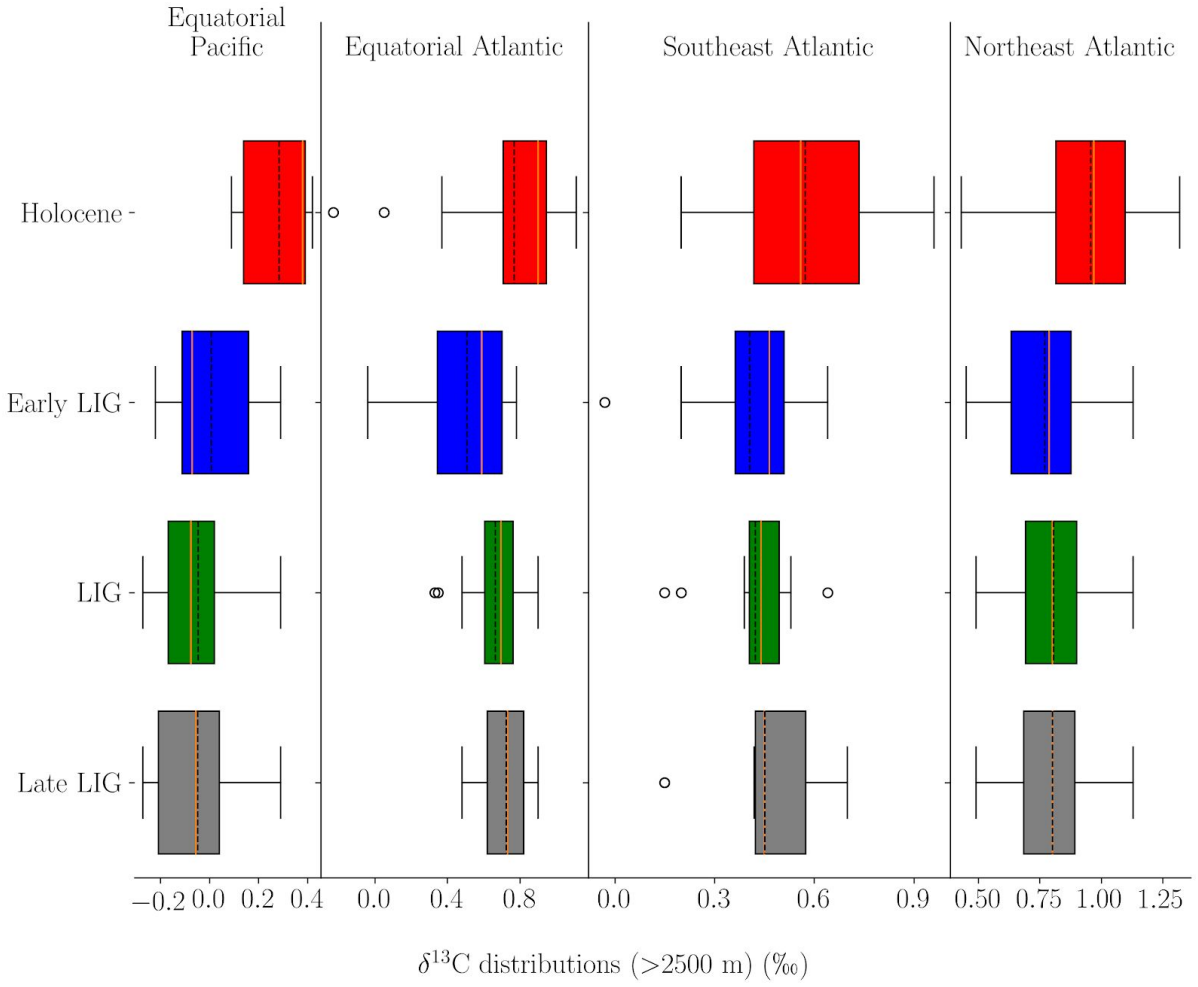

We have added the following accompanying paragraph to Section 3.1:

We also compare the distribution of d13C for cores deeper than 2,500 m for three overlapping periods within the LIG (early LIG: 128--123 ka BP; LIG: 125--120 ka BP; late LIG: 123--118 ka BP). The results for the four regions are shown in Fig. 5. The statistical characteristics do not show much variation between the LIG and late LIG d13C distributions. In the equatorial Pacific, the difference between the early LIG and the Holocene is smaller than between LIG and Holocene, but this is countered with a larger difference in the equatorial Atlantic between early LIG and Holocene. The spread in the data is generally larger during the Holocene than during the other time periods which might be due to the greater number of measurements during the Holocene. The spread of data during the early LIG is slightly larger than during the LIG and late LIG in the equatorial and southeast Atlantic. The equatorial Atlantic is the only region which displays significantly more points with lower d13C during the early LIG. Overall, these distributions do not suggest that the LIG-Holocene anomalies that we have determined would be significantly impacted by slight variations in the selected time window. We perform an analysis of variance (ANOVA) on each region and post hoc tests on the data. We find that the Holocene data is significantly different from the three LIG periods in the northeast Atlantic, the southeast Atlantic and the equatorial Pacific, while the three periods within the LIG are not significantly different from each other for any of the regions.

Additionally, we have improved our explanation of our selected time periods in the manuscript:

We then define the time periods within the LIG and the Holocene to perform our analyses. For the Holocene, as most of the available data is dated prior to 2 ka BP, we define the end of our Holocene time period as 2 ka BP. To capture as much of the Holocene data as possible, we include data back to 7 ka BP, ensuring that we do not include instability associated with the 8.2 kiloyear event (Alley et a., 2005; Thomas et al., 2007). This provides a time span of 5 ka of data that we will consider for our analysis of the Holocene.

For the LIG, we seek to avoid data associated with the end of the penultimate deglaciation, which is characterised by a benthic d13C increase in the Atlantic until ~128 ka BP (Govin et al., (2015); Menviel et al. (2019); Oliver et al. (2010), Fig. 4). In addition, a millennial-scale event has been identified in the North Atlantic between ~127 and 126 ka BP (Galaasen et al., 2014, Tzedakis et al., 2018). Considering the typical dating uncertainties associated with the LIG data (2 ka), we thus decide to start our LIG time period at 125 ka BP. To ensure that the two time periods are of same length (5 ka BP), we define the LIG period for our analysis to be 125-120 ka BP. We note that our definition should also avoid data associated with the glacial inception (Govin et al. (2015); Past Interglacial Working Group of PAGES, 2016). We verify that the LIG time period has sufficient data across the four selected regions, noting that the highest density of data falls within the 125-120 ka BP time period---particularly in the equatorial Atlantic and southeast Atlantic (Fig. 4b, c).

Line 85: While remineralization contributes to the lowering of NADW d13C as waters flow toward the Southern Ocean, the residence time of NADW is quite short in the Atlantic, minimizing the influence of remineralization. Mixing with 13C-depleted UCDW and AABW also contributes to the deep South Atlantic being 13C-depleted relative to the North Atlantic.

It is true that the remineralisation is not the only mechanism responsible for the decrease in d13C of NADW. We have rephrased the sentence to read:

Along its path through the Atlantic basin interior, organic matter remineralisation and mixing with southern source waters lowers δ13C, with δ13C values of ~0.5 ‰ in the deep Southern Ocean.

Line 87: This sentence is written in such a way to give the impression that the use of d13C as a circulation proxy is a recent phenomenon. But in the following sentence, there are citations of classic papers where d13C was used for exactly this purpose. Please clarify.

Sorry that this sentence was misleading. L79-80 has been changed to:

The tight relationship between the water masses' apparent oxygen utilisation, nutrient content and d13C allows d13C to be used as a water mass ventilation tracer (e.g. Boyle and Keigwin, 1987; Curry and Oppo, 2005; Duplessy et al., 1988; Eide et al., 2017).

Lines 285-305: The authors suggest that the -0.2 per mil difference in mean oceanic d13C during the LIG may have been due to less organic carbon in the land biosphere. Unfortunately, there is no effort to estimate how much land carbon would be required to create the d13C anomaly. While this would assume a closed atmosphere-biosphere-ocean system, making this assumption explicit would then allow for informed speculation on the

likely sources of terrestrial carbon. The estimate of terrestrial carbon loss could then be compared to various reservoirs (e.g. peats) to assess whether they are likely sources.

A mass balance calculation would imply that the system is closed. Given that the LIG and Holocene are more than 100,000 years apart, the closed system approximation is associated with uncertainties that are too large to be included in the main part of the manuscript. Nevertheless, we now include the d13C mass balance calculation in the supplementary materials. And reference it in the following paragraph in the revised discussion:

An alternative explanation for the anomaly is a change in the terrestrial carbon storage, which has a typical signature of approximately -37 to -20 ‰ for C3 derived plant material (Kohn, 2010) and -13 ‰ for C4 derived plant material (Basu et al., 2015). The total land carbon content at the LIG is poorly constrained. Proxies generally suggest extensive vegetation during the LIG compared to the Holocene (CAPE, 2006; Govin et al., 2015; Larrasoaña et al., 2013; Muhs et al., 2001; Tarasov et al., 2005; de Vernal and Hillaire-Marcel, 2008), which would imply a greater land carbon store. However, other terrestrial carbon stores including peatlands and permafrost may also have differed during the LIG compared to the Holocene. With an estimated ~550 Gt C stored in peats today (mean δ 13 305 C ~-28 ‰, Dioumaeva et al. (2002); Novák et al. (1999)) and ~1,000 Gt C in the active layer in permafrost, which may have been partially thawed during the LIG (Reyes et al., 2010; Schuur et al., 2015; Stapel et al., 2018), less carbon stored in peat and permafrost at the LIG could have led to a lower total land carbon store compared to the Holocene. However, it is not possible to infer this total land carbon change from the oceanic and atmospheric δ13C anomalies because it cannot be assumed that the mass of carbon and 13C is preserved within the ocean-atmosphere-land biosphere system on glacial-interglacial timescales.

There is indeed continuous exchange of carbon and 13C between the lithosphere and the coupled ocean, atmosphere and land biosphere carbon reservoirs. Isotopic perturbations associated with changes in the terrestrial biosphere are communicated to the burial fluxes of organic carbon and CaCO3 and are therefore removed on multi-millennial time scales (Jeltsch-Thömmes et al., 2019; Jeltsch-Thömmes and Joos, 2020). Nevertheless, when hypothetically neglecting any exchange with the lithosphere, we find that the change in terrestrial carbon needed to explain the difference in δ13C would be in the order of 295±44 Gt C less during the LIG than the Holocene (Text S1).

Lines 309-311: The idea about long-term imbalance between weathering and burial of carbon needs to be explained more thoroughly. How would these processes create the difference in LIG and Holocene d13C of DIC? The cited paper by Jeltsch-Thommes and Joos (2020) is a modeling study that evaluates the influence a large pulse of carbon introduced to the atmosphere, assuming that the carbon comes from the terrestrial biosphere. The simulations suggest that that oceanic d13C responds quickly to the addition of 500 Gt of terrestrial organic carbon, creating an oceanic anomaly of ~ -0.2 per mil within about 500 years. The d13C anomaly persists for 10 kyr, before slowly returning to its initial value after approximately 100 kyr (due to removal of light carbon through biogenic sedimentation). Are the authors suggesting that such a process could explain the apparent difference between LIG and Holocene d13C?

We agree with the Reviewer that the discussion on exchanges with the lithosphere as cause of the d13C anomaly was not clear. We have revised major parts of the discussion to better explore why we believe this mechanism is critical to understanding the anomaly.

The parts of the discussion exploring the possible mechanisms for the d13C anomaly now read:

Explanations for the 0.2 ‰ lower δ13C anomaly in the ocean may include a redistribution between the ocean-atmosphere system. Such a redistribution can result from a change in end-member values (Fig. 8). As fractionation during air-sea gas exchange is temperature dependent, globally higher SSTs at the LIG could lead to a lower oceanic δ13C. However, the effect of this is likely small (Brovkin et al., 2002) and this would also lead to a higher atmospheric δ13CO2 at the LIG, which is inconsistent with Antarctic ice core measurements that suggest an anomaly of -0.3 ‰ (Schneider et al., 2013). Lower nutrient utilisation in the North Atlantic would decrease surface ocean δ13C and thus the δ13C end-members. However, this would also imply that less organic carbon would be remineralised at depth. Therefore, it is unlikely that the lower average oceanic mean δ13C results from a change in end-members through lower surface ocean nutrient utilisation. Currently, there is still a lack of constraints on nutrient utilisation in these end-member regions during the LIG compared to the Holocene. Therefore, the lower δ13C in the ocean-atmosphere system cannot be explained by a simple redistribution of δ13C between the atmosphere and the ocean.

An alternative explanation for the anomaly is a change in the terrestrial carbon storage, which has a typical signature of approximately -37 to -20 ‰ for C3 derived plant material (Kohn, 2010) and -13 ‰ for C4 derived plant material (Basu et al., 2015). The total land carbon content at the LIG is poorly constrained. Proxies generally suggest extensive vegetation during the LIG compared to the Holocene (CAPE, 2006; Govin et al., 2015; Larrasoaña et al., 2013; Muhs et al., 2001; Tarasov et al., 2005; de Vernal and Hillaire-Marcel, 2008), which would imply a greater land carbon store. However, other terrestrial carbon stores including peatlands and permafrost may also have differed during the LIG compared to the Holocene. With an estimated ~550 Gt C stored in peats today (mean δ 13 305 C ~-28 ‰, Dioumaeva et al. (2002); Novák et al. (1999)) and ~1,000 Gt C in the active layer in permafrost, which may have been partially thawed during the LIG (Reyes et al., 2010; Schuur et al., 2015; Stapel et al., 2018), less carbon stored in peat and permafrost at the LIG could have led to a lower total land carbon store compared to the Holocene. However, it is not possible to infer this total land carbon change from the oceanic and atmospheric δ13C anomalies because it cannot be assumed that the mass of carbon and 13C is preserved within the ocean-atmosphere-land biosphere system on glacial-interglacial timescales.

There is indeed continuous exchange of carbon and 13C between the lithosphere and the coupled ocean, atmosphere and land biosphere carbon reservoirs. Isotopic perturbations associated with changes in the terrestrial biosphere are communicated to the burial fluxes of organic carbon and CaCO3 and are therefore removed on multi-millennial time scales (Jeltsch-Thömmes et al., 2019; Jeltsch-Thömmes and Joos, 2020). Nevertheless, when hypothetically neglecting any exchange with the lithosphere, we find that the change in terrestrial carbon needed to explain the difference in δ13C would be in the order of 295±44 Gt C less during the LIG than the Holocene (Text S1).

In addition, due to the warmer conditions at the LIG than during the Holocene, there could have been a release of methane clathrates which would have added isotopically light carbon

(δ 13C: ~-47 ‰) to the ocean-atmosphere system. However, available evidence suggests that geological CH4 sources are rather small (Bock et al., 2017; Hmiel et al., 2020; Petrenko et al., 2017; 320 Saunois et al., 2020) making this explanation unlikely, although we cannot completely exclude the possibility that the geological CH4 source was larger at the LIG than the Holocene. Similarly, since the δ 13C value of CO2 from volcanic outgassing is close to zero (Brovkin et al., 2016) and modelling suggests volcanic outgassing likely only had a minor impact on δ13CO2 (Roth and Joos, 2012), it is unlikely that volcanic outgassing of CO2 played a significant role in influencing the mean oceanic δ13C.

While we are not in the position to firmly pinpoint the exact mechanism, the LIG-Holocene differences in the isotopic signal of both the atmosphere and ocean were most likely due to a long-term imbalance between the isotopic fluxes to and from the lithosphere, including the net burial (or redissolution) of organic carbon and CaCO3 in deep-sea sediments, and changes in shallow water sedimentation and coral reef formation (Jeltsch-Thömmes and Joos, 2020).

Lower oceanic δ^{13}C during the Last Interglacial Period compared to the Holocene

Shannon A. Bengtson[1,2], Laurie C. Menviel[1], Katrin J. Meissner[1,2], Lise Missiaen[1], Carlye D. Peterson[3], Lorraine E. Lisiecki[4], and Fortunat Joos[5,6]

[1]Climate Change Research Centre, The University of New South Wales, Sydney, Australia
[2]The Australian Research Council Centre of Excellence for Climate Extremes, Australia
[3]Earth Sciences, University of California, Riverside, California, USA
[4]Department of Earth Science, University of California, Santa Barbara, California, USA
[5]Climate and Environmental Physics, Physics Institute, University of Bern, Bern, Switzerland
[6]Oeschger Centre for Climate Change Research, University of Bern, Bern, Switzerland

Correspondence: Shannon A. Bengtson (s.bengtson@unsw.edu.au)

Abstract.

The last time in Earth's history when ~~the~~ high latitudes were warmer than during pre-industrial times was the last interglacial period (LIG, 129–116 ka BP). Since the LIG is the most recent and best documented ~~warm time period~~interglacial, it can provide insights into climate processes in a warmer world. However, some key features of the LIG are not well constrained, notably the oceanic circulation and the global carbon cycle. Here, we use a new database of LIG benthic δ^{13}C to investigate these two aspects. We find that the oceanic mean δ^{13}C was ∼0.2 ‰ lower during the LIG (here defined as 125–120 ka BP) when compared to the ~~mid-Holocene (7–4~~ Holocene (7–2 ka BP). ~~As the LIG was slightly warmer than the Holocene, it is possible that terrestrial carbon was lower, which would~~ A lower terrestrial carbon content at the LIG than during the Holocene could have led to both a lower oceanic δ^{13}C and atmospheric $\delta^{13}CO_2$ as observed in paleo-records. However, given the multi-millennial timescale, the lower oceanic δ^{13}C most likely reflects a long-term imbalance between weathering and burial of carbon. The δ^{13}C distribution in the Atlantic Ocean suggests no significant difference in the latitudinal and depth extent of North Atlantic Deep Water (NADW) between the LIG and the ~~mid-Holocene~~Holocene. Furthermore, the data suggests that the multi-millennial mean NADW transport was similar between these two time periods.

1 Introduction

The most recent and well documented warm time period ~~,~~ is the last interglacial period (LIG), which is roughly equivalent to Marine Isotope Stage (MIS) 5e (Past Interglacial Working Group of PAGES, 2016; Shackleton, 1969). The LIG began at the end of the penultimate deglaciation (∼129 thousand years before present, ka BP hereafter) and ended with the last glacial inception (∼116 ka BP) ~~(Govin et al., 2015; Brewer et al., 2008; Dutton and Lambeck, 2012; Masson-Delmotte et al., 2013)~~ (Brewer et al., 2008; Dutton and Lambeck, 2012; Govin et al., 2015; Masson-Delmotte et al., 2013). The LIG was globally ~~somewhat~~ warmer than pre-industrial (PI, ∼1850–1900 (IPCC, 2013), Shackleton et al. (2020)~~; PI is~~ , with PI estimated to be ~~cooler by ~0.7~~ 0.4 °C cooler than the peak of the Holocene (~~∼5~~ 10–5 ka BP) (Marcott et al., 2013). Though not an exact

analogue for future warming, the LIG may still help shed light on future climates. In particular, we seek to constrain the mean LIG ocean circulation and estimate the global oceanic mean $\delta^{13}C$.

1.1 ~~Climate during the Last Interglacial~~

As greenhouse gas concentrations were comparable to the Holocene, the LIG was most likely relatively warm because of the high boreal summer insolation (Laskar et al., 2004). During the LIG, the atmospheric CO_2 concentration was relatively stable around ~280 p.p.m. (Bereiter et al., 2015; Lüthi et al., 2008), while during the Holocene CO_2 first decreased by about 5 p.p.m. starting at 11.7 ka BP before increasing by ~~28~~ 18 p.p.m. until reaching a mean of 279 p.p.m. at ~2 ka BP (Fig. 1a) ~~(Eggleston et al., 2016b). Additionally, during the LIG and the Holocene, N_2O peaked at around ~267 p.p.b (?Flückiger et al., 2002), while~~ (Köhler et al., 2017). CH_4 reached ~700 p.p.b ~~(Petit et al., 1999)~~ and ~675 p.p.b ~~respectively (Flückiger et al., 2002). Ice core data indicate strong polar warming in Greenland that was 8.5±2.5 °C higher during the peak of the LIG compared to PI (Landais et al., 2016). Similarly, EPICA DOME C record suggests that the highest Antarctic temperatures from the last 800 ka occurred during the LIG (Masson-Delmotte et al., 2010) (Fig.1b)~~during the LIG and the Holocene, respectively, and N_2O peaked at ~267 p.p.b during both periods (Flückiger et al., 2002; Petit et al., 1999; Spahni et al., 2005) . Global sea-level was 6–9 m higher at the LIG compared to PI (Dutton et al., 2015; Kopp et al., 2009), thus indicating significant ice-mass loss from both Antarctica and Greenland.

Strong polar warming is ~~also~~ supported by terrestrial and marine temperature reconstructions. ~~On land, proxy records from mid to high latitudes indicate higher temperatures during the LIG compared to PI, particularly in North America (Anderson et al., 2014; Montero-Serrano et al., 2011; Axford et al., 2011). In Alaska and Northern Europe, summer temperatures were higher by about 1–2 °C (Kaspar et al., 2005), though some Northern European records indicate a smaller temperature increase of up to 1 °C (Plikk et al., 2019), and there is some inconsistency in the European temperature records (Otto-Bliesner et al., 2020). Sea~~ A global analysis of sea surface temperature (SST) ~~reconstructions also indicate higher temperatures at the LIG compared to PI (e.g. the Mediterranean record in Fig. 1c). A global analysis of SST~~ records suggests that the mean surface ocean was 0.5±0.3 °C ~~higher~~ warmer during the LIG compared to 1870–1889 ~~, with the largest increases occurring at high latitudes (Hoffman et al., 2017). Another global reconstruction estimates that the global mean SST was~~ (Hoffman et al., 2017), similar to another global estimate which suggests SSTs were 0.7±0.6 °C higher during the LIG compared to ~~peak Holocene temperatures (McKay et al., 2011). During boreal summer, temperatures in the Arctic were likely 4–5 °C higher with reduced Arctic summer sea ice extent (Stein et al., 2017). Temperatures of surface waters off Greenland were likely 3–5 °C higher during the early to mid-LIG~~ the late Holocene (McKay et al., 2011). However, there were differences in the timing of these SST peaks in different regions compared to the ~~warmest period of the Holocene (Irvali et al., 2012) . North Atlantic summer SSTs were on average 1.1~~ 1870–1889 mean: North Atlantic SSTs peaked at +0.6±0.5 °C ~~higher than PI, while Southern Ocean austral summer SSTs are estimated to have been about 1.8~~ at 125 ka BP (e.g. Fig. 1b) and Southern Hemisphere extratropical SSTs peaked at +1.1±0.5 °C ~~higher at 127 ka BP than PI(Capron et al., 2017).~~ at 129 ka BP (Hoffman et al., 2017). On land, proxy records from mid to high latitudes indicate higher temperatures during the LIG compared to PI, particularly in North America (Anderson et al., 2014; Axford et al., 2011; Montero-Serrano et al., 2011)

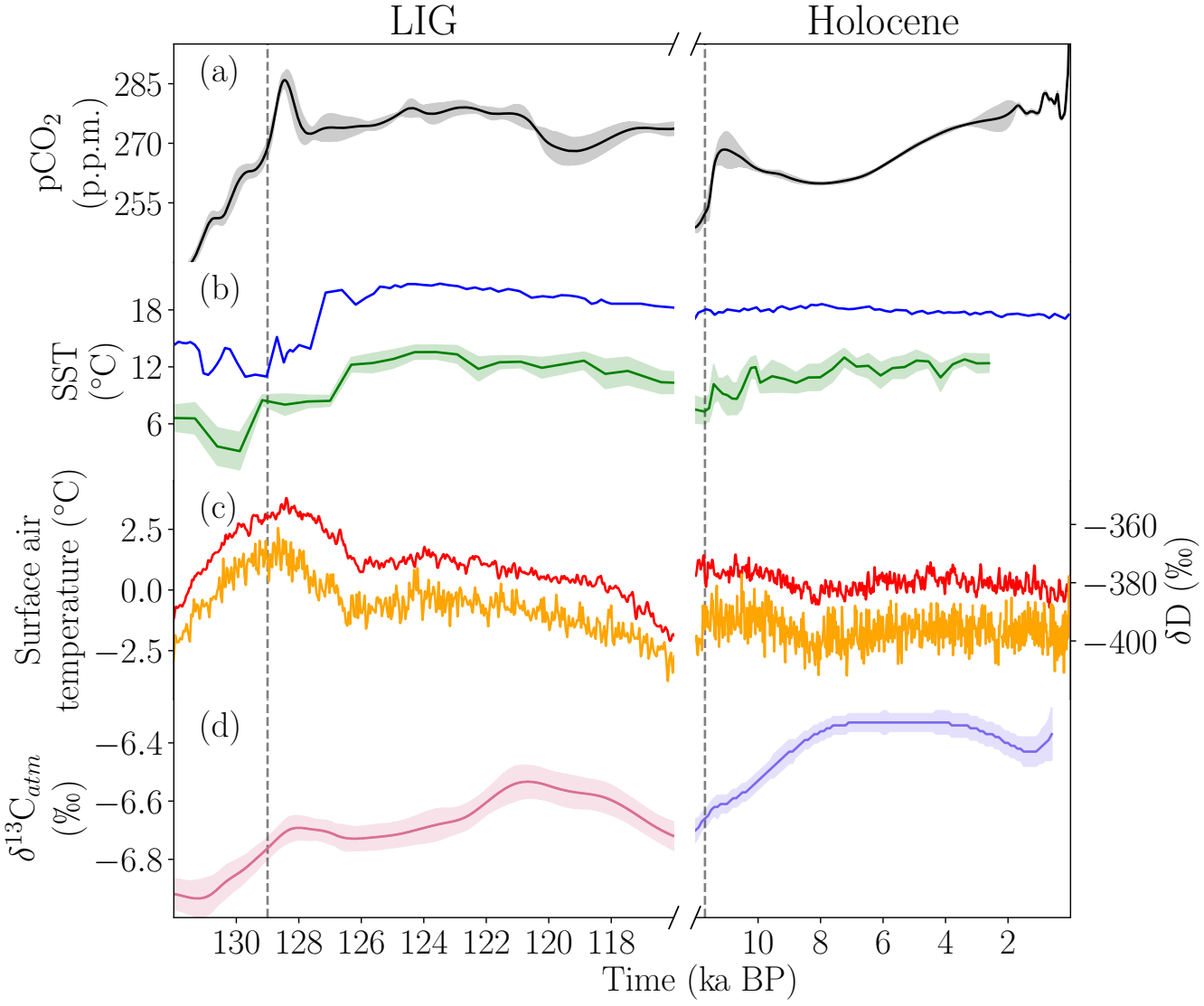

Figure 1. LIG and Holocene timeseries of a) ~~EPICA Dome C ice core~~ $pCO_{2,atm}$ ~~(Schneider et al., 2013; Eggleston et al., 2016a)~~ stack smoothed with a spline based on the age model AICC2012 (Köhler et al., 2017), b) ~~EPICA Dome C ice core surface air temperatures determined from deuterium measurements (Jouzel and Masson-Delmotte, 2007), c)~~ sea surface temperatures (~~SST~~SSTs) determined from alkenones and aligned with oxygen isotopes from the ~~Mediterranean marine sediment~~ Iberian Margin (MD01-2444, blue, Martrat et al. (2007b)) and the North Atlantic (GIK23414-6, green, Candy and Alonso-Garcia (2018)), c) EPICA Dome C ice core ~~ODP161-977A (Martrat et al., 2004)~~(EDC96) deuterium measurements (orange) and calculated surface air temperature (red, $\delta D = 6.2‰/°C * T + 5.5‰$) based on the EDC3 time scale relative to the mean of the last 1 ka (Jouzel et al., 2007) and d) spline of $\delta^{13}C_{atm}$ from EPICA Dome C and the Talos Dome ice ~~core~~ cores (Holocene, Eggleston et al. (2016a)) and Monte Carlo average of three Antarctic ice cores $\delta^{13}C_{atm}$ ~~(Elsig et al., 2009; Schneider et al., 2013)~~(LIG, Schneider et al. (2013)) both based on the age model AICC2012. Shading around the lines indicates 1σ. Vertical grey shading indicates the periods of analysis in this paper. Grey vertical dotted lines indicate the commencement of the LIG and Holocene~~periods~~.

. Similarly, the EPICA DOME C record suggests that the highest Antarctic temperatures from the last 800 ka occurred during the LIG (Masson-Delmotte et al., 2010) (Fig. 1c).

Polar warming was also associated with significant changes in vegetation. Pollen records suggest a contraction of tundra and an expansion of boreal forests across the Arctic (CAPE, 2006), in Russia (Tarasov et al., 2005), and in North America (Muhs et al., 2001; de Vernal and Hillaire-Marcel, 2008; Govin et al., 2015) (Govin et al., 2015; Muhs et al., 2001; de Vernal and Hillaire-Marcel, 2008). The few Saharan records suggest a green Sahara period during the LIG (Larrasoaña et al., 2013; Drake et al., 2011)(Drake et al., 2011; Larrasoaña et al., 2013), consistent with a stronger West African monsoon (Otto-Bliesner et al., 2020). Although these reconstructions indicate changes in vegetation distribution during the LIG, the total amount of carbon stored on land remains poorly constrained.

Recent numerical experiments of the LIG as part of the Paleomodel Intercomparison Project Phase 4 (PMIP4) simulate significant warming over Alaska and Siberia in boreal summer, with mean annual temperature anomalies of close to zero, which is in good agreement with the proxy record (Otto-Bliesner et al., 2020). Despite this and other recent data compilations and modelling efforts (including Bakker et al. (2013)), to date there are many open questions remaining about the LIG. In particular, stronger constraints are needed on the extent of Greenland and Antarctic ice sheets, on ocean circulation and the global carbon cycle, including $CaCO_3$ accumulation in shallow waters, and peat and permafrost carbon storage changes (Brovkin et al., 2016) .

1.1 Atlantic Meridional Overturning Circulation during the Last Interglacial

It is important to constrain the state of the Atlantic Meridional Overturning Circulation (AMOC) at the LIG given its significant role in modulating climate. Seven coupled climate models integrated with transient 130–115 ka BP boundary conditions simulate different AMOC trends, with some models producing a strengthening of the AMOC while others compute simulate a weakening during the LIG (Bakker et al., 2013). Paleoproxy records suggest equally strong and deep North Atlantic Deep Water (NADW) during the LIG and the Holocene (e.g. Böhm et al., 2015; Lototskaya and Ganssen, 1999), with a possible southward expansion of the Arctic front related to changes in the strength of the subpolar gyre (Mokeddem et al., 2014), and AMOC weakening during a few multi centennial-scale events between 127 and 115 ka BP (e.g. Galaasen et al., 2014b; Mokeddem et al., 2014; Tzedakis et al., 2018; Lehman et al., 2002; Helmens et al., 2015; Oppo et al., 2006; F (e.g. Galaasen et al., 2014b; Helmens et al., 2015; Lehman et al., 2002; Mokeddem et al., 2014; Oppo et al., 2006; Rowe et al., 2019; Tzed .

1.1 Oceanic δ^{13}C and the carbon cycle

Stable carbon isotopes are a powerful tool for investigating ocean circulation (e.g. Curry and Oppo, 2005; Eide et al., 2017) and the global carbon cycle (e.g. Menviel et al., 2017; Peterson et al., 2014). Since the largest carbon isotope fractionation occurs during photosynthesis, organic matter is enriched in ^{12}C (low δ^{13}C), while atmospheric CO_2 and surface water dissolved inorganic carbon (DIC) become enriched in ^{13}C (high δ^{13}C). On land , the different Organic matter on land includes the terrestrial biosphere, as well as carbon stored in soils, such as in peats and permafrosts. Different photosynthetic path-

ways (which differentiate C3 and C4 plants) fractionate carbon differently, producing typical signatures of about -37 to -20 ‰ for C3 plants (Kohn, 2010) and around -13 ‰ for C4 plants (Basu et al., 2015), though these values vary with a number of factors including precipitation, atmospheric CO_2 concentration and $\delta^{13}C$, light, nutrient availability, and plant species ~~(Diefendorf et al., 2010; Farquhar et al., 1989; Schubert and Jahren, 2012; Cernusak et al., 2013; Leavitt, 1992; Diefendorf and Freimuth,~~ (Cernusak et al., 2013; Diefendorf et al., 2010; Diefendorf and Freimuth, 2017; Farquhar, 1983; Farquhar et al., 1989; Keller et al., 2017; . In the ocean, phytoplankton using the C3 photosynthetic pathway are found to have fractionation during photosynthesis that depends on the concentration of dissolved CO_2. Thus, atmospheric $\delta^{13}CO_2$ during the LIG (Fig. 1d) is influenced by ~~plant type,~~ the cycling of organic carbon within the ocean, ~~the total~~ changes in the amount of carbon stored in vegetation and soils, temperature-dependent air-sea flux fractionation ~~(Zhang et al., 1995; Lynch-Stieglitz et al., 1995)~~ (Lynch-Stieglitz et al., 1995; Zhang et al., 1995), and, on longer time scales, by interactions with the lithosphere ~~. Today~~ (Tschumi et al., 2011). During PI, the mean surface DIC is thereby enriched by ∼8.5 ‰ compared to the atmosphere due to fractionation during air-sea gas exchange ~~(Schmittner et al., 2013; Menviel et al., 2015)~~(Menviel et al., 2015; Schmittner et al., 2013) .

NADW is characterised by low nutrients and high $\delta^{13}C$ as a result of a high nutrient and carbon utilisation by marine biota and fractionation during air-sea gas exchange in the northern North Atlantic. Along its path through the Atlantic basin interior, organic matter remineralisation and mixing with southern source waters lowers $\delta^{13}C$, ~~reducing~~ with $\delta^{13}C$ ~~to~~ values of ∼~~0~~ 0.5 ‰ ~~by the time these water masses reach the~~ in the deep Southern Ocean. ~~Conversely, Antarctic Bottom Water (AABW) has a high nutrient content and low $\delta^{13}C$.~~

The tight relationship between the water masses' apparent oxygen utilisation, nutrient content and $\delta^{13}C$ ~~has revealed the potential of~~ allows $\delta^{13}C$ to be used as a water mass ventilation tracer ~~(Eide et al., 2017)~~ (e.g. Boyle and Keigwin, 1987; Curry and Oppo, 2005; Duplessy et al., 1988; Eide et al., 2017). The $\delta^{13}C$ of benthic foraminifera shells, particularly of the species *Cibicides wuellerstorfi*, has been found to reliably represent the $\delta^{13}C$ signature of DIC ~~(Belanger et al., 1981; Zahn et al., 1986; Duplessy et al., 1984)~~ (Belanger et al., 1981; Duplessy et al., 1984; Zahn et al., 1986) and has therefore been used to better constrain the extent of different water masses. ~~A~~ Mass balances of $\delta^{13}C$ ~~mass balance~~ between the atmosphere, ocean and land ~~has~~ have been previously used to constrain changes in terrestrial carbon between the Last Glacial Maximum (∼20 ka BP) and Holocene (e.g. Peterson et al., 2014). However, ~~since~~ on longer time scales~~the exchange of carbon with the lithosphere~~ , exchanges with the lithosphere including volcanic outgassing (Hasenclever et al., 2017; Huybers and Langmuir, 2009), $CaCO_3$ burial in sediments and weathering, release of carbon from methane clathrates, and the net burial of organic carbon also influences the global mean $\delta^{13}C$~~, it cannot be applied to evaluate terrestrial carbon changes between the LIG and Holocene~~. It has been estimated that the amount of carbon both entering and exiting the lithosphere due to weathering and burial of organic carbon fluxes could be from 0.274 to 0.344 Gt C yr^{-1} (Schneider et al., 2013), though these vary through time (Hoogakker et al., 2006). Over timescales greater than 10 ka, the influence of weathering and burial of carbon might ~~therefore~~ dominate the $\delta^{13}C$ signal (Jeltsch-Thömmes et al., 2019; Jeltsch-Thömmes

and Joos, 2020b), so a mass balance cannot be accurately applied to evaluate terrestrial carbon changes between the LIG and Holocene.

Here, we present a new compilation of benthic δ^{13}C from *Cibicides* ~~*wuellestorfi*~~*wuellerstorfi* spanning the 130–118 ka BP time period. We use this data to compare the δ^{13}C signal of the LIG with that of the Holocene and to determine the difference in average ocean δ^{13}C between the two time periods. We then investigate the ~~Atlantic Meridional Overturning Circulation (AMOC)~~ AMOC during the LIG with our new benthic δ^{13}C database. Finally, we qualitatively explore the role of the various processes affecting the δ^{13}C difference between the LIG and the Holocene.

2 Database and methods

2.1 Database

We present a new compilation of benthic δ^{13}C records covering the LIG (130–118 ka BP) and, for comparison, the ~~mid-Holocene~~ Holocene period (8–2 ka BP). Our database only includes measurements on *Cibicides wuellerstorfi* as no significant fractionation between the calcite shells and the surrounding DIC has been measured in this species ~~(Belanger et al., 1981; Zahn et al., 1986; Duplessy et al., 1984)~~(Belanger et al., 1981; Duplessy et al., 1984; Zahn et al., 1986) .

Our compilation is predominantly based on Lisiecki and Stern (2016) (53 cores), but includes 14 cores described in Oliver et al. (2010), as well as a few other records (CH69-K09 ~~(?)~~(Labeyrie et al., 2017), MD03-2664 (Galaasen et al., 2014a), MD95-2042 ~~(Govin, 2012), IODP 303-U1308 (Hodell et al., 2008), and~~ (Martrat et al., 2007a), ODP 1063 ~~(Poirier and Billups, 2014))~~(Deaney et al., 2017)), and U1304 (Hodell and Channell, 2016). The full core ~~list and their respective locations is provided in the supplementary materials~~lists are provided in Tables 1 and 2 for the LIG and the Holocene, respectively.

2.2 Age models

Due to the lack of absolute age markers, such as tephra layers, the LIG age models mostly rely on alignment strategies that tie each record to a well-dated reference record. The age model tie-points used in this study are taken from the original age model publications. The reference records ~~used by Lisiecki and Stern (2016)~~(LS16, Lisiecki and Stern (2016)) consist of eight regional stacks (one for the intermediate and one for the deep ocean for each the North Atlantic, South Atlantic, Pacific and Indian Oceans) of benthic δ^{18}O that were dated through alignment with other climatic archives such as ice-rafted debris records, synthetic ice core records and speleothems. The use of regional stacks, rather than a single global stack, improved stratigraphic alignment targets and provided more robust age models. The estimated ~~uncertainty~~ age model uncertainty (2σ) for this group of cores is ~~±~~2 ka. Please refer to Lisiecki and Stern (2016) for further details. Oliver et al. (2010) defined their age tie points assuming that sea level minima and benthic δ^{18}O maxima are synchronous. The benthic δ^{18}O records were aligned with each other and then tied to the Dome Fuji chronology (based on O_2/N_2) (Kawamura et al., 2007). Please refer to Shackleton et al.

Table 1. List of cores for the last interglacial period (LIG). Provided is the core name ('Core'), latitude (Lat, °), longitude (Lon, °), depth (Dep, m), the region and the reference. Regions: NEA: northeast Atlantic, NWA: northwest Atlantic, SWA: southwest Atlantic, SEA: southeast Atlantic, SA: south Atlantic, NP: north Pacific, SP: south Pacific, I: Indian. Reference abbreviations: BW96: Bickert and Wefer (1996), CL82: Curry and Lohmann (1982), dA03: de Abreu et al. (2003), KJ8994: Keigwin and Jones (1989, 1994), KS02: Keigwin and Schlegel (2002), L99: Labeyrie et al. (1999), MB99: Mackensen and Bickert (1999), OH00: Oppo and Horowitz (2000), SH84: Shackleton and Hall (1984), SS0405: Skinner and Shackleton (2004, 2005), VH02: Venz and Hodell (2002), V99: Venz et al. (1999), ZM1011: Zarriess and Mackensen (2010, 2011).

Core	Lat	Lon	Dep (m)	Region	Reference
ODP758	5.38	90.36	2,935	I	Chen et al. (1995)
RC12-339	9.13	90.03	3,010	I	{CLIMAP Project Members} (2006)
GEOB3004-1	14.61	52.92	1,803	I	Schmiedl and Mackensen (2006)
MD01-2378	-13.08	121.79	1,783	I	Holbourn et al. (2005)
Y69-71	0.1	-95.65	2,740	NP	Lyle et al. (2002)
ODP677	1.2	-83.73	3,450	NP	SH84, Shackleton et al. (1990)
ODP849	0.18	-110.52	3,839	NP	Shackleton et al. (1990)
V24-109	0.43	158.8	2,367	NP	Duplessy et al. (1984)
Y69-106	2.98	-86.55	2,870	NP	Lyle et al. (2002); Pisias and Mix (1997)
ODP807A	3.61	156.63	2,804	NP	Zhang et al. (2007)
GIK17961-2	8.51	112.33	1,795	NP	Wang et al. (1999)
MD97-2151	8.73	109.87	1,598	NP	Lee et al. (1999); Wei et al. (2006)
ODP1143	9.36	113.29	2,772	NP	Cheng et al. (2004)
V28-304	28.53	134.13	2,942	NP	Duplessy et al. (1984)
V32-128	36.47	177.17	3,623	NP	Duplessy et al. (1984)
PS2495	-41.28	-14.49	3,134	SA	Mackensen et al. (2001)
ODP1089	-40.94	9.89	4,621	SA	Hodell et al. (2001)
PS2082	-43.22	11.74	4,610	SA	McCorkle and Holder (2001)
MD06-3018	-23	166.15	2,470	SP	Russon et al. (2009)
RC13-110	-0.1	-95.65	3,231	SP	Mix et al. (1991)
ODP846	-3.1	-90.82	3,296	SP	Shackleton et al. (1995)
V19-27	-0.47	-82.07	1,373	SP	Mix et al. (1991)
GEOB1101	1.66	-10.98	4,588	NEA	BW96
GIK13519-1	5.67	-19.85	2,862	NEA	Zahn et al. (1986)
GIK16402	14.42	-20.54	4,202	NEA	Sarnthein et al. (1994)
GIK12392-1	25.17	-16.85	2,573	NEA	Shackleton (1977); Zahn et al. (1986)
GIK16004	29.98	-10.65	1,512	NEA	Sarnthein et al. (1994)
GEOB4216	30.63	-12.4	2,324	NEA	Freudenthal et al. (2002)
GIK15669	34.89	-7.82	2,022	NEA	Sarnthein et al. (1994)
GIK15612-2	44.36	-26.54	3,050	NEA	Sarnthein et al. (1994)
NO79-28	45.63	-22.75	3,625	NEA	Duplessy (1996)
GIK23416-4	51.57	-20.0	3,616	NEA	Sarnthein et al. (1994)
NEAP18K	52.77	-30.35	3,275	NEA	Chapman and Shackleton (1999)
GIK23415-9	53.18	-19.15	2,472	NEA	CL82, Sarnthein et al. (1994)
GIK23414-9	53.54	-20.29	2,196	NEA	Sarnthein et al. (1994)
CH73-139	54.63	-16.35	2,209	NEA	Curry et al. (1988); Sarnthein et al. (1994)
GIK17049-6	55.26	-26.73	3,331	NEA	Sarnthein et al. (1994)
V28-56	68.03	-6.12	2,941	NEA	Ruddiman and Members (1982)
ODP984	61	-24	1,650	NEA	Raymo et al. (2004)
V29-202	61	-21	2,658	NEA	Oppo and Lehman (1995)
ODP664	0.11	-23.23	3,806	NEA	Raymo et al. (1997)
SU90-39	52.5	-22	3,955	NEA	Cortijo (2003)
ODP983	60.4	-23.64	1,984	NEA	McIntyre et al. (1999)
SU90-03	40.05	-32	2,475	NEA	Chapman and Shackleton (1999)
U1308	49.88	-24.24	3,883	NEA	Hodell et al. (2008)
ODP980	55.49	-14.7	2,168	NEA	McManus et al. (1999); Oppo et al. (1998)
ODP982	57.51	-15.85	1,134	NEA	Jansen et al. (1996), V99, VH02
EW9209-1JPC	5.91	-44.2	4,056	NWA	Curry and Oppo (1997)
GEOB4403-2	6.13	-43.44	4,503	NWA	Bickert and Mackensen (2003)
ODP1063	33.68	-57.62	4,584	NWA	Deaney et al. (2017)
CH69-K9	41.75	-47.35	4,100	NWA	L99, Waelbroeck et al. (2001)
SU90-11	44.07	-40.02	3,645	NWA	Jullien et al. (2006); Labeyrie et al. (1995)
U1304	53.06	-33.53	3065	NWA	Hodell and Channell (2016)
V27-20	54.0	-46.2	3,510	NWA	Ruddiman and Members (1982)
MD03_2664	57.44	-48.61	3,442	NWA	Galaasen et al. (2014a)
ODP925	4.2	-43.49	3,040	NWA	Bickert et al. (1997)
ODP926	3.72	-42.91	3,598	NWA	Curry et al. (1995)
ODP928	5.46	-43.75	4,012	NWA	Bickert et al. (1997)
V28-127	11.65	-80.13	3,237	NWA	Oppo and Fairbanks (1987)
KNR140-37JPC	31.41	-75.26	3,000	NWA	Curry and Oppo (2005), KS02
GEOB3801-6	-29.51	-8.31	4,546	SEA	Bickert and Mackensen (2003)
GEOB1214	-24.69	7.24	3,210	SEA	BW96
GEOB1211	-24.48	7.53	4,084	SEA	BW96
GEOB1710	-23.43	11.7	2,987	SEA	Schmiedl and Mackensen (1997)
GEOB1034	-21.74	5.42	3,772	SEA	BW96
GEOB1035	-21.59	5.03	4,453	SEA	BW96
GEOB1028-5	-20.1	9.19	2,209	SEA	Bickert and Mackensen (2003)
V22-174	-10.07	-12.82	2,630	SEA	Shackleton (1977)
GEOB1112	-5.78	-10.75	3,125	SEA	BW96, MB99
GEOB1115	-3.56	-12.56	2,945	SEA	BW96, MB99
GEOB1041	-3.48	-7.6	4,033	SEA	BW96, MB99
GIK16867	-2.2	5.1	3,891	SEA	Sarnthein et al. (1994)
GEOB1105	-1.67	-12.43	3,225	SEA	BW96, MB99
GIK16772-1	-1.34	-11.97	3,911	SEA	Sarnthein (2003)
V29-135	-19.7	8.88	2,675	SEA	Sarnthein et al. (1994)
RC13-228	-22.33	11.2	3,204	SEA	Bickert and Mackensen (2003)
ODP1087	-31.46	15.31	1,372	SEA	Lynch-Stieglitz et al. (2006)
MD96-2080	-36.27	19.48	2,488	SEA	Rau et al. (2002)
GEOB2109-1	-27.91	-45.88	2,504	SWA	Vidal et al. (1999)
V22-38	-9.55	-34.25	3,797	SWA	Ruddiman and Members (1982)
GEOB1117	-3.82	-14.9	3,984	SWA	BW96, MB99
GEOB1118	-3.56	-16.43	4,675	SWA	BW96, MB99

(2000) and Oliver et al. (2010) for an extensive method description. The ~~estimated~~ age model uncertainty on this group of cores is estimated to range from ~~±~~1 to ~~±~~2.5 ka.

The published age models for the additional cores were determined using similar alignment techniques: SSTs were correlated to the NGRIP Greenland ice core for CH69-K09 and MD95-2042 (Govin et al., 2012). The age model for MD03-2664 was determined by correlating MD03-2664 δ^{18}O with previously dated MD95-2042 δ^{18}O (Galaasen et al., 2014b). ~~IODP 303-U1308 δ^{18}O and~~ ODP 1063 and U1304 δ^{18}O were originally aligned to the LR04 stack (Lisiecki and Raymo, 2005). In order to align all of the records, adjustments to the age models of cores from Oliver et al. (2010) and the five additional cores (CH69-K09, MD95-2042, MD03-2664, ODP 1063 and U1304) were made by aligning the δ^{18}O minima during the LIG to the corresponding δ^{18}O minima of the nearest LS16 stack. The δ^{18}O data before and after the alignment is given in Fig. S1.

The Holocene age models ~~have been generally~~ are based on planktonic foraminifera radiocarbon dates ~~(Waelbroeck et al., 2001; Stern and Lisiecki, 2014)~~(Stern and Lisiecki, 2014; Waelbroeck et al., 2001), which have been converted into calendar ages using IntCal13 and using reservoir ages based on modern observations (Key et al., 2004), which are assumed to have remained fairly stable across the Holocene. The age uncertainty associated with these Holocene radiocarbon-based age models is generally less than ~~±~~0.5 ka. However, it is important to note that Holocene age models from Oliver et al.

Table 2. List of cores for the Holocene. Provided is the core name ('Core'), latitude (Lat, °), longitude (Lon, °), depth (Dep, m) the region and the reference. Regions: NEA: northeast Atlantic, NWA: northwest Atlantic, SWA: southwest Atlantic, SEA: southeast Atlantic, SA: south Atlantic, NP: north Pacific, SP: south Pacific, I: Indian. Reference abbreviations: BW96: Bickert and Wefer (1996), CL82: Curry and Lohmann (1982), dA03: de Abreu et al. (2003), KJ8994Keigwin and Jones (1989, 1994), KS02: Keigwin and Schlegel (2002), L99: Labeyrie et al. (1999), MB99: Mackensen and Bickert (1999), OH00: Oppo and Horowitz (2000), SH84: Shackleton and Hall (1984), SS0405: Skinner and Shackleton (2004, 2005), VH02: Venz and Hodell (2002), V99: Venz et al. (1999), ZM1011: Zarriess and Mackensen (2010, 2011).

Core	Lat	Lon	Dep (m)	Region	Reference
ODP758	5.38	90.36	2,935	I	Chen et al. (1995)
GEOB3004-1	14.61	52.92	1,803	I	Schmiedl and Mackensen (2006)
M5-3A-422	24.39	58.04	2,732	I	Sirocko et al. (2000)
MD01-2378	-13.08	121.79	1,783	I	Holbourn et al. (2005)
MD79-254	-17.53	38.4	1,934	I	Curry et al. (1988)
RC11-120	-43.52	79.87	3,193	I	CL82
MD88-770	-46.02	96.46	3,290	I	Labeyrie et al. (1996); Sowers et al. (1993)
V35-5	7.2	112.08	1,953	NP	Wang et al. (1999)
V24-109	0.43	158.8	2,367	NP	Duplessy et al. (1984)
Y69-106	2.98	-86.55	2,870	NP	Lyle et al. (2002); Pisias and Mix (1997)
ODP807A	3.61	156.63	2,804	NP	Zhang et al. (2007)
GIK17964-2	6.16	112.21	1,556	NP	Wang et al. (1999)
GIK17961-2	8.51	112.33	1,795	NP	Wang et al. (1999)
MD97-2151	8.73	109.87	1,598	NP	Lee et al. (1999); Wei et al. (2006)
GIK17940-2	20.12	117.38	1,727	NP	Wang et al. (1999)
V28-304	28.53	134.13	2,942	NP	Duplessy et al. (1984)
EW9504-05	32.48	-118.13	1,818	NP	Stott et al. (2000)
MD02-2489	54.39	-148.92	3,640	NP	Gebhardt et al. (2008)
ODP1090	-42.91	8.9	3,702	SA	Hodell et al. (2000, 2003)
ODP1089	-40.94	9.89	4,621	SA	Hodell et al. (2001)
PS2082	-43.22	11.74	4,610	SA	McCorkle and Holder (2001)
MD07-3076	-44.07	-14.21	3,770	SA	Waelbroeck et al. (2011)
MD06-3018	-23	166.15	2,470	SP	Russon et al. (2009)
RC13-110	-0.1	-95.65	3,231	SP	Mix et al. (1991)
ODP846	-3.1	-90.82	3,296	SP	Shackleton et al. (1995)
V19-27	-0.47	-82.07	1,373	SP	Mix et al. (1991)
H214	-36.92	177.43	2,045	SP	Samson et al. (2005)
RS147-07	-45.15	146.28	3,300	SP	Sikes et al. (2009)
MD97-2120	-45.53	174.93	1,210	SP	Pahnke and Zahn (2005)
GEOB1101	1.66	-10.98	4,588	NEA	BW96
EN066-29	2.46	-19.76	5,105	NEA	Sarnthein et al. (1994)
EN066-32	2.47	-19.73	4,998	NEA	Sarnthein et al. (1994)
EN066-26	3.09	-20.02	4,745	NEA	Sarnthein et al. (1994)
EN066-21	4.23	-20.63	3,792	NEA	Sarnthein et al. (1994)
EN066-36	4.31	-20.21	4,095	NEA	Boyle (1992)
EN066-38	4.92	-20.5	2,937	NEA	Sarnthein et al. (1994)
EN066-44	5.26	-21.71	3,423	NEA	Sarnthein et al. (1994)
EN066-16	5.45	-21.14	3,160	NEA	Boyle (1992)
GIK13519-1	5.67	-19.85	2,862	NEA	Zahn et al. (1986)
EN066-10	6.64	-21.9	3,527	NEA	Sarnthein et al. (1994)
GEOB9526	12.44	-18.06	3,223	NEA	ZM1011, Zarriess et al. (2011)
GIK16402	14.42	-20.54	4,202	NEA	Sarnthein et al. (1994)
GEOB9508-5	14.5	-17.95	2,384	NEA	Mulitza et al. (2008)
GIK12347-2	15.83	-17.86	2,576	NEA	Sarnthein et al. (1994)
GEOB7920-2	20.75	-18.58	2,278	NEA	Collins et al. (2011); Tjallingii et al. (2008)
GIK12328-5	21.15	-18.57	2,778	NEA	Sarnthein et al. (1994)
GIK16030	21.24	-18.06	1,516	NEA	Sarnthein et al. (1994)
GIK12379-3	23.14	-17.75	2,136	NEA	Sarnthein et al. (1994)
GIK12392-1	25.17	-16.85	2,573	NEA	Shackleton (1977); Zahn et al. (1986)
GEOB4240	28.89	-13.23	1,358	NEA	Freudenthal et al. (2002)
GIK16004	29.98	-10.65	1,512	NEA	Sarnthein et al. (1994)
GEOB4216	30.63	-12.4	2,324	NEA	Freudenthal et al. (2002)
GIK15672	34.86	-8.13	2,460	NEA	CL82, Sarnthein et al. (1994)
GIK15669	34.89	-7.82	2,022	NEA	Sarnthein et al. (1994)
GIK11944-2	35.65	-8.06	1,765	NEA	Sarnthein et al. (1994)
KF13	37.58	-31.84	2,690	NEA	Curry et al. (1988)
MD99-2334	37.8	-10.17	3,146	NEA	Skinner et al. (2003), SS0405
MD95-2040	40.58	-9.86	2,465	NEA	dA03, Schönfeld et al. (2003)
CHN82-24	41.72	-32.85	3,427	NEA	Boyle and Keigwin (1985)
GIK15612-2	44.36	-26.54	3,050	NEA	Sarnthein et al. (1994)
NO79-28	45.63	-22.75	3,625	NEA	Duplessy (1996)
GIK17055-1	48.22	-27.06	2,558	NEA	Sarnthein et al. (1994)
U1308	49.88	-24.24	3,883	NEA	Hodell et al. (2008)
GIK23417-1	50.67	-19.43	3,850	NEA	Sarnthein et al. (1994)
GIK23416-4	51.57	-20.0	3,616	NEA	Sarnthein et al. (1994)
GIK23418-8	52.55	-20.33	2,841	NEA	Sarnthein et al. (1994)
GIK23415-9	53.18	-19.15	2,472	NEA	CL82, Sarnthein et al. (1994)
GIK23414-9	53.54	-20.29	2,196	NEA	Sarnthein et al. (1994)
GIK23419	54.96	-19.76	1,487	NEA	Sarnthein et al. (1994)
GIK17049-6	55.26	-26.73	3,331	NEA	Sarnthein et al. (1994)
DSDP552	56.04	-23.22	2,311	NEA	SH84
GIK17051	56.16	-31.99	2,295	NEA	Sarnthein et al. (1994)
GIK23519	64.8	-29.6	1,893	NEA	Millo et al. (2006)
ODP984	61	-24	1,650	NEA	Raymo et al. (2004)
V29-202	61	-21	2,658	NEA	Oppo and Lehman (1995)
MD95-2042	37.8	-10.17	3,146	NEA	Martrat et al. (2007a)
SU90-39	52.5	-22	3,955	NEA	Cortijo (2003)
ODP983	60.4	-23.64	1,984	NEA	McIntyre et al. (1999)
V22-197	14.17	-18.58	3,167	NEA	Sarnthein et al. (1994)
ODP659	18.08	-21.03	3,082	NEA	Sarnthein et al. (1994)
V30-49	18.43	-21.08	3,093	NEA	Mix and Fairbanks (1985)
MD03-2698	38.24	-10.39	4,602	NEA	Lebreiro et al. (2009)
SU90-03	40.05	-32	2,475	NEA	Chapman and Shackleton (1999)
V23-81	54.25	-16.83	2,393	NEA	Sarnthein et al. (1994)
NA87-22	55.48	-14.68	2,161	NEA	Sarnthein et al. (1994)
ODP980	55.49	-14.7	2,168	NEA	Oppo et al. (1998); McManus et al. (1999)
ODP982	57.51	-15.85	1,134	NEA	Jansen et al. (1996), V99, VH02
V28-14	64.78	-29.57	1,855	NEA	Duplessy et al. (1984)
KNR110-50	4.87	-43.21	3,995	NWA	Curry et al. (1988)
KNR110-55	4.95	-42.89	4,556	NWA	Curry et al. (1988)
EW9209-1JPC	5.91	-44.2	4,056	NWA	Curry and Oppo (1997)
GEOB4403-2	6.13	-43.44	4,503	NWA	Bickert and Mackensen (2003)
KNR31-GPC5	33.69	-57.63	4,583	NWA	KJ8994, Keigwin et al. (1991)
CH69-K9	41.75	-47.35	4,100	NWA	L99, Waelbroeck et al. (2001)
U1304	53.06	-33.53	3065	NWA	Hodell and Channell (2016)
ODP925	4.2	-43.49	3,040	NWA	Bickert et al. (1997)
V25-59	1.37	-33.48	3,824	NWA	Mix and Fairbanks (1985)
ODP926	3.72	-42.91	3,598	NWA	Curry et al. (1995)
KNR110-75	4.34	-43.41	3,063	NWA	Curry et al. (1988)
KNR110-82	4.34	-43.49	2,816	NWA	Curry et al. (1988)
KNR110-71	4.36	-43.7	3,164	NWA	Curry et al. (1988)
KNR110-66	4.56	-43.38	3,547	NWA	CL82, Curry et al. (1988)
KNR110-91	4.76	-43.31	3,810	NWA	Curry et al. (1988)
KNR110-58	4.79	-43.04	4,341	NWA	Curry et al. (1988)
ODP927	5.46	-44.48	3,326	NWA	Bickert et al. (1997)
ODP928	5.46	-43.75	4,012	NWA	Bickert et al. (1997)
ODP929	5.98	-43.74	4,369	NWA	Bickert et al. (1997)
V28-127	11.65	-80.13	3,237	NWA	Oppo and Fairbanks (1987)
M35003-4	12.09	-61.24	1,299	NWA	Hüls (1999); Zahn and Stüber (2002)
KNR140-37JPC	31.41	-75.26	3,000	NWA	Curry and Oppo (2005), KS02
V26-176	36.05	-72.38	3,942	NWA	Curry et al. (1988)
GEOB1214	-24.69	7.24	3,210	SEA	BW96
GEOB1211	-24.48	7.53	4,084	SEA	BW96
GEOB1710	-23.43	11.7	2,987	SEA	Schmiedl and Mackensen (1997)
GEOB1032	-22.92	6.04	2,505	SEA	BW96, Bickert et al. (2003)
GEOB1034	-21.74	5.42	3,772	SEA	BW96
GEOB1035	-21.59	5.03	4,453	SEA	BW96
GEOB1028-5	-20.1	9.19	2,209	SEA	Bickert and Mackensen (2003)
GEOB1112	-5.78	-10.75	3,125	SEA	BW96, MB99
BT4	-4.0	10.0	1,000	SEA	Sarnthein et al. (1994)
GEOB1115	-3.56	-12.56	2,945	SEA	BW96, MB99
GEOB1041	-3.48	-7.6	4,033	SEA	BW96, MB99
GIK16867	-2.2	5.1	3,891	SEA	Sarnthein et al. (1994)
GEOB1105	-1.67	-12.43	3,225	SEA	BW96, MB99
V29-135	-19.7	8.88	2,675	SEA	Sarnthein et al. (1994)
RC13-229	-25.5	11.3	4,194	SEA	Sarnthein et al. (1994)
RC13-228	-22.33	11.2	3,204	SEA	Bickert and Mackensen (2003)
ODP1087	-31.46	15.31	1,372	SEA	Lynch-Stieglitz et al. (2006)
MD96-2080	-36.27	19.48	2,488	SEA	Rau et al. (2002)
GEOB2109-1	-27.91	-45.88	2,504	SWA	Vidal et al. (1999)
KNR159-36	-27.51	-46.47	1,268	SWA	Came et al. (2003), OH00
GEOB1117	-3.82	-14.9	3,984	SWA	BW96, MB99
GEOB1118	-3.56	-16.43	4,675	SWA	BW96, MB99
RC16-84	-26.7	-43.33	2,438	SWA	OH00
RC16-119	-27.7	-46.52	1,567	SWA	OH00
V24-253	-26.95	-44.67	2,069	SWA	OH00

(2010) were derived using the same method as their LIG age models, leading to larger age uncertainties of about ~~±1 – ±2.5~~ 1–2.5 ka for this set of Holocene records (~~14~~ 4 cores).

The tie points were used to derive a full age-depth model assuming a constant sedimentation rate between tie-points (i.e. linear interpolation).

2.3 Spatial coverage

The spatial distribution of the database for the Holocene and the LIG is shown in Fig. 2 ~~.~~and the depth distribution of each ocean basin is shown in Fig. 3. There is more data in the Atlantic Ocean (~~69 LIG, 113~~ 65 LIG, 118 Holocene) than in the Pacific (~~18~~ 15 LIG, 19 Holocene) and Indian (~~4~~ 3 LIG, 7 Holocene) Oceans. We used this database to determine 1) if there is a significant difference in the average ocean δ^{13}C signal at the LIG compared to the Holocene, and 2) if ocean circulation patterns were comparable. Due to the sparsity of data in the Indian and Pacific Oceans, our investigation is primarily focused on the Atlantic. Additionally, the temporal uncertainties (∼2 ka) do not permit an investigation of centennial-scale events, and therefore we restrict our analysis to mean LIG and Holocene conditions.

3 Results

The δ^{13}C signal varies significantly regionally and with depth. The highest average δ^{13}C values are associated with NADW and are generally found at intermediate depths (∼1,500–3,000 m) in the North Atlantic, with organic matter remineralisation and mixing with southern source waters leading to a δ^{13}C decrease along the NADW path. The lowest δ^{13}C values are in the deep south Atlantic (>4,000 m) because the AABW end member is much lower than its NADW counterpart. Since the Indian and Pacific Oceans are mostly ventilated from southern-sourced water masses, δ^{13}C generally decreases northward in these two basins.

Since the number of cores is not consistent across the two time periods, and given the high regional variability observed in δ^{13}C, it is not possible to simply average all available data to determine the global mean δ^{13}C. Furthermore, the spatial heterogeneity of the data density adds to the complexity of the problem. To address these points, we first analyse differences between the LIG and Holocene records for pre-defined small regions with high data density. We then calculate regional volume-weighted δ^{13}C means for larger regions from which we estimate the global LIG-Holocene anomaly.

3.1 Regional reconstruction of δ^{13}C

We define regions with high densities of cores to reconstruct regional mean δ^{13}C (Fig. 2). These regions need to be small enough to assume reasonably small spatial variability in the δ^{13}C signal and yet still have enough data to establish a reliable statistical difference between the two time periods.

Based on these requirements, four regions are selected: the northeast Atlantic, the equatorial Atlantic, a region off the Namibian Coast (southeast Atlantic), and a region around the Galapagos Islands (eastern equatorial Pacific). The boundaries of each region are defined in Table 3~~, with values of records deeper than 2~~.

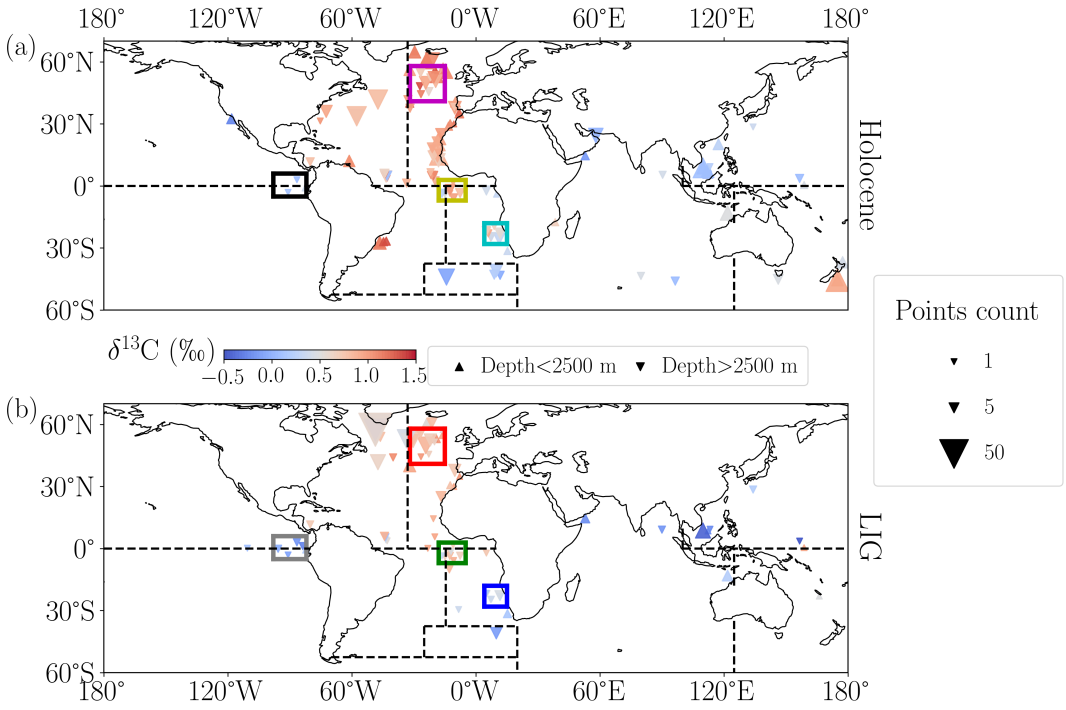

Figure 2. Global distribution of benthic foraminifera δ^{13}C covering the periods studied here: the Holocene (~~8–2~~ 7–2 ka BP) (a) and LIG (~~130–118~~ 125–120 ka BP) (b). Symbol size indicates the number of values per core, colour indicates average δ^{13}C, and the triangle direction indicates the proxy depth (upward-pointing triangle: between 1,000 and 2,500 m depth, downward-pointing triangle: deeper than 2,500 m). Four specific regions used in Sect. 3.1 are outlined: eastern equatorial Pacific (black, grey), equatorial Atlantic (yellow, green), southeast Atlantic (cyan, blue), and northeast Atlantic (magenta, red). ~~Panel c: box plots for each region showing data below 2,500 m (box colours correspond~~ Regional boundaries used to calculate the ~~region outline colours)~~global volume-weighted mean δ^{13}C (Sect. ~~Orange vertical~~ 3.2) are indicated by dotted black lines ~~show the median~~as defined in Peterson et al. (2014).~~The whiskers indicate the lower and upper fences of the data, and the clear circles are outliers.~~

We then define the time periods within the LIG and the Holocene to perform our analyses. For the Holocene, ~~500 m represented in the box plots of Fig. 2c. The statistical characteristics shown in all of the box plots are consistently lower at the LIG compared to the Holocene ranging from 0.1 to 0.3 lower, which suggests that independent of regional differences, the LIG exhibits lower δ^{13}C values than the Holocene(Fig. 2). However, these box plots include all the data from 130–118 ka BPand 8–2 ka BP, and might therefore capture more than the mean LIG and Holocene states, i.e. they might include parts of the deglaciations or the beginning of the glacial inception for the LIG~~as most of the available data is dated prior to 2 ka BP, we define the end of our Holocene time period as 2 ka BP. To capture as much of the Holocene data as possible, we include data back to 7 ka BP, ensuring that we do not include instability associated with the 8.2 kiloyear event (Alley and Ágústsdóttir, 2005; Thomas et al., 2007). This provides a time span of 5 ka of data that we will consider for our analysis of the Holocene.

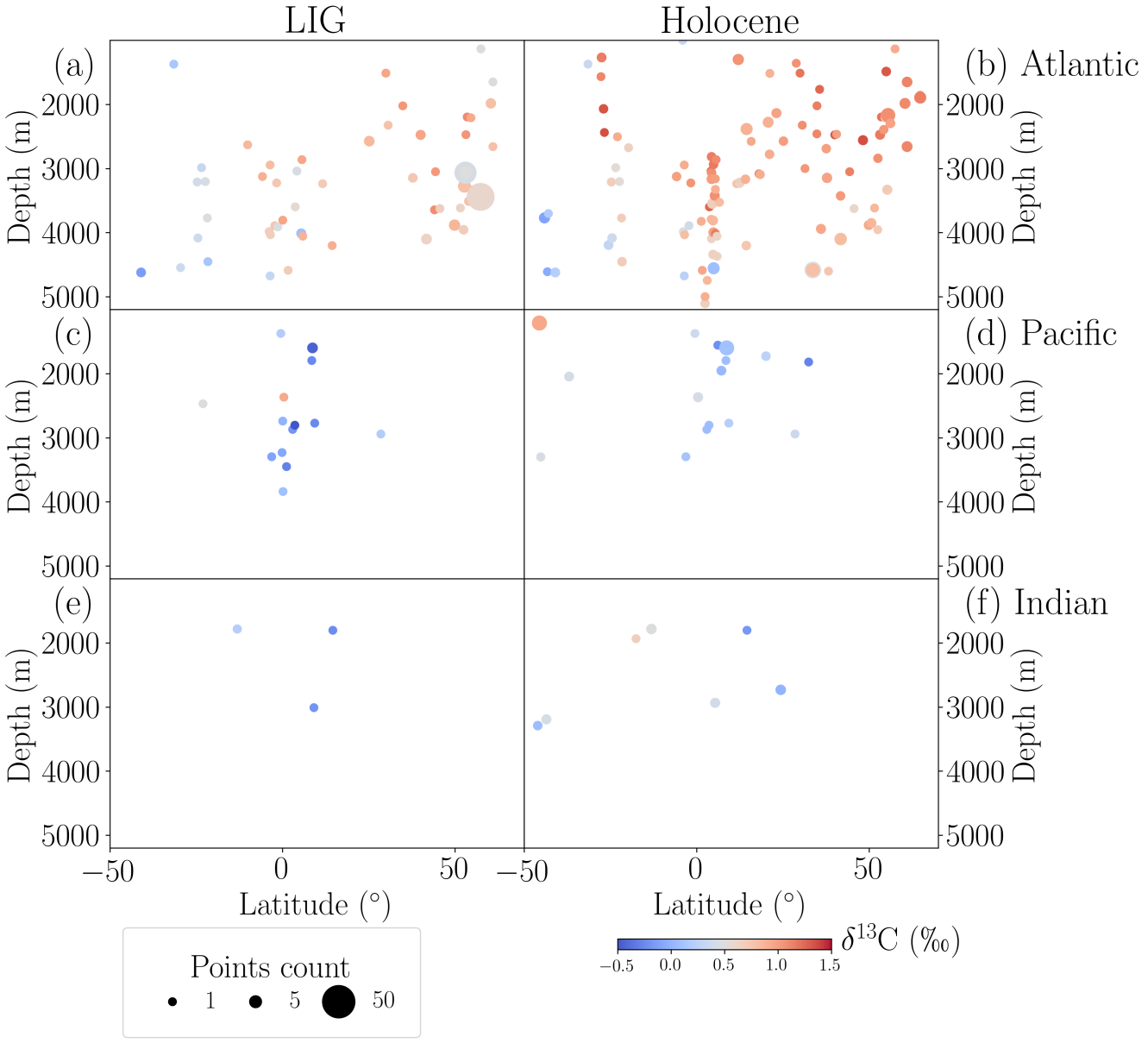

Figure 3. Zonal distribution of benthic foraminifera δ^{13}C (‰) during the LIG (125–120 ka BP; a, c, e) and the Holocene (7–2 ka BP; b, d, f) in the Atlantic Ocean (a, b), Pacific Ocean (c, d) and Indian Ocean (e, f). Symbol size indicates the number of measurements per core and colour indicates average δ^{13}C.

Table 3. Regional summary of δ^{13}C below 2,500 m depth for the LIG (125–120 ka BP) and ~~mid-Holocene~~ Holocene (~~7–4~~ 7–2 ka BP) using a single value per core for each time slice. Shown are the means (δ^{13}C, ‰), standard deviations (σ, ‰), and counts (N) for both time periods, along with the time period regional anomalies ($\Delta\delta^{13}$C, ‰), propagated standard deviations for the anomaly (σ, ‰), and p-values from two-sample t-tests between the two time periods.

			Holocene			LIG			LIG-Holocene		
Region	Latitude	Longitude	$\delta^{13}C$ (‰)	σ (‰)	N	$\delta^{13}C$ (‰)	σ (‰)	N	$\Delta\delta^{13}C$ (‰)	σ (‰)	P value
Northeast Atlantic	41N-58N	32E-15E	0.89	0.21	34	0.76	0.11	23	-0.13	0.12	0.0096
Equatorial Atlantic	7S-3N	18E-5E	0.79	0.32	22	0.62	0.23	14	-0.17	0.20	0.1110
Southeast Atlantic	28S-18S	4W-15W	0.55	0.22	27	0.40	0.11	12	-0.15	0.12	0.0361
Equatorial Pacific	5S-6N	98E-82E	0.09	0.05	4	-0.11	0.10	8	-0.20	0.06	0.0056

~~Most δ^{13}C time series display a significant increase in~~ For the LIG, we seek to avoid data associated with the end of the penultimate deglaciation, which is characterised by a benthic δ^{13}C ~~between 130 and 127~~ increase in the Atlantic until ~128 ka BP (Govin et al. (2015); Menviel et al. (2019); Oliver et al. (2010), Fig. 4). ~~Given the uncertainties in the age models, this increase could be~~ In addition, a millennial-scale event has been identified in the North Atlantic between ~127 and 126 ka BP (Galaasen et al., 2014b; Tzedakis et al., 2018). Considering the typical dating uncertainties associated with the ~~penultimate deglaciation (Oliver et al., 2010; Menviel et al., 2019). To avoid the relatively low δ^{13}C values which could be~~ LIG data (2 ka), we thus decide to start our LIG time period at 125 ka BP. To ensure that the two time periods are of same length (5 ka BP), we define the LIG period for our analysis to be 125–120 ka BP. We note that our definition should also avoid data associated with the ~~penultimate deglaciation and glacial inception , we focus our analysis on the period~~ glacial inception (Govin et al., 2015; Past Interglacial Working Group of PAGES, 2016). We verify that the LIG time period has sufficient data across the selected four regions, noting that the highest density of data falls within the 125–120 ka BP time period—particularly in the equatorial Atlantic and southeast Atlantic (Fig. 4~~a). b~~, c).

We round the data to the nearest 1 ka, find an average per 1 ka, and refer to this as a time slice. We consider the LIG-Holocene anomaly across these two time periods for the four regions selected, and consider qualitatively the influence of changes in the average depth in which the proxies were recorded, as indicated by the direction of the black triangles in Fig. 4. ~~To make a meaningful comparison with the Holocene, we also restrict the Holocene data to a relatively stable δ^{13}C period, spanning from 7 to 4 ka BP for the Holocene–the mid-Holocene. The number of data points per 1 ka time slice deteriorates on either side of these two periods.~~

The average δ^{13}C anomaly between the LIG and ~~mid-Holocene stable periods as defined above~~ Holocene periods for cores deeper than 2,500 m is consistent across the different regions despite their geographic separation, suggesting a significantly lower δ^{13}C during the LIG than the ~~mid-Holocene~~Holocene, with differences ranging from ~~0.13~~ -0.13 ‰ in the ~~south-east Atlantic to 0.19~~ northeast Atlantic to -0.20 ‰ in the equatorial ~~Atlantic~~ Pacific (Table 3). The statistical significance between the two time periods is established using a two-tailed t-test on data ~~that has one~~ of one mean value per core and spans the entire time slices (125–120 ka BP and ~~7–4~~ 7–2 ka BP). The t-test shows that there is a statistically significant difference everywhere except in the ~~southeast~~ equatorial Atlantic, with confidence intervals varying from ~~0.14 in the Equatorial Atlantic to 0.06 in the Equatorial Pacific~~0.13 in the equatorial Atlantic to 0.04 in the northeast Atlantic. When using a single tail t-test instead, the

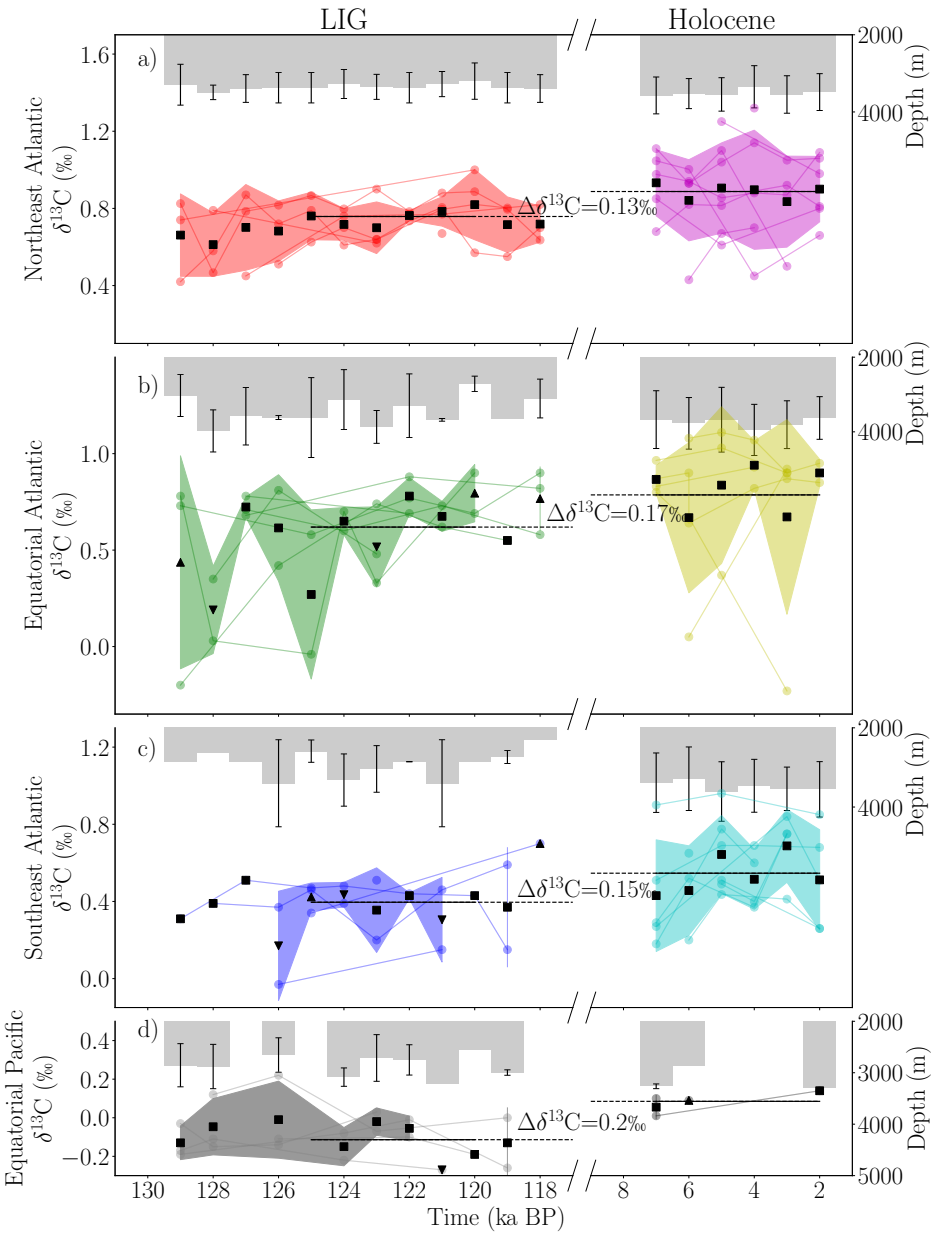

Figure 4. Benthic foraminifera δ^{13}C (left y-axis, ‰) during the LIG (left) and Holocene (right) for four defined regions; northeast Atlantic (a), equatorial Atlantic (b), southeast Atlantic (c), and eastern equatorial Pacific (d). Data is presented in discrete time slices spanning 1 ka~~,~~ ~~only~~. Only cores deeper than 2,500 m are shown. Circular, coloured points connected by lines show each average δ^{13}C value per core per time slice. Black symbols represent δ^{13}C averages per slice. Each slice has a corresponding averaged depth (right y-axis, m), with 1 standard deviation on either side shown in the bars. Slices with an average depth within ±300 m of the mean core depth of all slices are represented with a square point. Slices with an average depth shallower than ~~the~~ 300 m less than the mean are shown with an upward triangle, and deeper than 300 m more than the mean are shown with a downward triangle. Shading shows 1 standard deviation on either side of the mean for slices where more than 1 point exists.

difference becomes significant in the ~~southeast~~ equatorial Atlantic, giving a new p-value of ~~0.002. Figure~~ 0.02. Fig. 4 suggests that ~~depth variations between time slices likely explain the variability in this region, making it difficult to establish a difference between the two time periods. However,~~ the ~~mean depth in each region~~ difficulty in determining significance in this region for cores deeper than 2,500 m might be due to a singular outlier measurement in the equatorial Atlantic; a value of -0.23 ‰ from GeoB1118 at ∼3.5 ka BP. If this value is excluded, then an anomaly of -0.22 with a p-value less than 0.005 is observed.

We also compare the distribution of δ^{13}C for cores deeper than 2,500 m for three overlapping periods within the LIG (early LIG: 128–123 ka BP; LIG: 125–120 ka BP; late LIG: 123–118 ka BP). The results for the four regions are shown in Fig. 5. The statistical characteristics do not show much variation between the LIG and ~~the mid-Holocene are similar (with a maximum difference of 135 m).~~

~~Within this stable period during the LIG, a small~~ late LIG δ^{13}C ~~increase can be observed in the northeast Atlantic between 125 and 120 ka BP (Fig. 4a). Over that period, a linear regression fitted to the mean of the points suggests an increase in~~ C distributions. In the equatorial Pacific, the difference between the early LIG and the Holocene is smaller than between LIG and Holocene, but this is countered with a larger difference in the equatorial Atlantic between early LIG and Holocene. The spread in the data is generally larger during the Holocene than during the other time periods which might be due to the greater number of measurements during the Holocene. The spread of data during the early LIG is slightly larger than during the LIG and late LIG in the equatorial and southeast Atlantic. The equatorial Atlantic is the only region which displays significantly more points with lower δ^{13}C ~~of 0.02 ka^{-1}, with a p-value of 0.001 and an R^2 of 0.93, suggesting that while the trend is small, it is statistically significant~~during the early LIG. Overall, these distributions do not suggest that the LIG-Holocene anomalies that we have determined would be significantly impacted by slight variations in the selected time window. We perform an analysis of variance (ANOVA) on each region and post hoc tests on the data. We find that the Holocene data is significantly different from the three LIG periods in the northeast Atlantic, the southeast Atlantic and the equatorial Pacific, while the three periods within the LIG are not significantly different from each other for any of the regions.

3.2 Volume-weighted regional δ^{13}C

The second approach we use to further constrain the LIG-Holocene δ^{13}C anomaly is to estimate the volume-weighted regional δ^{13}C. We define our regional boundaries based on the regions described in Peterson et al. (2014), however we only include the regions where there is enough data to justify an analysis. For all the data in each of these regions, we calculate a mean value by taking the direct averages of all data~~below 1,000 m depth~~. We divide the ocean basins into eight regions (Table 4, shown in Fig. ~~?? (Peterson et al., 2014)~~2) and calculate the volume-weighted averages δ^{13}C for each of these regions. Since the Atlantic and Pacific Oceans have more data than the Indian Ocean, there is greater confidence in the δ^{13}C estimates for these regions. These regional averages are then used to calculate a global volume-weighted δ^{13}C.

Results for the Atlantic and Pacific Oceans are given in Fig. 6, and show a mean LIG-Holocene anomaly of ~~-0.22~~ -0.21 ‰ and ~~-0.24~~ -0.27 ‰ respectively, slightly higher than the range of estimates for the four regions selected in Sect. 3.1. ~~The slightly~~ There is a higher offset estimated in ~~the Atlantic compared to our previous regional analysis (~~this definition of the southwest Atlantic (-0.45 ‰) than in Sect. 3.1~~) could be due to the δ^{13}C records in cores located in the southwest Atlantic, which were~~

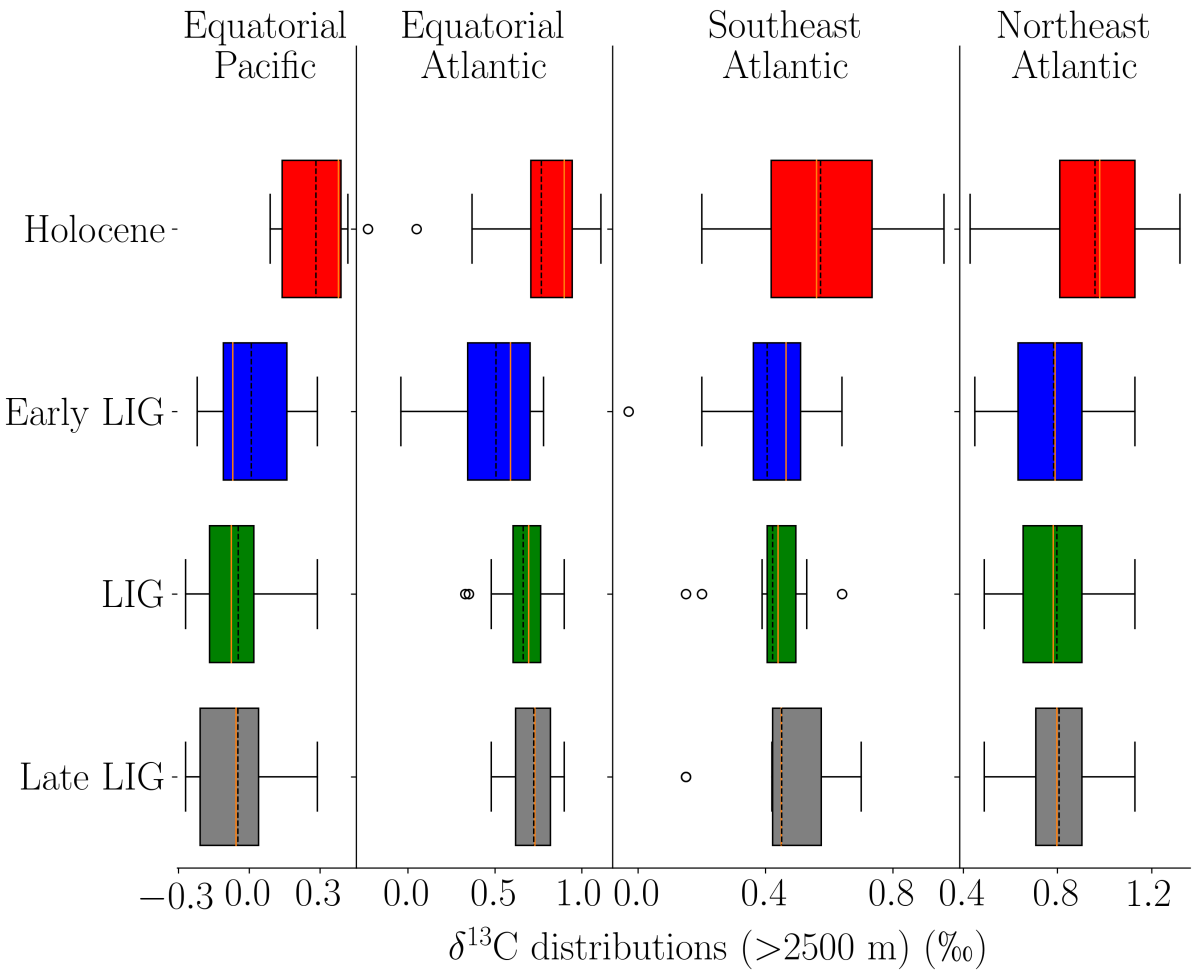

Figure 5. Distributions of $\delta^{13}C$ for all core measurements deeper than 2,500 m during the Holocene (7–2 ka BP, red), the early LIG (128–123 ka BP), the LIG (125–120 ka BP), and the late LIG (123–118 ka BP) across four regions (equatorial Pacific, equatorial Atlantic, southeast Atlantic, northeast Atlantic). Lower end of the box indicates quartile 1 (Q1) and the upper end indicates quartile 3 (Q3). Orange vertical lines show the median and dotted vertical lines show the mean. The whiskers indicate the lower and upper fences of the data calculated as Q1-1.5*(Q3-Q1) and Q3+1.5*(Q3-Q1), respectively, and the clear circles are outliers.

Table 4. Regional breakdown of δ^{13}C data for all depths during the ~~mid-Holocene~~ Holocene (~~7–4~~ 7–2 ka BP) and LIG (125–120 ka BP) averaged across the 1 ka time slices. For each region: the average number of data points (labelled as 'Points') and cores per time slice (labelled as 'Cores'), the average standard deviation of δ^{13}C per time slices (‰), the mean depth (m) across time slices, and the standard deviation of depth (m) between time slices (σ_{depth}). NEA: northeast Atlantic, NWA: northwest Atlantic, SA: south Atlantic, SEA: southeast Atlantic, SWA: southwest Atlantic, I: Indian, NP: north Pacific, SP: south Pacific.

	Holocene						LIG					
Area	δ^{13}C (‰)	Points	Cores	$\sigma_{\delta^{13}C}$ (‰)	Mean depth (m)	σ_{depth} (m)	δ^{13}C (‰)	Points	Cores	$\sigma_{\delta^{13}C}$ (‰)	Mean depth (m)	σ_{depth} (m)
NEA	0.94	73	47	0.19	2853	944	0.76	32	22	0.21	2746	789
NWA	0.81	28	13	0.27	3698	867	0.64	41	9	0.27	3679	455
SA	0.08	6	4	0.18	4103	429	-0.14	3	2	0.11	4533	120
SEA	0.63	13	12	0.26	3306	787	0.55	14	14	0.23	3163	799
SWA	0.96	6	4	0.32	2302	929	0.51	2	2	0.12	4156	172
I	0.23	6	4	0.26	2287	529	0.06	4	4	0.19	2347	581
NP	0.03	14	7	0.20	2015	448	-0.10	9	8	0.24	2815	673
SP	0.45	12	5	0.30	2285	924	0.06	3	3	0.15	2724	709

~~not included in our regional analysis. There~~ , however there are only 4 cores available in this region during the Holocene ~~, and 1~~ and 2 during the LIG.

The estimated LIG-Holocene anomaly in the south Pacific is relatively high at ~~-0.4~~ -0.39 ‰~~. However, the relatively large LIG to Holocene~~ , giving a relatively large Pacific anomaly estimate of ~~-0.4~~ -0.27 ‰~~.~~ This could be due in part to the deeper location of the LIG ~~core~~ cores compared to the mean of the Holocene cores (~~881 m~~ 439 m difference, Table 4). There is less confidence in the estimate of the Pacific volume-weighted mean since the proxy data is sparse, and the majority of cores are from the eastern equatorial Pacific ~~(4 LIG, 11 Holocene)~~ as shown in Fig. 2.

~~Similar to the trend highlighted in the northeast Atlantic (Fig. 4a)~~We also note that the average depths of cores from the Pacific Ocean (LIG: 2,~~there is~~ 711 m, Holocene: 2,131 m) and Indian Ocean (LIG: 2,383 m, Holocene: 2,303 m) are shallower than that of the Atlantic Ocean (LIG: 3,531 m, Holocene: 3,157 m; Fig. 3). However, as the vertical gradient below 2,000 m depth in the Pacific Ocean is small (e.g. Eide et al., 2017), this might not significantly impact our results.

There is a small positive trend in the average Atlantic δ^{13}C from 125 ka BP, reaching a maximum value at ~~121~~ 118 ka BP (Fig. ~~4~~6). The average core depth over ~~this~~ the 125–120 ka BP time period does not suggest that a change in the mean depth could explain this variation. Fitting a linear regression over this period indicates an increase in δ^{13}C of 0.03 ‰ ka^{-1} in the Atlantic, with a p-value of ~~0.03~~ 0.01 and an R^2 of ~~0.72, similar to the trend seen in the northeast Atlantic~~ 0.85 (Fig. 4a). ~~This ~0.15 Atlantic Ocean δ^{13}C increase is also concurrent with the ~0.3 atmospheric $\delta^{13}CO_2$ increase.~~ For the Pacific, there is a ~~0.18~~ 0.13 ‰ increase in δ^{13}C between 7 and 5 ka BP, which could be associated with the early Holocene terrestrial regrowth (Menviel and Joos, 2012).

For the Indian Ocean, we only include ~~two~~ four cores, as these are the only ones spanning both the LIG and ~~mid-Holocene~~Holocene. An LIG anomaly of -0.13 ‰ in the Indian Ocean compared to the ~~mid-Holocene~~ Holocene is therefore associated with higher uncertainties. The whole ocean mean LIG δ^{13}C anomaly is ~~-0.21~~ -0.25 ‰, but it is associated with higher uncertainties than each region anomaly.

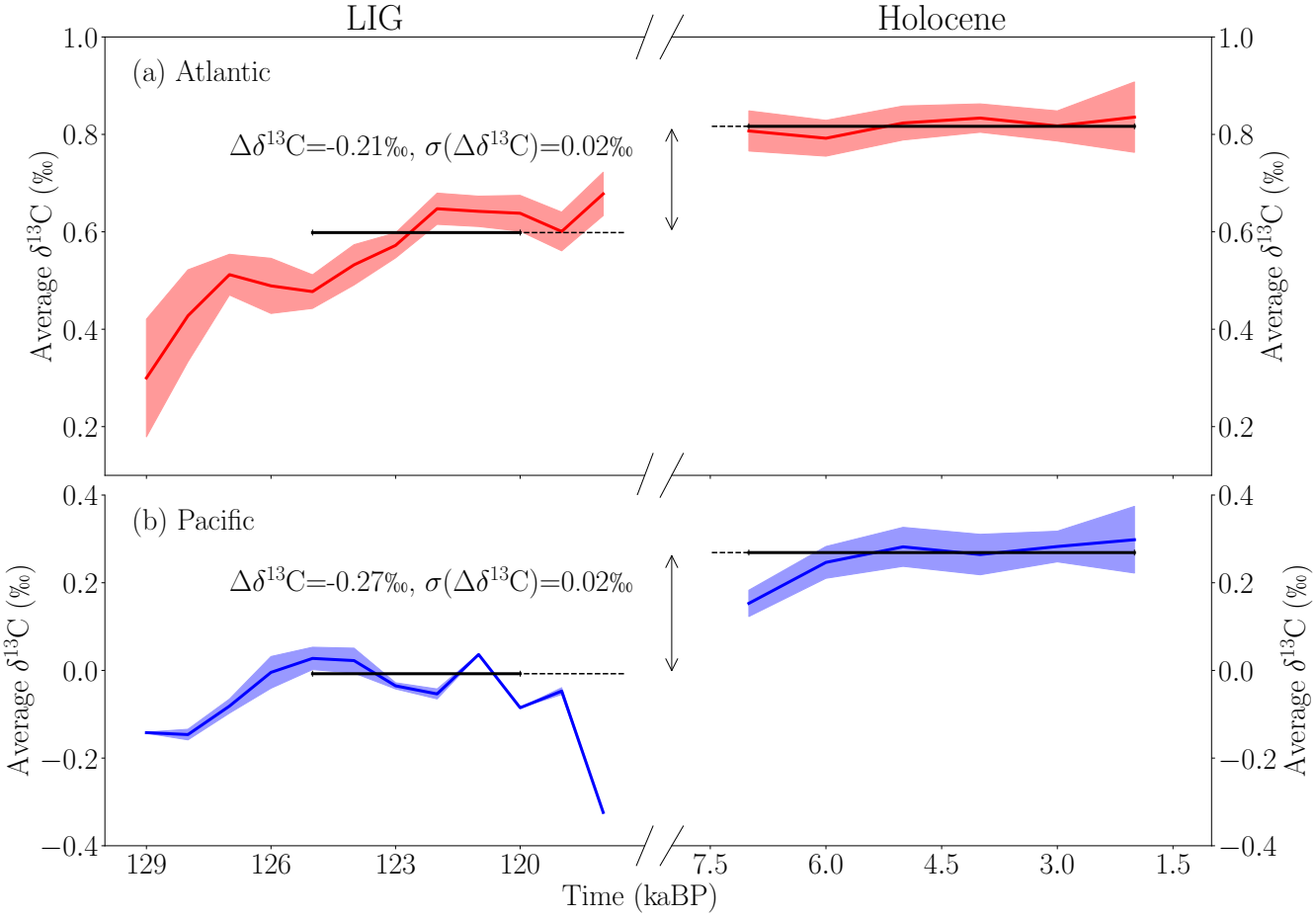

Figure 6. Comparison of volume-weighted δ^{13}C for the Atlantic (red) and Pacific (blue) for the LIG and ~~mid-Holocene~~Holocene, calculated using the regions from Peterson et al. (2014) from data covering all depths. Solid coloured lines indicate the mean volume-weighted δ^{13}C, and the shading indicates the volume-weighted sum of square deviations from the mean. The horizontal bars indicate the mean of the stable period determined from the regional analysis as defined in Sect. 3.1 (LIG: 125–120 ka BP, ~~mid-Holocene~~Holocene: ~~7–4~~ 7–2 ka BP), with the ~~$\Delta\delta^{13}$~~ $\Delta\delta^{13}$C indicating the mean anomaly between these two average and the standard deviation ($\sigma(\delta^{13}$C), ‰).

Both the regional analysis of our new database and our volume-weighted estimate indicate that the global mean δ^{13}C was about 0.2 ‰ lower during the LIG than during the ~~mid-Holocene. There are three possible explanations for this difference. Firstly, an AMOC change might influence the global estimate due to overrepresentation of the Atlantic Ocean in the data. Since in total only 22 points originate from the Pacific and Indian basins compared to 69 in the Atlantic during the LIG, and a change in AMOC would significantly impact Atlantic benthic δ^{13}C (Menviel et al., 2015), an assessment of possible mean LIG AMOC change would provide additional confidence in a global mean ocean δ^{13}C change. Secondly, the global estimate might be influenced by lower LIG than mid-Holocene stores of organic carbon in either the land biosphere or dissolved organic matter. Thirdly, changes in sedimentary and lithospheric carbon both in terms of quantity and mean δ^{13}C value can impact the global mean δ^{13}C (Jeltsch-Thömmes and Joos, 2020a; Schneider et al., 2013). These three possibilities are explored below.~~ Holocene. We further test the robustness of this result in the next section.

3.3 Reconstruction of the LIG Atlantic Meridional Overturning Circulation

In this section, we analyse the spatial δ^{13}C distribution in the Atlantic Ocean to assess potential changes in the penetration depth and southward expansion of NADW during the LIG, defined here as 125–120 ka BP, with respect to the ~~mid-Holocene~~Holocene. A change in NADW might influence our estimate of the mean δ^{13}C, given that most of the available data is localised in the Atlantic Ocean.

We use simple statistical regression models to reconstruct NADW and AABW separately with a quadratic-with-depth and linear-with-latitude equation following the method of Bengtson et al. (2019). For consistency, the regression algorithm only includes records from cores that span both the LIG and ~~mid-Holocene~~ Holocene and uses a weighted least squares approach, where the weighting equals the number of samples per core. The modelled region is defined between 40° S and 60° N as this is the region where we can expect to find both the NADW and AABW δ^{13}C signals.

The results are shown in Fig. 7. We test the robustness of our statistical model using the jackknifing technique. We systematically exclude each individual core from the database one at a time, fit the parameters using this modified database, and compare the model prediction against the core which was excluded. This produces small variations in the average mean response of the statistical models (the standard deviations were ~~0.04~~ 0.01 ‰ ~~and 0.03 for~~ for both the LIG and ~~mid-Holocene~~Holocene, respectively).

We calculate end-member values based on proxies located near the water mass sources. These are taken as 0.79 ‰ and 1.02 ‰ for NADW for the LIG and ~~mid-Holocene~~Holocene, respectively, and -0.09 ‰ and ~~0.22~~ 0.23 ‰ for AABW for the LIG and ~~mid-Holocene~~Holocene, respectively. The end-member values are calculated as the average of cores shallower than 3,000 m but deeper than 1,000 m and located between 50° N and 70° N for NADW. The NADW end-member cores have an average depth of ~~2043~~ 2,043 m and a standard deviation of 478 m during the LIG. For the AABW end-member, the only eligible core is ODP1089, which is at ∼41° S and ~~4621~~ 4,621 m.

The mean volume-weighted δ^{13}C for the Atlantic Ocean between 40° S and 60° N based on this interpolation is 0.53 ‰ for the LIG and ~~0.69~~ 0.70 ‰ for the ~~mid-Holocene~~ Holocene (Fig. 7). This suggests a ~~0.16~~ 0.17 ‰ lower Atlantic δ^{13}C at the LIG

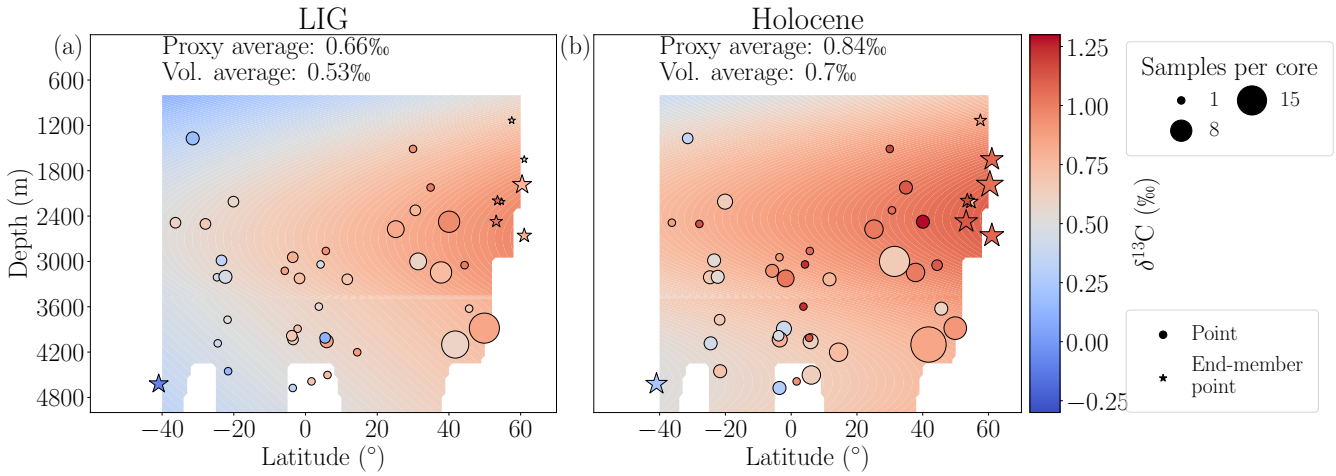

Figure 7. Reconstructed Atlantic δ^{13}C (‰) meridional section during the LIG (125–120 ka BP) and ~~mid-Holocene~~Holocene (7–2 ka BP). The circular points represent the proxy data, showing the average δ^{13}C with colour and the number of points per core with size. The stars represent the proxy data which make up the end-members. Background shading shows the reconstructed δ^{13}C using a quadratic statistical regression of the proxy data following the method described in Bengtson et al. (2019).

than the ~~mid-Holocene~~Holocene. Our statistical reconstruction points to a very similar NADW depth (~2,600 m) for both time periods (Fig. 7). The NADW depth is defined here as the depth of maximum δ^{13}C in the North Atlantic.

We also investigate the meridional gradient in δ^{13}C in the Atlantic Ocean to determine whether the NADW southward penetration, transport and remineralisation rates were significantly different during the LIG compared to the ~~mid-Holocene~~Holocene. We only consider cores that are located between depths of 1,000 and 3,000 m in order to stay within the main pathway of NADW (Fig. 8a). Though there is significant scatter, in accordance with our previous findings, a moving average through the Holocene and the LIG data shows that LIG δ^{13}C is typically lower than the ~~mid-Holocene~~ Holocene counterparts. However, the ~~slopes of the~~ meridional δ^{13}C statistical model gradients are not very different for the LIG (~~0.0050~~ 0.0035 ‰ °latitude^{-1}) and the ~~mid-Holocene (0.0045~~ Holocene (0.0046 ‰ °latitude^{-1}) (Fig. 8a), suggesting a similar southward penetration of NADW.

Using δ^{13}C of the end-members for NADW and AABW, we use a simple binary mixing model for all cores deeper than 1,000 m to estimate changes in NADW penetration (Fig. 8b). The LIG and ~~mid-Holocene~~ Holocene δ^{13}C slopes in the Atlantic are similar, indicating similar southward penetration of NADW during both time periods. This suggests that the differences in δ^{13}C between the two time periods is most likely due to change in end-member values, while the mean Atlantic oceanic circulation was likely similar.

Based on our analysis, there appears to be no significant difference in the mean time-averaged AMOC between the LIG and the ~~mid-Holocene~~Holocene. Negative LIG-Holocene anomalies are found for each of the smaller regions selected (northeast Atlantic, equatorial Atlantic, southeast Atlantic, and eastern equatorial Pacific), with statistical significance seen in all regions except the ~~southeast~~ equatorial Atlantic, where ~~depth variations between time slices likely explain the increased variability in~~

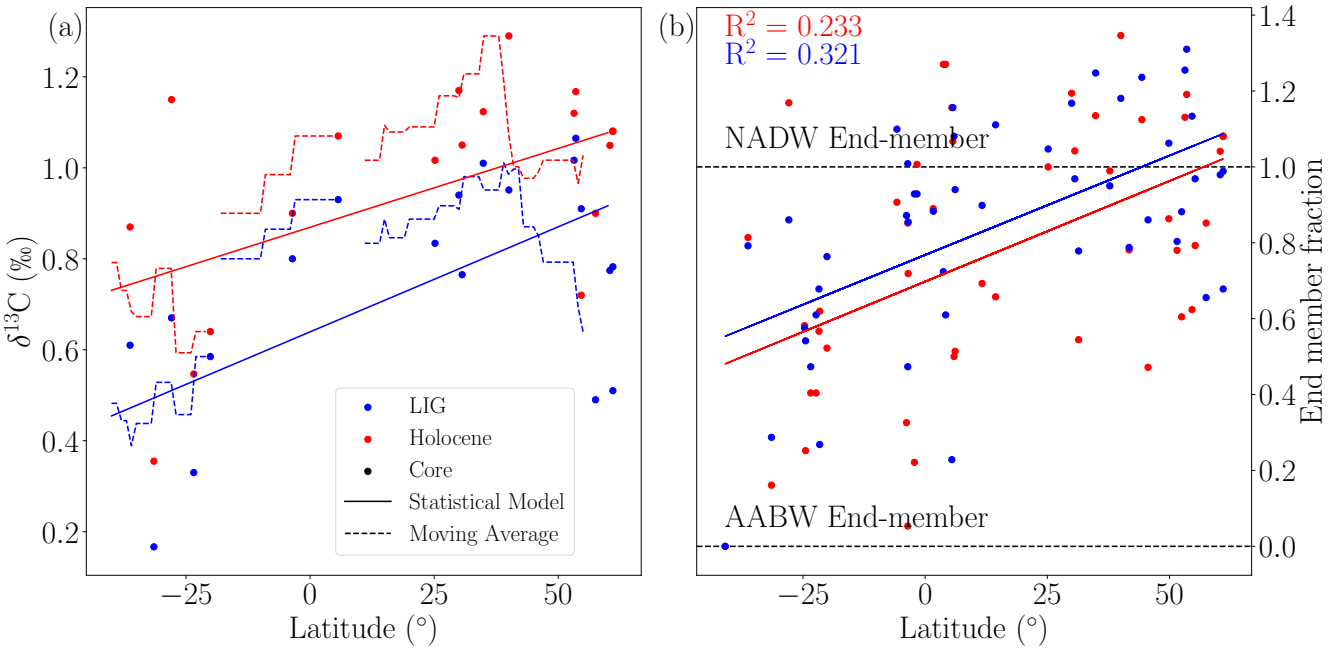

Figure 8. The meridional gradient of the Atlantic Ocean benthic δ^{13}C (‰). a) ~~Mid-Holocene~~ Holocene (red) and LIG (blue) ~~$\delta^{13}C$~~ δ^{13}C for each core (points) between 1,000 m and 3,000 m. Dotted lines are the moving averages of the cores. Solid lines indicate the results of our statistical model at 2,000 m. b) Average δ^{13}C for each record deeper than 1,000 m as a proportion of the end-members. A value of one indicates the NADW end-member and a value of zero the AABW end-member. Solid lines show the linear regressions of the records.

~~this region~~an unusual low δ^{13}C value in one core is responsible for narrowing the difference between the two period means. Additionally, our volume-weighted mean δ^{13}C estimates ~~display~~ have similar anomalies in the Atlantic and Pacific Oceans (~~-0.22~~ -0.21 ‰ and ~~-0.24~~ -0.27 ‰ respectively).

4 Discussion

One of the goals of our study is to assess the mean change in oceanic δ^{13}C between the LIG and the Holocene. Given the uncertainties in the chronologies~~and to avoid taking into account data that would pertain to deglaciations,~~ , avoiding data that pertains to deglaciation, and capturing the same length of time during the LIG and the Holocene, we chose the periods 125 to 120 ka BP for the LIG and 7 to ~~4~~ 2 ka BP for the ~~mid-Holocene~~Holocene. Using a similar geographical distribution of data points for both periods, we find that the oceanic δ^{13}C was ~0.2 ‰ lower during the LIG than the ~~mid-Holocene~~Holocene.

Our analysis of the δ^{13}C signal suggests consistent LIG-Holocene δ^{13}C anomalies in different regions of the Atlantic basins, as well as in the Pacific and Indian Oceans, even if there are significant uncertainties with the later due to fewer available records. The δ^{13}C distribution in the Atlantic Ocean suggests that there was no significant mean change in the southward penetration or depth of NADW during the LIG (125–120 ka BP) compared to the ~~mid-Holocene. However, because of the~~

relatively large time slices that were used in our analysis (1 ka) and with a typical age model uncertainty of ±2 ka, our analysis suggests that there is no difference in the mean oceanic circulation between the periods Holocene (7–2 ka BP). A statistical reconstruction of the early LIG (128–123 ka BP) δ^{13}C compared to our 125–120 ka BP reconstruction does not reveal a significant difference in either the NADW core depth or NADW extent as indicated by the meridional δ^{13}C gradients (Fig. S2). The volume weighted average δ^{13}C during the early LIG is 0.06 ‰ lighter than during the LIG period considered here (125–120 ka BPand 7–4 ka BPwithout being able). Since both time slices (128–123 ka BP and 125–120 ka BP) are 5 ka averages and include dating uncertainties of ∼2 ka, it is not possible to resolve potential centennial-scale oceanic circulation changes (e.g. Tzedakis et al., 2018)(e.g. Galaasen et al., 2014b; Tzedakis et al., 2018).

The overall Explanations for the 0.2 ‰ lower oceanic δ^{13}C could potentially be due to a anomaly in the ocean may include a redistribution between the ocean-atmosphere system. Such a redistribution can result from a change in end-member values (Fig. 8). As fractionation during air-sea gas exchange is temperature dependent, globally higher SSTs at the LIG could lead to a lower oceanic δ^{13}C. However, this the effect of this is likely small (Brovkin et al., 2002) and this would also lead to a higher atmospheric $\delta^{13}CO_2$ at the LIG, which is inconsistent with Antarctic ice core measurements (Schneider et al., 2013). Nutrient utilisation decrease that suggest an anomaly of -0.3 ‰ (Schneider et al., 2013). Lower nutrient utilisation in the North Atlantic could also would decrease surface ocean δ^{13}C and thus the δ^{13}C end-members. However, because the vast amount of organic carbon is remineralised and therefore remains as DIC (Sarmiento et al., 2002), nutrient utilisation impact on the end-members should not have influenced the this would also imply that less organic carbon would be remineralised at depth. Therefore, it is unlikely that the lower average oceanic mean δ^{13}C , unlike the process of air-sea gas exchangeresults from a change in end-members through lower surface ocean nutrient utilisation. Currently, there is still a lack of constraints on nutrient utilisation in these end-member regions during the LIG compared to the Holocene.

Since both the atmospheric and oceanic Therefore, the lower δ^{13}C were lower at the LIG than during the Holocene, this could indicate a significant release of low in the ocean-atmosphere system cannot be explained by a simple redistribution of δ^{13}C terrestrial carbon into the system. While changes between the atmosphere and the ocean.

An alternative explanation for the anomaly is a change in the terrestrial biosphere are not well constrained during the LIG, the proxies do indicate that there was possibly a greener Sahara (Larrasoaña et al., 2013) and a greater forest coverage at high latitudes (CAPE, 2006; Tarasov et al., 2005; Muhs et al., 2001; de Vernal and Hillaire-Marcel, 2008; Govin et al., 2015), which should have increased the carbon stored in the terrestrial vegetation. This does not account for other factors though, such as the intensity of fires, which can have a significant impact on the terrestrial carbon storage (Bowman et al., 2009). A lower terrestrial carbon reservoir could also be explained by a decrease in soil carbon, including changes in carbon stored in carbon storage, which has a typical signature of approximately -37 to -20 ‰ for C3 derived plant material (Kohn, 2010) and -13 ‰ for C4 derived plant material (Basu et al., 2015). The total land carbon content at the LIG is poorly constrained. Proxies generally suggest extensive vegetation during the LIG compared to the Holocene (CAPE, 2006; Govin et al., 2015; Larrasoaña et al., 2013; Muhs et al., 2001; Tarasov et al., 2005; de Vernal and Hillaire-Marcel, 2008) , which would imply a greater land carbon store. However, other terrestrial carbon stores including peatlands and permafrost . While, to our knowledge, no comprehensive proxy-based reconstruction of soil carbon may also have differed during the

LIG ~~exists, one modelling study found that the increase in carbon storage during the LIG was almost offset by an increase in heterotrophic respiration caused by higher temperatures at high latitudes (Schurgers et al., 2006), which gives credence to a lower soil carbon reservoir between the LIG and the mid-Holocene.~~

~~Furthermore, it is estimated that~~ compared to the Holocene. With an estimated ~550 Gt C ~~are stored in high northern latitude peats today (Yu et al., 2010), with a~~ stored in peats today (mean $\delta^{13}C$ ~~value of~~ ~-28 ‰ ~~(Dioumaeva et al., 2002; Novák et al., 1999) . Any variation in peat accumulation rates could therefore significantly impact the total terrestrial carbon storage. Though it is associated with large uncertainties, a modelling study indicated higher accumulation of carbon in peat during the LIG than during the Holocene (Kleinen et al., 2012). Recent estimates suggest that~~ , Dioumaeva et al. (2002); Novák et al. (1999)) and ~1,~~500 Gt C are stored in permafrost, with about 1,~~000 Gt C in the active layer ~~(Schuur et al., 2015). Even though quantitative estimates are lacking, there is some evidence in Siberia and Alaska for thawing permafrost during the LIG due to warmer conditions, potentially leading to a carbon release (e.g. Reyes et al., 2010; Stapel et al., 2018). Currently, both our understanding of the carbon stored in permafrost in the past and the potential evolution of permafrost in the future is limited (Turetsky et al., 2020). Further research to constrain this aspect of the climate system is needed~~in permafrost, which may have been partially thawed during the LIG (Reyes et al., 2010; Schuur et al., 2015; Stapel et al., 2018), less carbon stored in peat and permafrost at the LIG could have led to a lower total land carbon store compared to the Holocene. However, it is not possible to infer this total land carbon change from the oceanic and atmospheric $\delta^{13}C$ anomalies because it cannot be assumed that the mass of carbon and ^{13}C is preserved within the ocean-atmosphere-land biosphere system on glacial-interglacial timescales.

~~While there is possibility of carbon stored in vegetation and soils contributing to the $\delta^{13}C$ anomaly that we have observed, we are unable to verify this through the use of a mass balance, since the atmosphere–biosphere–ocean system cannot be assumed to be closed (Jeltsch-Thömmes and Joos, 2020b)~~There is indeed continuous exchange of carbon and ^{13}C between the lithosphere and the coupled ocean, atmosphere and land biosphere carbon reservoirs. Isotopic perturbations associated with changes in the terrestrial biosphere are communicated to the burial fluxes of organic carbon and $CaCO_3$ and are therefore removed on multi-millennial time scales (Jeltsch-Thömmes et al., 2019; Jeltsch-Thömmes and Joos, 2020b). Nevertheless, when hypothetically neglecting any exchange with the lithosphere, we find that the change in terrestrial carbon needed to explain the difference in $\delta^{13}C$ would be in the order of 295±44 Gt C less during the LIG than the Holocene (Text S1).

~~At the LIG, both atmospheric~~ In addition, due to the warmer conditions at the LIG than during the Holocene, there could have been a release of methane clathrates which would have added isotopically light carbon ($\delta^{13}C$: ~-47 ‰) to the ocean-atmosphere system. However, available evidence suggests that geological CH_4 sources are rather small (Bock et al., 2017; Hmiel et al., 2020; Petrenko et al., 2017; Saunois et al., 2020) making this explanation unlikely, although we cannot completely exclude the possibility that the geological CH_4 source was larger at the LIG than the Holocene. Similarly, since the $\delta^{13}C$ value of CO_2 ~~and~~ from volcanic outgassing is close to zero (Brovkin et al., 2016) and modelling suggests volcanic outgassing likely only had a minor impact on $\delta^{13}CO_2$ (Roth and Joos, 2012), it is unlikely that volcanic outgassing of CO_2 played a significant role in influencing the mean oceanic $\delta^{13}C$~~were lower than during the mid-Holocene, with atmosphere and ocean anomalies being 0.3 (Schneider et al., 2013) and 0.2 respectively. Such multi-millenial~~ .

While we are not in the position to firmly pinpoint the exact mechanism, the LIG-Holocene differences in the isotopic signal of both the atmosphere and ocean were most likely due to a long-term imbalance between ~~weathering and sedimentation of carbon~~ the isotopic fluxes to and from the lithosphere, including the net burial (or redissolution) of organic carbon and $CaCO_3$ in deep-sea sediments, and changes in shallow water sedimentation and coral reef formation (Jeltsch-Thömmes and Joos, 2020b).

5 Conclusions

We present a new compilation of benthic $\delta^{13}C$ from 130 to 115 ka BP covering the LIG. Over this time period, benthic $\delta^{13}C$ generally display a maximum value at ~121 ka BP (±2 ka), in phase with the maximum atmospheric $\delta^{13}CO_2$ (LIG value of -6.5 ‰ at ~120 ka BP). As there are significant chronological uncertainties associated with LIG records, we ~~identify a relatively stable period ranging~~ analyse data between 125 and 120 ka BP to avoid data associated with millennial-scale events and deglaciations. We compare this LIG benthic $\delta^{13}C$ data to a similar database covering the ~~mid-Holocene (7-4~~ Holocene (7–2 ka BP). We find that during these specific time periods, LIG oceanic $\delta^{13}C$ was about 0.2 ‰ lower than during the ~~mid-Holocene~~Holocene. This anomaly is consistent across different regions in the Atlantic Ocean. Even though there are less records available, benthic $\delta^{13}C$ data from the Pacific Ocean also support an anomaly of about 0.2 ‰.

An analysis of $\delta^{13}C$ gradients across the Atlantic Ocean suggests that there were no significant changes in mean, long-term ocean circulation across the two intervals. While reduced high northern latitude peat and permafrost caused by higher temperatures at the LIG than during the ~~mid-Holocene~~ Holocene (Otto-Bliesner et al., 2020) could also lead to a lower atmospheric and oceanic $\delta^{13}C$, the most likely explanation for the lower LIG oceanic $\delta^{13}C$ is a long term imbalance in the weathering and burial of carbon. Additional studies are required to further constrain the LIG carbon balance.

Data availability. The data is published on Research Data Australia at DOI https://doi.org/10.26190/5efe841541f3b.

6 ~~Regional Boundaries~~

~~Global distribution of benthic foraminifera $\delta^{13}C$ () during the Holocene (a) and LIG (b) showing the regional boundaries used to calculate the global volume-weighted mean $\delta^{13}C$. Dotted black lines indicate the regional boundaries. Symbol size indicates the number of values per core, colour indicates average $\delta^{13}C$, and the triangle direction indicates the proxy depth (upward-pointing triangle: shallower than 2,500 m, downward-pointing triangle: deeper than 2,500 m).~~

Author contributions. SAB, LCM, and KJM designed the research. CDP and LEL provided significant portions of the $\delta^{13}C$ data. SAB, LCM, KJM, and LM analysed the data and developed the methodology. FJ assisted in the interpretation of the results. SAB prepared the manuscript with contributions from all co-authors.

Competing interests. The authors declare that they have no conflict of interest.

Acknowledgements. Shannon Bengtson acknowledges funding from the Australian Government Research Training Program Scholarship. Laurie Menviel and Katrin Meissner acknowledge funding from the Australian Research Council grants FT180100606 (to Laurie Menviel) and DP180100048 (to Katrin Meissner and Laurie Menviel). Computational resources were provided by the NCI National Facility at the Australian National University, through awards under the Merit Allocation Scheme, the Intersect allocation scheme, and the UNSW HPC at NCI Scheme. Fortunat Joos acknowledges funding from the Swiss National Science Foundation (#200020_172476). This study was facilitated by the PAGES QUIGS working group.

References

Alley, R. B. and Ágústsdóttir, A. M.: The 8k Event: Cause and Consequences of a Major Holocene Abrupt Climate Change, Quaternary Science Reviews, 24, 1123–1149, https://doi.org/10.1016/j.quascirev.2004.12.004, 2005.

Anderson, R. S., Jiménez-Moreno, G., Ager, T., and Porinchu, D. F.: High-Elevation Paleoenvironmental Change during MIS 6–4 in the Central Rockies of Colorado as Determined from Pollen Analysis, Quaternary Research, 82, 542–552, https://doi.org/10.1016/j.yqres.2014.03.005, 2014.

Axford, Y., Briner, J., R. Francis, D., H. Miller, G., R. Walker, I., and Wolfe, A.: Chironomids Record Terrestrial Temperature Changes throughout Arctic Interglacials of the Past 200,000 Yr, Geological Society of America Bulletin, 123, 1275–1287, https://doi.org/10.1130/B30329.1, 2011.

Bakker, P., Stone, E. J., Charbit, S., Gröger, M., Krebs-Kanzow, U., Ritz, S. P., Varma, V., Khon, V., Lunt, D. J., Mikolajewicz, U., Prange, M., Renssen, H., Schneider, B., and Schulz, M.: Last Interglacial Temperature Evolution – a Model Inter-Comparison, Climate of the Past, 9, 605–619, https://doi.org/10.5194/cp-9-605-2013, 2013.

Basu, S., Agrawal, S., Sanyal, P., Mahato, P., Kumar, S., and Sarkar, A.: Carbon Isotopic Ratios of Modern C3–C4 Plants from the Gangetic Plain, India and Its Implications to Paleovegetational Reconstruction, Palaeogeography Palaeoclimatology Palaeoecology, 440, https://doi.org/10.1016/j.palaeo.2015.08.012, 2015.

Belanger, P. E., Curry, W. B., and Matthews, R. K.: Core-Top Evaluation of Benthic Foraminiferal Isotopic Ratios for Paleo-Oceanographic Interpretations, Palaeogeography, Palaeoclimatology, Palaeoecology, 33, 205–220, https://doi.org/10.1016/0031-0182(81)90039-0, 1981.

Bengtson, S. A., Meissner, K. J., Menviel, L., A. Sisson, S., and Wilkin, J.: Evaluating the Extent of North Atlantic Deep Water and the Mean Atlantic $\Delta^{13}C$ from Statistical Reconstructions, Paleoceanography and Paleoclimatology, https://doi.org/10.1029/2019PA003589, 2019.

Bereiter, B., Eggleston, S., Schmitt, J., Nehrbass-Ahles, C., Stocker, T. F., Fischer, H., Kipfstuhl, S., and Chappellaz, J.: Revision of the EPICA Dome C CO_2 Record from 800 to 600 Kyr before Present, Geophysical Research Letters, 42, 542–549, https://doi.org/10.1002/2014GL061957, 2015.

Bickert, T. and Mackensen, A.: Last Glacial to Holocene Changes in South Atlantic Deep Water Circulation, in: The South Atlantic in the Late Quaternary: Reconstruction of Material Budgets and Current Systems, edited by Wefer, G., Mulitza, S., and Ratmeyer, V., pp. 671–693, Springer, Berlin, Heidelberg, 2003.

Bickert, T. and Wefer, G.: Late Quaternary Deep Water Circulation in the South Atlantic: Reconstruction from Carbonate Dissolution and Benthic Stable Isotopes, in: The South Atlantic: Present and Past Circulation, edited by Wefer, G., Berger, W. H., Siedler, G., and Webb, D. J., pp. 599–620, Springer, Berlin, Heidelberg, 1996.

Bickert, T., Curry, W. B., and Wefer, G.: Late Pliocene to Holocene (2.6 – 0 Ma) Western Equatorial Atlantic Deep-Water Circulation: Inferences from Benthic Stable Isotopes, vol. 154, pp. 239–254, Proc. Ocean Drill. Program Sci. Results, 1997.

Bickert, T., Wefer, G., and Müller, P. J.: Stable Isotopes and Sedimentology of Core GeoB1032-2, PANGAEA, https://doi.org/10.1594/PANGAEA.103613, 2003.

Bock, M., Schmitt, J., Beck, J., Seth, B., Chappellaz, J., and Fischer, H.: Glacial/Interglacial Wetland, Biomass Burning, and Geologic Methane Emissions Constrained by Dual Stable Isotopic CH_4 Ice Core Records, Proceedings of the National Academy of Sciences, 114, E5778–E5786, https://doi.org/10.1073/pnas.1613883114, 2017.

Böhm, E., Lippold, J., Gutjahr, M., Frank, M., Blaser, P., Antz, B., Fohlmeister, J., Frank, N., Andersen, M. B., and Deininger, M.: Strong and Deep Atlantic Meridional Overturning Circulation during the Last Glacial Cycle, Nature, 517, 73–76, https://doi.org/10.1038/nature14059, 2015.

Bowman, D. M. J. S., Balch, J. K., Artaxo, P., Bond, W. J., Carlson, J. M., Cochrane, M. A., D'Antonio, C. M., DeFries, R. S., Doyle, J. C., Harrison, S. P., Johnston, F. H., Keeley, J. E., Krawchuk, M. A., Kull, C. A., Marston, J. B., Moritz, M. A., Prentice, I. C., Roos, C. I., Scott, A. C., Swetnam, T. W., van der Werf, G. R., and Pyne, S. J.: Fire in the Earth System, Science, 324, 481–484, https://doi.org/10.1126/science.1163886, 2009.

Boyle, E. A.: Cadmium and Δ^{13}C Paleochemical Ocean Distributions During the Stage 2 Glacial Maximum, Annual Review of Earth and Planetary Sciences, 20, 245–287, https://doi.org/10.1146/annurev.ea.20.050192.001333, 1992.

Boyle, E. A. and Keigwin, L.: North Atlantic Thermohaline Circulation during the Past 20,000 Years Linked to High-Latitude Surface Temperature, Nature, 330, 35–40, https://doi.org/10.1038/330035a0, 1987.

Boyle, E. A. and Keigwin, L. D.: Comparison of Atlantic and Pacific Paleochemical Records for the Last 215,000 Years: Changes in Deep Ocean Circulation and Chemical Inventories, Earth and Planetary Science Letters, 76, 135–150, https://doi.org/10.1016/0012-821X(85)90154-2, 1985.

Brewer, S., Guiot, J., Sánchez-Goñi, M. F., and Klotz, S.: The Climate in Europe during the Eemian: A Multi-Method Approach Using Pollen Data, Quaternary Science Reviews, 27, 2303–2315, https://doi.org/10.1016/j.quascirev.2008.08.029, 2008.

Brovkin, V., Bendtsen, J., Claussen, M., Ganopolski, A., Kubatzki, C., Petoukhov, V., and Andreev, A.: Carbon Cycle, Vegetation, and Climate Dynamics in the Holocene: Experiments with the CLIMBER-2 Model, Global Biogeochemical Cycles, 16, 86–1–86–20, https://doi.org/10.1029/2001GB001662, 2002.

Brovkin, V., Brücher, T., Kleinen, T., Zaehle, S., Joos, F., Roth, R., Spahni, R., Schmitt, J., Fischer, H., Leuenberger, M., Stone, E. J., Ridgwell, A., Chappellaz, J., Kehrwald, N., Barbante, C., Blunier, T., and Dahl Jensen, D.: Comparative Carbon Cycle Dynamics of the Present and Last Interglacial, Quaternary Science Reviews, 137, 15–32, https://doi.org/10.1016/j.quascirev.2016.01.028, 2016.

Came, R. E., Oppo, D. W., and Curry, W. B.: Atlantic Ocean Circulation during the Younger Dryas: Insights from a New Cd/Ca Record from the Western Subtropical South Atlantic, Paleoceanography, 18, https://doi.org/10.1029/2003PA000888, 2003.

Candy, S. and Alonso-Garcia, M.: Sea Surface Temperature Reconstruction for Sediment Core GIK23414-6, PANGAEA, https://doi.org/10.1594/PANGAEA.894428, 2018.

CAPE: Last Interglacial Arctic Warmth Confirms Polar Amplification of Climate Change, Quaternary Science Reviews, 25, 1383–1400, https://doi.org/10.1016/j.quascirev.2006.01.033, 2006.

Capron, E., Govin, A., Feng, R., Otto-Bliesner, B. L., and Wolff, E. W.: Critical Evaluation of Climate Syntheses to Benchmark CMIP6/PMIP4 127 Ka Last Interglacial Simulations in the High-Latitude Regions, Quaternary Science Reviews, 168, 137–150, https://doi.org/10.1016/j.quascirev.2017.04.019, 2017.

Cernusak, L. A., Ubierna, N., Winter, K., Holtum, J. A. M., Marshall, J. D., and Farquhar, G. D.: Environmental and Physiological Determinants of Carbon Isotope Discrimination in Terrestrial Plants, New Phytologist, 200, 950–965, https://doi.org/10.1111/nph.12423, 2013.

Chapman, M. and Shackleton, N.: Late Quaternary North Atlantic IRD and Isotope Data, IGBP PAGES/World Data Center for Paleoclimatology, 1999.

Chen, J., Farrell, J. W., Murray, D. W., and Prell, W. L.: Timescale and Paleoceanographic Implications of a 3.6 m.y. Oxygen Isotope Record from the Northeast Indian Ocean (Ocean Drilling Program Site 758), Paleoceanography, 10, 21–47, https://doi.org/10.1029/94PA02290, 1995.

Cheng, X., Tian, J., and Wang, P.: Stable Isotopes from Site 1143, Tech. Rep. 184, 2004.

{CLIMAP Project Members}: Stable Isotopes Measured on Foraminifera from the 120 Kyr Time Slice Reconstruction in Sediment Core RC12-339, PANGAEA, https://doi.org/10.1594/PANGAEA.358927, 2006.

Collins, J. A., Schefuß, E., Heslop, D., Mulitza, S., Prange, M., Zabel, M., Tjallingii, R., Dokken, T. M., Huang, E., Mackensen, A., Schulz, M., Tian, J., Zarriess, M., and Wefer, G.: Interhemispheric Symmetry of the Tropical African Rainbelt over the Past 23,000 Years, Nature Geoscience, 4, 42–45, https://doi.org/10.1038/ngeo1039, 2011.

Cortijo, E.: Stable Isotope Analysis on Sediment Core SU90-39, PANGAEA, https://doi.org/10.1594/PANGAEA.106761, 2003.

Curry, W., Shackleton, N., and Richter, C.: Proc. ODP, Init. Repts, 154: College Station, TX (Ocean Drilling Program), https://doi.org/10.2973/odp.proc.ir.154.1995, 1995.

Curry, W. B. and Lohmann, G. P.: Carbon Isotopic Changes in Benthic Foraminifera from the Western South Atlantic: Reconstruction of Glacial Abyssal Circulation Patterns, Quaternary Research, 18, 218–235, https://doi.org/10.1016/0033-5894(82)90071-0, 1982.

Curry, W. B. and Oppo, D. W.: Synchronous, High-Frequency Oscillations in Tropical Sea Surface Temperatures and North Atlantic Deep Water Production during the Last Glacial Cycle, Paleoceanography, 12, 1–14, https://doi.org/10.1029/96PA02413, 1997.

Curry, W. B. and Oppo, D. W.: Glacial Water Mass Geometry and the Distribution of $\Delta^{13}C$ of ΣCO_2 in the Western Atlantic Ocean, Paleoceanography, 20, https://doi.org/10.1029/2004PA001021, 2005.

Curry, W. B., Duplessy, J. C., Labeyrie, L., and Shackleton, N. J.: Changes in the Distribution of $\Delta^{13}C$ of Deep Water ΣCO_2 between the Last Glaciation and the Holocene, Paleoceanography, 3, 317–341, https://doi.org/10.1029/PA003i003p00317, 1988.

de Abreu, L., Shackleton, N. J., Schönfeld, J., Hall, M., and Chapman, M.: Millennial-Scale Oceanic Climate Variability off the Western Iberian Margin during the Last Two Glacial Periods, Marine Geology, 196, 1–20, https://doi.org/10.1016/S0025-3227(03)00046-X, 2003.

de Vernal, A. and Hillaire-Marcel, C.: Natural Variability of Greenland Climate, Vegetation, and Ice Volume During the Past Million Years, Science, 320, 1622–1625, https://doi.org/10.1126/science.1153929, 2008.

Deaney, E. L., Barker, S., and van de Flierdt, T.: Timing and Nature of AMOC Recovery across Termination 2 and Magnitude of Deglacial CO_2 Change, Nature Communications, 8, 1–10, https://doi.org/10.1038/ncomms14595, 2017.

Diefendorf, A. F. and Freimuth, E. J.: Extracting the Most from Terrestrial Plant-Derived n-Alkyl Lipids and Their Carbon Isotopes from the Sedimentary Record: A Review, Organic Geochemistry, 103, 1–21, https://doi.org/10.1016/j.orggeochem.2016.10.016, 2017.

Diefendorf, A. F., Mueller, K. E., Wing, S. L., Koch, P. L., and Freeman, K. H.: Global Patterns in Leaf ^{13}C Discrimination and Implications for Studies of Past and Future Climate, Proceedings of the National Academy of Sciences, 107, 5738–5743, https://doi.org/10.1073/pnas.0910513107, 2010.

Dioumaeva, I., Trumbore, S., Schuur, E. A. G., Goulden, M. L., Litvak, M., and Hirsch, A. I.: Decomposition of Peat from Upland Boreal Forest: Temperature Dependence and Sources of Respired Carbon, Journal of Geophysical Research: Atmospheres, 107, WFX 3–1–WFX 3–12, https://doi.org/10.1029/2001JD000848, 2002.

Drake, N. A., Blench, R. M., Armitage, S. J., Bristow, C. S., and White, K. H.: Ancient Watercourses and Biogeography of the Sahara Explain the Peopling of the Desert, Proceedings of the National Academy of Sciences, 108, 458–462, https://doi.org/10.1073/pnas.1012231108, 2011.

Duplessy, J.: Quaternary Paleoceanography: Unpublished Stable Isotope Records. IGBP PAGES/World Data Center for Paleoclimatology Data Contribution Series: #1996-035., Tech. rep., NOAA/NGDC Paleoclimatology Program, Boulder, Colorado, USA, 1996.

Duplessy, J.-C., Shackleton, N. J., Matthews, R. K., Prell, W., Ruddiman, W. F., Caralp, M., and Hendy, C. H.: ^{13}C Record of Benthic Foraminifera in the Last Interglacial Ocean: Implications for the Carbon Cycle and the Global Deep Water Circulation, Quaternary Research, 21, 225–243, https://doi.org/10.1016/0033-5894(84)90099-1, 1984.

Duplessy, J. C., Shackleton, N. J., Fairbanks, R. G., Labeyrie, L., Oppo, D. W., and Kallel, N.: Deepwater Source Variations during the Last Climatic Cycle and Their Impact on the Global Deepwater Circulation, Paleoceanography, 3, 343–360, https://doi.org/10.1029/PA003i003p00343, 1988.

Dutton, A. and Lambeck, K.: Ice Volume and Sea Level During the Last Interglacial, Science, 337, 216–219, https://doi.org/10.1126/science.1205749, 2012.

Dutton, A., Carlson, A. E., Long, A. J., Milne, G. A., Clark, P. U., DeConto, R., Horton, B. P., Rahmstorf, S., and Raymo, M. E.: Sea-Level Rise Due to Polar Ice-Sheet Mass Loss during Past Warm Periods, Science, 349, aaa4019, https://doi.org/10.1126/science.aaa4019, 2015.

Eggleston, S., Schmitt, J., Bereiter, B., Schneider, R., and Fischer, H.: CO_2 Concentration and Stable Isotope Ratios of Three Antarctic Ice Cores Covering the Period from 149.4 - 1.5 Kyr before 1950, PANGAEA, https://doi.org/10.1594/PANGAEA.859181, 2016a.

Eggleston, S., Schmitt, J., Bereiter, B., Schneider, R., and Fischer, H.: Evolution of the Stable Carbon Isotope Composition of Atmospheric CO_2 over the Last Glacial Cycle, Paleoceanography, 31, 2015PA002 874, https://doi.org/10.1002/2015PA002874, 2016b.

Eide, M., Olsen, A., Ninnemann, U. S., and Johannessen, T.: A Global Ocean Climatology of Preindustrial and Modern Ocean $\Delta^{13}C$, Global Biogeochemical Cycles, 31, 515–534, https://doi.org/10.1002/2016GB005473, 2017.

Elsig, J., Schmitt, J., Leuenberger, D., Schneider, R., Eyer, M., Leuenberger, M., Joos, F., Fischer, H., and Stocker, T. F.: Carbon Isotopic Record of CO_2 from the Holocene of the Dome C Ice Core, PANGAEA, https://doi.org/10.1594/PANGAEA.728699, 2009.

Farquhar, G. D.: On the Nature of Carbon Isotope Discrimination in C4 Species, Functional Plant Biology, 10, 205–226, https://doi.org/10.1071/pp9830205, 1983.

Farquhar, G. D., Ehleringer, J. R., and Hubick, K. T.: Carbon Isotope Discrimination and Photosynthesis, Annual Review of Plant Physiology and Plant Molecular Biology, 40, 503–537, https://doi.org/10.1146/annurev.pp.40.060189.002443, 1989.

Flückiger, J., Monnin, E., Stauffer, B., Schwander, J., Stocker, T. F., Chappellaz, J., Raynaud, D., and Barnola, J.-M.: High-Resolution Holocene N_2O Ice Core Record and Its Relationship with CH_4 and CO_2, Global Biogeochemical Cycles, 16, 10–1–10–8, https://doi.org/10.1029/2001GB001417, 2002.

Freudenthal, T., Meggers, H., Henderiks, J., Kuhlmann, H., Moreno, A., and Wefer, G.: Upwelling Intensity and Filament Activity off Morocco during the Last 250,000 Years, Deep Sea Research Part II: Topical Studies in Oceanography, 49, 3655–3674, https://doi.org/10.1016/S0967-0645(02)00101-7, 2002.

Galaasen, E. V., Ninnemann, U. S., Irvalı, N., Kleiven, H. F., Rosenthal, Y., Kissel, C., and Hodell, D. A.: Stable Isotope Ratios of C. Wuellerstorfi from Sediment Core MD03-2664, Bjerknes Centre for Climate Research, https://doi.org/10.1594/PANGAEA.830079, 2014a.

Galaasen, E. V., Ninnemann, U. S., Irvalı, N., Kleiven, H. K. F., Rosenthal, Y., Kissel, C., and Hodell, D. A.: Rapid Reductions in North Atlantic Deep Water During the Peak of the Last Interglacial Period, Science, 343, 1129–1132, https://doi.org/10.1126/science.1248667, 2014b.

Gebhardt, H., Sarnthein, M., Grootes, P. M., Kiefer, T., Kuehn, H., Schmieder, F., and Röhl, U.: Paleonutrient and Productivity Records from the Subarctic North Pacific for Pleistocene Glacial Terminations I to V, Paleoceanography, 23, https://doi.org/10.1029/2007PA001513, 2008.

Govin, A.: 4) Planktic and Benthic Foraminiferal Stable Isotope Data from Core MD95-2042: Revised Chronology for the Last Interglacial (Period 135-110 Ka), In supplement to: Govin, Aline; Braconnot, Pascale; Capron, Emilie; Cortijo, Elsa; Duplessy, Jean-Claude; Jansen, Eystein; Labeyrie, Laurent D; Landais, Amaelle; Marti, O; Michel, Elisabeth; Mosquet, E; Risebrobakken, Bjørg; Swingedouw, Didier; Waelbroeck, Claire (2012): Persistent influence of ice sheet melting on high northern latitude climate during the early Last Interglacial. Climate of the Past, 8, 483-507, https://doi.org/10.5194/cp-8-483-2012, https://doi.org/10.1594/PANGAEA.777659, 2012.

Govin, A., Braconnot, P., Capron, E., Cortijo, E., Duplessy, J.-C., Jansen, E., Labeyrie, L., Landais, A., Marti, O., Michel, E., Mosquet, E., Risebrobakken, B., Swingedouw, D., and Waelbroeck, C.: Persistent Influence of Ice Sheet Melting on High Northern Latitude Climate during the Early Last Interglacial, Climate of the Past, 8, 483–507, https://doi.org/10.5194/cp-8-483-2012, 2012.

Govin, A., Capron, E., Tzedakis, P. C., Verheyden, S., Ghaleb, B., Hillaire-Marcel, C., St-Onge, G., Stoner, J. S., Bassinot, F., Bazin, L., Blunier, T., Combourieu-Nebout, N., El Ouahabi, A., Genty, D., Gersonde, R., Jimenez-Amat, P., Landais, A., Martrat, B., Masson-Delmotte, V., Parrenin, F., Seidenkrantz, M. S., Veres, D., Waelbroeck, C., and Zahn, R.: Sequence of Events from the Onset to the Demise of the Last Interglacial: Evaluating Strengths and Limitations of Chronologies Used in Climatic Archives, Quaternary Science Reviews, 129, 1–36, https://doi.org/10.1016/j.quascirev.2015.09.018, 2015.

Hasenclever, J., Knorr, G., Rüpke, L. H., Köhler, P., Morgan, J., Garofalo, K., Barker, S., Lohmann, G., and Hall, I. R.: Sea Level Fall during Glaciation Stabilized Atmospheric CO_2 by Enhanced Volcanic Degassing, Nature Communications, 8, 15 867, https://doi.org/10.1038/ncomms15867, 2017.

Helmens, K. F., Salonen, J. S., Plikk, A., Engels, S., Väliranta, M., Kylander, M., Brendryen, J., and Renssen, H.: Major Cooling Intersecting Peak Eemian Interglacial Warmth in Northern Europe, Quaternary Science Reviews, 122, 293–299, https://doi.org/10.1016/j.quascirev.2015.05.018, 2015.

Hmiel, B., Petrenko, V. V., Dyonisius, M. N., Buizert, C., Smith, A. M., Place, P. F., Harth, C., Beaudette, R., Hua, Q., Yang, B., Vimont, I., Michel, S. E., Severinghaus, J. P., Etheridge, D., Bromley, T., Schmitt, J., Faïn, X., Weiss, R. F., and Dlugokencky, E.: Preindustrial $^{14}CH_4$ Indicates Greater Anthropogenic Fossil CH_4 Emissions, Nature, 578, 409–412, https://doi.org/10.1038/s41586-020-1991-8, 2020.

Hodell, D., Charles, C., Curtis, J., Mortyn, P., Ninnemann, U., and Venz, K.: Data Report: Oxygen Isotope Stratigraphy of ODP Leg 177 Sites 1088, 1089, 1090, 1093, and 1094, in: Proc. Ocean Drill. Prog. Sci. Results, vol. 177, College Station TX (Ocean Drilling Program), 2003.

Hodell, D. A. and Channell, J. E. T.: Mode Transitions in Northern Hemisphere Glaciation: Co-Evolution of Millennial and Orbital Variability in Quaternary Climate, Climate of the Past, 12, 1805–1828, https://doi.org/10.5194/cp-12-1805-2016, 2016.

Hodell, D. A., Charles, C. D., and Ninnemann, U. S.: Comparison of Interglacial Stages in the South Atlantic Sector of the Southern Ocean for the Past 450 Kyr: Implifications for Marine Isotope Stage (MIS) 11, Global and Planetary Change, 24, 7–26, https://doi.org/10.1016/S0921-8181(99)00069-7, 2000.

Hodell, D. A., Charles, C. D., and Sierro, F. J.: Late Pleistocene Evolution of the Ocean's Carbonate System, Earth and Planetary Science Letters, 192, 109–124, https://doi.org/10.1016/S0012-821X(01)00430-7, 2001.

Hodell, D. A., Channell, J. E. T., Curtis, J. H., Romero, O. E., and Röhl, U.: Oxygen and Carbon Isotopes of the Benthic Foraminifer Cibicoides Wuellerstorfi of IODP Site 303-U1308, In supplement to: Hodell, DA et al. (2008): Onset of 'Hudson Strait' Heinrich Events in the eastern North Atlantic at the end of the middle Pleistocene transition (~640 ka)? Paleoceanography, 23(4), PA4218, https://doi.org/10.1029/2008PA001591, https://doi.org/10.1594/PANGAEA.831735, 2008.

Hoffman, J. S., Clark, P. U., Parnell, A. C., and He, F.: Regional and Global Sea-Surface Temperatures during the Last Interglaciation, Science, 355, 276–279, https://doi.org/10.1126/science.aai8464, 2017.

Holbourn, A., Kuhnt, W., Schulz, M., and Erlenkeuser, H.: Impacts of Orbital Forcing and Atmospheric Carbon Dioxide on Miocene Ice-Sheet Expansion, Nature, 438, 483–487, https://doi.org/10.1038/nature04123, 2005.

Hoogakker, B. A. A., Rohling, E. J., Palmer, M. R., Tyrrell, T., and Rothwell, R. G.: Underlying Causes for Long-Term Global Ocean $\Delta^{13}C$ Fluctuations over the Last 1.20 Myr, Earth and Planetary Science Letters, 248, 15–29, https://doi.org/10.1016/j.epsl.2006.05.007, 2006.

Hüls, M.: Calculated Sea Surface Temperature of Sediment Core M35003-4, PANGAEA, https://doi.org/10.1594/PANGAEA.55761, 1999.

Huybers, P. and Langmuir, C.: Feedback between Deglaciation, Volcanism, and Atmospheric CO_2, Earth and Planetary Science Letters, 286, 479–491, https://doi.org/10.1016/j.epsl.2009.07.014, 2009.

IPCC: Climate Change 2013: The Physical Science Basis. Contribution of Working Group I to the Fifth Assessment Report of the Intergovernmental Panel on Climate Change, Tech. rep., Cambridge University Press, Cambridge, United Kingdom and New York, NY, USA, 2013.

Irvalı, N., Ninnemann, U., Galaasen, E., Rosenthal, Y., Kroon, D., W. Oppo, D., Kleiven, H., Darling, K., and Kissel, C.: Rapid Switches in Subpolar North Atlantic Hydrography and Climate during the Last Interglacial (MIS 5e), Paleoceanography, 27, https://doi.org/10.1029/2011PA002244, 2012.

Jansen, E., Raymo, M., and Blum, P.: Proc. ODP, Init. Repts, 154: College Station, TX (Ocean Drilling Program), https://doi.org/10.2973/odp.proc.ir.162.1996, 1996.

Jeltsch-Thömmes, A. and Joos, F.: Modeling the Evolution of Pulse-like Perturbations in Atmospheric Carbon and Carbon Isotopes: The Role of Weathering–Sedimentation Imbalances, Climate of the Past, 16, 423–451, https://doi.org/10.5194/cp-16-423-2020, 2020a.

Jeltsch-Thömmes, A. and Joos, F.: The Response to Pulse-like Perturbations in Atmospheric Carbon and Carbon Isotopes, Climate of the Past Discussions, pp. 1–36, https://doi.org/10.5194/cp-2019-107, 2020b.

Jeltsch-Thömmes, A., Battaglia, G., Cartapanis, O., Jaccard, S. L., and Joos, F.: Low Terrestrial Carbon Storage at the Last Glacial Maximum: Constraints from Multi-Proxy Data, Climate of the Past, 15, 849–879, https://doi.org/z‘, 2019.

Jouzel, J. and Masson-Delmotte, V.: EPICA Dome C Ice Core 800KYr Deuterium Data and Temperature Estimates, PANGAEA, https://doi.org/10.1594/PANGAEA.683655, 2007.

Jouzel, J., Masson-Delmotte, V., Cattani, O., Dreyfus, G., Falourd, S., Hoffmann, G., Minster, B., Nouet, J., Barnola, J. M., Chappellaz, J., Fischer, H., Gallet, J. C., Johnsen, S., Leuenberger, M., Loulergue, L., Luethi, D., Oerter, H., Parrenin, F., Raisbeck, G., Raynaud, D., Schilt, A., Schwander, J., Selmo, E., Souchez, R., Spahni, R., Stauffer, B., Steffensen, J. P., Stenni, B., Stocker, T. F., Tison, J. L., Werner, M., and Wolff, E. W.: Orbital and Millennial Antarctic Climate Variability over the Past 800,000 Years, Science, 317, 793–796, https://doi.org/10.1126/science.1141038, 2007.

Jullien, E., Grousset, F. E., Hemming, S. R., Peck, V. L., Hall, I. R., Jeantet, C., and Billy, I.: Contrasting Conditions Preceding MIS3 and MIS2 Heinrich Events, Global and Planetary Change, 54, 225–238, https://doi.org/10.1016/j.gloplacha.2006.06.021, 2006.

Kaspar, F., Kühl, N., Cubasch, U., and Litt, T.: A Model-Data Comparison of European Temperatures in the Eemian Interglacial, Geophysical Research Letters, 32, https://doi.org/10.1029/2005GL022456, 2005.

Kawamura, K., Parrenin, F., Lisiecki, L., Uemura, R., Vimeux, F., Severinghaus, J. P., Hutterli, M. A., Nakazawa, T., Aoki, S., Jouzel, J., Raymo, M. E., Matsumoto, K., Nakata, H., Motoyama, H., Fujita, S., Goto-Azuma, K., Fujii, Y., and Watanabe, O.: Northern Hemisphere Forcing of Climatic Cycles in Antarctica over the Past 360,000 Years, Nature, 448, 912–916, https://doi.org/10.1038/nature06015, 2007.

Keigwin, L. D. and Jones, G. A.: Glacial-Holocene Stratigraphy, Chronology, and Paleoceanographic Observations on Some North Atlantic Sediment Drifts, Deep Sea Research Part A. Oceanographic Research Papers, 36, 845–867, https://doi.org/10.1016/0198-0149(89)90032-0, 1989.

Keigwin, L. D. and Jones, G. A.: Western North Atlantic Evidence for Millennial-Scale Changes in Ocean Circulation and Climate, Journal of Geophysical Research: Oceans, 99, 12 397–12 410, https://doi.org/10.1029/94JC00525, 1994.

Keigwin, L. D. and Schlegel, M. A.: Ocean Ventilation and Sedimentation since the Glacial Maximum at 3 Km in the Western North Atlantic, Geochemistry, Geophysics, Geosystems, 3, 1–14, https://doi.org/10.1029/2001GC000283, 2002.

Keigwin, L. D., Jones, G. A., Lehman, S. J., and Boyle, E. A.: Deglacial Meltwater Discharge, North Atlantic Deep Circulation, and Abrupt Climate Change, Journal of Geophysical Research: Oceans, 96, 16 811–16 826, https://doi.org/10.1029/91JC01624, 1991.

Keller, K. M., Lienert, S., Bozbiyik, A., Stocker, T. F., Churakova (Sidorova), O. V., Frank, D. C., Klesse, S., Koven, C. D., Leuenberger, M., Riley, W. J., Saurer, M., Siegwolf, R., Weigt, R. B., and Joos, F.: 20th Century Changes in Carbon Isotopes and Water-Use Efficiency: Tree-Ring-Based Evaluation of the CLM4.5 and LPX-Bern Models, Biogeosciences, 14, 2641–2673, https://doi.org/10.5194/bg-14-2641-2017, 2017.

Key, R. M., Kozyr, A., Sabine, C. L., Lee, K., Wanninkhof, R., Bullister, J. L., Feely, R. A., Millero, F. J., Mordy, C., and Peng, T.-H.: A Global Ocean Carbon Climatology: Results from Global Data Analysis Project (GLODAP), Global Biogeochemical Cycles, 18, https://doi.org/10.1029/2004GB002247, 2004.

Kleinen, T., Brovkin, V., and Schuldt, R. J.: A Dynamic Model of Wetland Extent and Peat Accumulation: Results for the Holocene, Biogeosciences, 9, 235–248, https://doi.org/10.5194/bg-9-235-2012, 2012.

Köhler, P., Nehrbass-Ahles, C., Schmitt, J., Stocker, T. F., and Fischer, H.: Continuous Record of the Atmospheric Greenhouse Gas Carbon Dioxide (CO_2), Raw Data, PANGAEA, https://doi.org/10.1594/PANGAEA.871265, 2017.

Kohn, M. J.: Carbon Isotope Compositions of Terrestrial C3 Plants as Indicators of (Paleo)Ecology and (Paleo)Climate, Proceedings of the National Academy of Sciences, 107, 19 691–19 695, https://doi.org/10.1073/pnas.1004933107, 2010.

Kopp, R. E., Simons, F. J., Mitrovica, J. X., Maloof, A. C., and Oppenheimer, M.: Probabilistic Assessment of Sea Level during the Last Interglacial Stage, Nature, 462, 863–867, https://doi.org/10.1038/nature08686, 2009.

Labeyrie, L., Vidal, L., Cortijo, E., Paterne, M., Arnold, M., Duplessy, J. C., Vautravers, M., Labracherie, M., Duprat, J., Turon, J. L., Grousset, F., and Van Weering, T.: Surface and Deep Hydrology of the Northern Atlantic Ocean during the Past 150 000 Years, Philosophical Transactions: Biological Sciences, 348, 255–264, 1995.

Labeyrie, L., Labracherie, M., Gorfti, N., Pichon, J. J., Vautravers, M., Arnold, M., Duplessy, J.-C., Paterne, M., Michel, E., Duprat, J., Caralp, M., and Turon, J.-L.: Hydrographic Changes of the Southern Ocean (Southeast Indian Sector) Over the Last 230 Kyr, Paleoceanography, 11, 57–76, https://doi.org/10.1029/95PA02255, 1996.

Labeyrie, L., Leclaire, H., Waelbroeck, C., Cortijo, E., Duplessy, J.-C., Vidal, L., Elliot, M., Coat, B. L., and Auffret, G.: Temporal Variability of the Surface and Deep Waters of the North West Atlantic Ocean at Orbital and Millenial Scales, in: Mechanisms of Global Climate Change at Millennial Time Scales, pp. 77–98, American Geophysical Union (AGU), 1999.

Labeyrie, L. D., Leclaire, H., Waelbroeck, C., Cortijo, E., Duplessy, J.-C., Vidal, L., Elliot, M., and Le Coat, B.: Foraminiferal Stable Isotopes of Sediment Core CH69-K09, PANGAEA, https://doi.org/10.1594/PANGAEA.881464, 2017.

Landais, A., Masson-Delmotte, V., Capron, E., Langebroek, P. M., Bakker, P., Stone, E. J., Merz, N., Raible, C. C., Fischer, H., Orsi, A., Prié, F., Vinther, B., and Dahl-Jensen, D.: How Warm Was Greenland during the Last Interglacial Period?, Climate of the Past, 12, 1933–1948, https://doi.org/10.5194/cp-12-1933-2016, 2016.

Larrasoaña, J. C., Roberts, A. P., and Rohling, E. J.: Dynamics of Green Sahara Periods and Their Role in Hominin Evolution, PLOS ONE, 8, e76 514, https://doi.org/10.1371/journal.pone.0076514, 2013.

Laskar, J., Robutel, P., Joutel, F., Gastineau, M., Correia, A. C. M., and Levrard, B.: A Long-Term Numerical Solution for the Insolation Quantities of the Earth, Astronomy & Astrophysics, 428, 261–285, https://doi.org/10.1051/0004-6361:20041335, 2004.

Leavitt, S. W.: Systematics of Stable-Carbon Isotopic Differences between Gymnosperm and Angiosperm Trees, Plant Physiol. (Life Sci. Adv.), 11, 257–262, 1992.

Lebreiro, S. M., Voelker, A. H. L., Vizcaino, A., Abrantes, F. G., Alt-Epping, U., Jung, S., Thouveny, N., and Gràcia, E.: Sediment Instability on the Portuguese Continental Margin under Abrupt Glacial Climate Changes (Last 60kyr), Quaternary Science Reviews, 28, 3211–3223, https://doi.org/10.1016/j.quascirev.2009.08.007, 2009.

Lee, M., Wei, K. C. J., and Chen, Y.-G.: High Resolution Oxygen Isotope Stratigraphy for the Last 150,000 Years in the Southern South China Sea: Core MD972151, Terrestrial Atmospheric and Oceanic Sciences, https://doi.org/10.3319/tao.1999.10.1.239(images), 1999.

Lehman, S. J., Sachs, J. P., Crotwell, A. M., Keigwin, L. D., and Boyle, E. A.: Relation of Subtropical Atlantic Temperature, High-Latitude Ice Rafting, Deep Water Formation, and European Climate 130,000–60,000 Years Ago, Quaternary Science Reviews, 21, 1917–1924, https://doi.org/10.1016/S0277-3791(02)00078-1, 2002.

Lisiecki, L. E. and Raymo, M. E.: A Pliocene-Pleistocene Stack of 57 Globally Distributed Benthic Δ^{18}O Records, Paleoceanography, 20, PA1003, https://doi.org/10.1029/2004PA001071, 2005.

Lisiecki, L. E. and Stern, J. V.: Regional and Global Benthic Δ^{18}O Stacks for the Last Glacial Cycle, Paleoceanography, 31, 2016PA003 002, https://doi.org/10.1002/2016PA003002, 2016.

Lototskaya, A. and Ganssen, G. M.: The Structure of Termination II (Penultimate Deglaciation and Eemian) in the North Atlantic, Quaternary Science Reviews, 18, 1641–1654, https://doi.org/10.1016/S0277-3791(99)00011-6, 1999.

Lüthi, D., Le Floch, M., Bereiter, B., Blunier, T., Barnola, J.-M., Siegenthaler, U., Raynaud, D., Jouzel, J., Fischer, H., Kawamura, K., and Stocker, T. F.: High-Resolution Carbon Dioxide Concentration Record 650,000–800,000 Years before Present, Nature, 453, 379–382, https://doi.org/10.1038/nature06949, 2008.

Lyle, M., Mix, A., and Pisias, N.: Patterns of $CaCO^3$ Deposition in the Eastern Tropical Pacific Ocean for the Last 150 Kyr: Evidence for a Southeast Pacific Depositional Spike during Marine Isotope Stage (MIS) 2, Paleoceanography, 17, 3–1, https://doi.org/10.1029/2000PA000538, 2002.

Lynch-Stieglitz, J., Stocker, T. F., Broecker, W. S., and Fairbanks, R. G.: The Influence of Air-Sea Exchange on the Isotopic Composition of Oceanic Carbon: Observations and Modeling, Global Biogeochemical Cycles, 9, 653–665, https://doi.org/10.1029/95GB02574, 1995.

Lynch-Stieglitz, J., Curry, W. B., Oppo, D. W., Ninneman, U. S., Charles, C. D., and Munson, J.: Meridional Overturning Circulation in the South Atlantic at the Last Glacial Maximum, Geochemistry, Geophysics, Geosystems, 7, https://doi.org/10.1029/2005GC001226, 2006.

Mackensen, A. and Bickert, T.: Stable Carbon Isotopes in Benthic Foraminifera: Proxies for Deep and Bottom Water Circulation and New Production, in: Use of Proxies in Paleoceanography: Examples from the South Atlantic, edited by Fischer, G. and Wefer, G., pp. 229–254, Springer, Berlin, Heidelberg, 1999.

Mackensen, A., Rudolph, M., and Kuhn, G.: Late Pleistocene Deep-Water Circulation in the Subantarctic Eastern Atlantic, Global and Planetary Change, 30, 197–229, https://doi.org/10.1016/S0921-8181(01)00102-3, 2001.

Marcott, S. A., Shakun, J. D., Clark, P. U., and Mix, A. C.: A Reconstruction of Regional and Global Temperature for the Past 11,300 Years, Science, 339, 1198–1201, https://doi.org/10.1126/science.1228026, 2013.

Martrat, B., Grimalt, J. O., López-Martinez, C., Cacho, I., Sierro, F. J., Flores, J.-A., Zahn, R., Canals, M., Curtis, J. H., and Hodell, D. A.: Sea Surface Temperatures, Alkenones and Sedimentation Rate from ODP Hole 161-977A, https://doi.org/10.1594/PANGAEA.787811, 2004.

Martrat, B., Grimalt, J. O., Shackleton, N. J., de Abreu, L., Hutterli, M. A., and Stocker, T. F.: Sea Surface Temperature Estimation for the Iberian Margin, Supplement to: Martrat, B et al. (2007): Four climate cycles of recurring deep and surface water destabilizations on the Iberian Margin. Science, 317(5837), 502-507, https://doi.org/10.1126/science.1139994, https://doi.org/10.1594/PANGAEA.771894, 2007a.

Martrat, B., Grimalt, J. O., Shackleton, N. J., de Abreu, L., Hutterli, M. A., and Stocker, T. F.: (Table S2) Sea Surface Temperature Estimation for ODP Hole 161-977A, PANGAEA, https://doi.org/10.1594/PANGAEA.771890, 2007b.

Masson-Delmotte, V., Stenni, B., Pol, K., Braconnot, P., Cattani, O., Falourd, S., Kageyama, M., Jouzel, J., Landais, A., Minster, B., Barnola, J. M., Chappellaz, J., Krinner, G., Johnsen, S., Röthlisberger, R., Hansen, J., Mikolajewicz, U., and Otto-Bliesner, B.: EPICA Dome C Record of Glacial and Interglacial Intensities, Quaternary Science Reviews, 29, 113–128, https://doi.org/10.1016/j.quascirev.2009.09.030, 2010.

Masson-Delmotte, V., Schulz, M., Abe-Ouchi, A., Beer, J., Ganopolski, J., González Rouco, J. F., Jansen, E., Lambeck, K., Luterbacher, J., Naish, T., Osborn, T., Otto-Bliesner, B., Quinn, T., Ramesh, R., Rojas, M., Shao, X., and Timmermann, A.: Information from Paleoclimate Archives, in: Climate Change 2013: The Physical Science Basis. Contribution of Working Group I to the Fifth Assessment Report of the Intergovernmental Panel on Climate Change, edited by Stocker, T. F., Qin, D., Plattner, G.-K., Tignor, M., Allen, S. K., Doschung, J., Nauels, A., Xia, Y., Bex, V., and Midgley, P. M., pp. 383–464, Cambridge University Press, Cambridge, UK, https://doi.org/10.1017/CBO9781107415324.013, 2013.

McCorkle, D. and Holder, A.: Calibration Studies of Benthic Foraminiferal Isotopic Composition: Results from the Southeast Pacific, AGU Fall Meeting Abstracts, 2001.

McIntyre, K., Ravelo, A. C., and Delaney, M. L.: North Atlantic Intermediate Waters in the Late Pliocene to Early Pleistocene, Paleoceanography, 14, 324–335, https://doi.org/10.1029/1998PA900005, 1999.

McKay, N. P., Overpeck, J. T., and Otto-Bliesner, B. L.: The Role of Ocean Thermal Expansion in Last Interglacial Sea Level Rise, Geophysical Research Letters, 38, https://doi.org/10.1029/2011GL048280, 2011.

McManus, J. F., Oppo, D. W., and Cullen, J. L.: A 0.5-Million-Year Record of Millennial-Scale Climate Variability in the North Atlantic, Science, 283, 971–975, https://doi.org/10.1126/science.283.5404.971, 1999.

Menviel, L. and Joos, F.: Toward Explaining the Holocene Carbon Dioxide and Carbon Isotope Records: Results from Transient Ocean Carbon Cycle-Climate Simulations, Paleoceanography, 27, https://doi.org/10.1029/2011PA002224, 2012.

Menviel, L., Mouchet, A., J. Meissner, K., Joos, F., and H. England, M.: Impact of Oceanic Circulation Changes on Atmospheric $\Delta^{13}CO^2$, Global Biogeochemical Cycles, 29, 1944–1961, https://doi.org/10.1002/2015GB005207, 2015.

Menviel, L., Yu, J., Joos, F., Mouchet, A., Meissner, K. J., and England, M. H.: Poorly Ventilated Deep Ocean at the Last Glacial Maximum Inferred from Carbon Isotopes: A Data-Model Comparison Study, Paleoceanography, 32, 2–17, https://doi.org/10.1002/2016PA003024, 2017.

Menviel, L., Capron, E., Govin, A., Dutton, A., Tarasov, L., Abe-Ouchi, A., Drysdale, R. N., Gibbard, P. L., Gregoire, L., He, F., Ivanovic, R. F., Kageyama, M., Kawamura, K., Landais, A., Otto-Bliesner, B. L., Oyabu, I., Tzedakis, P. C., Wolff, E., and Zhang, X.: The Penultimate Deglaciation: Protocol for Paleoclimate Modelling Intercomparison Project (PMIP) Phase 4 Transient Numerical Simulations between 140 and 127 Ka, Version 1.0, Geoscientific Model Development, 12, 3649–3685, https://doi.org/10.5194/gmd-12-3649-2019, 2019.

Millo, C., Sarnthein, M., Voelker, A., and Erlenkeuser, H.: Variability of the Denmark Strait Overflow during the Last Glacial Maximum, Boreas, 35, 50–60, https://doi.org/10.1080/03009480500359244, 2006.

Mix, A. C. and Fairbanks, R. G.: North Atlantic Surface-Ocean Control of Pleistocene Deep-Ocean Circulation, Earth and Planetary Science Letters, 73, 231–243, https://doi.org/10.1016/0012-821X(85)90072-X, 1985.

Mix, A. C., Pisias, N. G., Zahn, R., Rugh, W., Lopez, C., and Nelson, K.: Carbon 13 in Pacific Deep and Intermediate Waters, 0-370 Ka: Implications for Ocean Circulation and Pleistocene CO_2, Paleoceanography, 6, 205–226, https://doi.org/10.1029/90PA02303, 1991.

Mokeddem, Z., McManus, J. F., and Oppo, D. W.: Oceanographic Dynamics and the End of the Last Interglacial in the Subpolar North Atlantic, Proceedings of the National Academy of Sciences, 111, 11 263–11 268, https://doi.org/10.1073/pnas.1322103111, 2014.

Montero-Serrano, J.-C., Bout-Roumazeilles, V., Carlson, A. E., Tribovillard, N., Bory, A., Meunier, G., Sionneau, T., Flower, B. P., Martinez, P., Billy, I., and Riboulleau, A.: Contrasting Rainfall Patterns over North America during the Holocene and Last Interglacial as Recorded by Sediments of the Northern Gulf of Mexico, Geophysical Research Letters, 38, https://doi.org/10.1029/2011GL048194, 2011.

Muhs, D. R., Ager, T. A., and Begét, J. E.: Vegetation and Paleoclimate of the Last Interglacial Period, Central Alaska, Quaternary Science Reviews, 20, 41–61, https://doi.org/10.1016/S0277-3791(00)00132-3, 2001.

Mulitza, S., Prange, M., Stuut, J.-B., Zabel, M., von Dobeneck, T., Itambi, A. C., Nizou, J., Schulz, M., and Wefer, G.: Sahel Megadroughts Triggered by Glacial Slowdowns of Atlantic Meridional Overturning, Paleoceanography, 23, https://doi.org/10.1029/2008PA001637, 2008.

Novák, M., Buzek, F., and Adamová, M.: Vertical Trends in $\Delta^{13}C$, $\Delta^{15}N$ and $\Delta^{34}S$ Ratios in Bulk Sphagnum Peat, Soil Biology and Biochemistry, 31, 1343–1346, 1999.

Oliver, K. I. C., Hoogakker, B. A. A., Crowhurst, S., Henderson, G. M., Rickaby, R. E. M., Edwards, N. R., and Elderfield, H.: A Synthesis of Marine Sediment Core $\Delta^{13}C$ Data over the Last 150 000 Years, Climate of the Past, 5, 2497–2554, https://doi.org/10.5194/cpd-5-2497-2009, 2010.

Oppo, D. W. and Fairbanks, R. G.: Variability in the Deep and Intermediate Water Circulation of the Atlantic Ocean during the Past 25,000 Years: Northern Hemisphere Modulation of the Southern Ocean, Earth and Planetary Science Letters, 86, 1–15, https://doi.org/10.1016/0012-821X(87)90183-X, 1987.

Oppo, D. W. and Horowitz, M.: Glacial Deep Water Geometry: South Atlantic Benthic Foraminiferal Cd/Ca and $\Delta^{13}C$ Evidence, Paleoceanography, 15, 147–160, https://doi.org/10.1029/1999PA000436, 2000.

Oppo, D. W. and Lehman, S. J.: Suborbital Timescale Variability of North Atlantic Deep Water during the Past 200,000 Years, Paleoceanography, 10, 901–910, https://doi.org/10.1029/95PA02089, 1995.

Oppo, D. W., McManus, J. F., and Cullen, J. L.: Abrupt Climate Events 500,000 to 340,000 Years Ago: Evidence from Subpolar North Atlantic Sediments, Science, 279, 1335–1338, https://doi.org/10.1126/science.279.5355.1335, 1998.

Oppo, D. W., McManus, J. F., and Cullen, J. L.: Evolution and Demise of the Last Interglacial Warmth in the Subpolar North Atlantic, Quaternary Science Reviews, 25, 3268–3277, https://doi.org/10.1016/j.quascirev.2006.07.006, 2006.

Otto-Bliesner, B., Brady, E., Zhao, A., Brierley, C., Axford, Y., Capron, E., Govin, A., Hoffman, J., Isaacs, E., Kageyama, M., Scussolini, P., Tzedakis, P. C., Williams, C., Wolff, E., Abe-Ouchi, A., Braconnot, P., Ramos Buarque, S., Cao, J., de Vernal, A., Guarino, M. V., Guo, C., LeGrande, A. N., Lohmann, G., Meissner, K., Menviel, L., Nisancioglu, K., O'ishi, R., Salas Y Melia, D., Shi, X., Sicard, M., Sime, L., Tomas, R., Volodin, E., Yeung, N., Zhang, Q., Zhang, Z., and Zheng, W.: Large-Scale Features of Last Interglacial Climate: Results from Evaluating the Lig127k Simulations for CMIP6-PMIP4, Climate of the Past Discussions, https://doi.org/10.5194/cp-2019-174, 2020.

Pahnke, K. and Zahn, R.: Southern Hemisphere Water Mass Conversion Linked with North Atlantic Climate Variability, Science (New York, N.Y.), 307, 1741–1746, https://doi.org/10.1126/science.1102163, 2005.

Past Interglacial Working Group of PAGES: Interglacials of the Last 800,000 Years, Reviews of Geophysics, 54, 162–219, https://doi.org/10.1002/2015RG000482, 2016.

Peterson, C. D., Lisiecki, L. E., and Stern, J. V.: Deglacial Whole-Ocean $\Delta^{13}C$ Change Estimated from 480 Benthic Foraminiferal Records, Paleoceanography, 29, 549–563, https://doi.org/10.1002/2013PA002552, 2014.

Petit, J. R., Jouzel, J., Raynaud, D., Barkov, N. I., Barnola, J.-M., Basile, I., Bender, M., Chappellaz, J., Davis, M., Delaygue, G., Delmotte, M., Kotlyakov, V. M., Legrand, M., Lipenkov, V. Y., Lorius, C., Pépin, L., Ritz, C., Saltzman, E., and Stievenard, M.: Climate and Atmospheric History of the Past 420,000 Years from the Vostok Ice Core, Antarctica, Nature, 399, 429–436, https://doi.org/10.1038/20859, 1999.

Petrenko, V. V., Smith, A. M., Schaefer, H., Riedel, K., Brook, E., Baggenstos, D., Harth, C., Hua, Q., Buizert, C., Schilt, A., Fain, X., Mitchell, L., Bauska, T., Orsi, A., Weiss, R. F., and Severinghaus, J. P.: Minimal Geological Methane Emissions during the Younger Dryas–Preboreal Abrupt Warming Event, Nature, 548, 443–446, https://doi.org/10.1038/nature23316, 2017.

Pisias, N. G. and Mix, A. C.: Spatial and Temporal Oceanographic Variability of the Eastern Equatorial Pacific during the Late Pleistocene: Evidence from Radiolaria Microfossils, Paleoceanography, 12, 381–393, https://doi.org/10.1029/97PA00583, 1997.

Plikk, A., Engels, S., Luoto, T. P., Nazarova, L., Salonen, J. S., and Helmens, K. F.: Chironomid-Based Temperature Reconstruction for the Eemian Interglacial (MIS 5e) at Sokli, Northeast Finland, Journal of Paleolimnology, 61, 355–371, https://doi.org/10.1007/s10933-018-00064-y, 2019.

Poirier, R. K. and Billups, K.: The Intensification of Northern Component Deepwater Formation during the Mid-Pleistocene Climate Transition: Mid-Pleistocene Deep Water Circulation, Paleoceanography, 29, 1046–1061, https://doi.org/10.1002/2014PA002661, 2014.

Rau, A. J., Rogers, J., Lutjeharms, J. R. E., Giraudeau, J., Lee-Thorp, J. A., Chen, M. T., and Waelbroeck, C.: A 450-Kyr Record of Hydrological Conditions on the Western Agulhas Bank Slope, South of Africa, Marine Geology, 180, 183–201, https://doi.org/10.1016/S0025-3227(01)00213-4, 2002.

Raymo, M. E., Oppo, D. W., and Curry, W.: The Mid-Pleistocene Climate Transition: A Deep Sea Carbon Isotopic Perspective, Paleoceanography, 12, 546–559, https://doi.org/10.1029/97PA01019, 1997.

Raymo, M. E., Oppo, D. W., Flower, B. P., Hodell, D. A., McManus, J. F., Venz, K. A., Kleiven, K. F., and McIntyre, K.: Stability of North Atlantic Water Masses in Face of Pronounced Climate Variability during the Pleistocene, Paleoceanography, 19, https://doi.org/10.1029/2003PA000921, 2004.

Reyes, A. V., Froese, D. G., and Jensen, B. J. L.: Permafrost Response to Last Interglacial Warming: Field Evidence from Non-Glaciated Yukon and Alaska, Quaternary Science Reviews, 29, 3256–3274, https://doi.org/10.1016/j.quascirev.2010.07.013, 2010.

Roth, R. and Joos, F.: Model Limits on the Role of Volcanic Carbon Emissions in Regulating Glacial–Interglacial CO_2 Variations, Earth and Planetary Science Letters, 329-330, 141–149, https://doi.org/10.1016/j.epsl.2012.02.019, 2012.

Rowe, P. J., Wickens, L. B., Sahy, D., Marca, A. D., Peckover, E., Noble, S., Özkul, M., Baykara, M. O., Millar, I. L., and Andrews, J. E.: Multi-Proxy Speleothem Record of Climate Instability during the Early Last Interglacial in Southern Turkey, Palaeogeography, Palaeoclimatology, Palaeoecology, p. 109422, https://doi.org/10.1016/j.palaeo.2019.109422, 2019.

Ruddiman, W. F. and Members, C. P.: Stable Isotope Data of the 120 k Time Slice, PANGAEA, https://doi.org/10.1594/PANGAEA.51932, 1982.

Russon, T., Elliot, M., Kissel, C., Cabioch, G., Deckker, P. D., and Corrège, T.: Middle-Late Pleistocene Deep Water Circulation in the Southwest Subtropical Pacific, Paleoceanography, 24, https://doi.org/10.1029/2009PA001755, 2009.

Samson, C. R., Sikes, E. L., and Howard, W. R.: Deglacial Paleoceanographic History of the Bay of Plenty, New Zealand, Paleoceanography, 20, https://doi.org/10.1029/2004PA001088, 2005.

Sarmiento, J., Dunne, J., Gnanadesikan, A., Key, R., Matsumoto, K., and Slater, R.: A New Estimate of the $CaCO_3$ to Organic Carbon Export Ratio, Global Biogeochemical Cycles, 16, https://doi.org/10.1029/2002GB001919, 2002.

Sarnthein, M.: Age Model of Sediment Core GIK16772-1, PANGAEA, https://doi.org/10.1594/PANGAEA.134239, 2003.

Sarnthein, M., Winn, K., Jung, S. J. A., Duplessy, J.-C., Labeyrie, L., Erlenkeuser, H., and Ganssen, G.: Changes in East Atlantic Deepwater Circulation over the Last 30,000 Years: Eight Time Slice Reconstructions, Paleoceanography, 9, 209–267, https://doi.org/10.1029/93PA03301, 1994.

Saunois, M., Stavert, A. R., Poulter, B., Bousquet, P., Canadell, J. G., Jackson, R. B., Raymond, P. A., Dlugokencky, E. J., Houweling, S., Patra, P. K., Ciais, P., Arora, V. K., Bastviken, D., Bergamaschi, P., Blake, D. R., Brailsford, G., Bruhwiler, L., Carlson, K. M., Carrol, M., Castaldi, S., Chandra, N., Crevoisier, C., Crill, P. M., Covey, K., Curry, C. L., Etiope, G., Frankenberg, C., Gedney, N., Hegglin, M. I., Höglund-Isaksson, L., Hugelius, G., Ishizawa, M., Ito, A., Janssens-Maenhout, G., Jensen, K. M., Joos, F., Kleinen, T., Krummel, P. B., Langenfelds, R. L., Laruelle, G. G., Liu, L., Machida, T., Maksyutov, S., McDonald, K. C., McNorton, J., Miller, P. A., Melton, J. R., Morino, I., Müller, J., Murguia-Flores, F., Naik, V., Niwa, Y., Noce, S., O'Doherty, S., Parker, R. J., Peng, C., Peng, S., Peters, G. P., Prigent, C., Prinn, R., Ramonet, M., Regnier, P., Riley, W. J., Rosentreter, J. A., Segers, A., Simpson, I. J., Shi, H., Smith, S. J., Steele, L. P., Thornton, B. F., Tian, H., Tohjima, Y., Tubiello, F. N., Tsuruta, A., Viovy, N., Voulgarakis, A., Weber, T. S., van Weele, M., van der Werf, G. R., Weiss, R. F., Worthy, D., Wunch, D., Yin, Y., Yoshida, Y., Zhang, W., Zhang, Z., Zhao, Y., Zheng, B., Zhu, Q., Zhu, Q., and Zhuang, Q.: The Global Methane Budget 2000–2017, Earth System Science Data, 12, 1561–1623, https://doi.org/10.5194/essd-12-1561-2020, 2020.

Schmiedl, G. and Mackensen, A.: Late Quaternary Paleoproductivity and Deep Water Circulation in the Eastern South Atlantic Ocean: Evidence from Benthic Foraminifera, Palaeogeography, Palaeoclimatology, Palaeoecology, 130, 43–80, https://doi.org/10.1016/S0031-0182(96)00137-X, 1997.

Schmiedl, G. and Mackensen, A.: Multispecies Stable Isotopes of Benthic Foraminifers Reveal Past Changes of Organic Matter Decomposition and Deepwater Oxygenation in the Arabian Sea, Paleoceanography, 21, https://doi.org/10.1029/2006PA001284, 2006.

Schmittner, A., Gruber, N., Mix, A. C., Key, R. M., Tagliabue, A., and Westberry, T. K.: Biology and Air–Sea Gas Exchange Controls on the Distribution of Carbon Isotope Ratios ($\Delta^{13}C$) in the Ocean, Biogeosciences, 10, 5793–5816, https://doi.org/10.5194/bg-10-5793-2013, 2013.

Schneider, R., Schmitt, J., Köhler, P., Joos, F., and Fischer, H.: A Reconstruction of Atmospheric Carbon Dioxide and Its Stable Carbon Isotopic Composition from the Penultimate Glacial Maximum to the Last Glacial Inception, Climate of the Past, 9, 2507–2523, https://doi.org/10.5194/cp-9-2507-2013, 2013.

Schönfeld, J., Zahn, R., and de Abreu, L.: Surface and Deep Water Response to Rapid Climate Changes at the Western Iberian Margin, Global and Planetary Change, 36, 237–264, https://doi.org/10.1016/S0921-8181(02)00197-2, 2003.

Schubert, B. A. and Jahren, A. H.: The Effect of Atmospheric CO_2 Concentration on Carbon Isotope Fractionation in C3 Land Plants, Geochimica et Cosmochimica Acta, 96, 29–43, https://doi.org/10.1016/j.gca.2012.08.003, 2012.

Schurgers, G., Mikolajewicz, U., Gröger, M., Maier-Reimer, E., Vizcaíno, M., and Winguth, A.: Dynamics of the Terrestrial Biosphere, Climate and Atmospheric CO_2 Concentration during Interglacials: A Comparison between Eemian and Holocene, Climate of the Past, 2, 205–220, https://doi.org/10.5194/cp-2-205-2006, 2006.

Schuur, E. a. G., McGuire, A. D., Schädel, C., Grosse, G., Harden, J. W., Hayes, D. J., Hugelius, G., Koven, C. D., Kuhry, P., Lawrence, D. M., Natali, S. M., Olefeldt, D., Romanovsky, V. E., Schaefer, K., Turetsky, M. R., Treat, C. C., and Vonk, J. E.: Climate Change and the Permafrost Carbon Feedback, Nature, 520, 171–179, https://doi.org/10.1038/nature14338, 2015.

Shackleton, N., Hall, M., and Pate, D.: Pliocene Stable Isotope Stratigraphy of ODP Site 846, Tech. Rep. 138, 1995.

Shackleton, N. J.: The Last Interglacial in the Marine and Terrestrial Records, Proceedings of the Royal Society of London. Series B. Biological Sciences, 174, 135–154, https://doi.org/10.1098/rspb.1969.0085, 1969.

Shackleton, N. J.: Stable Carbon and Oxygen Isotope Ratios of Benthic and Planktic Foraminifera from the Atlantic Ocean, Supplement to: Shackleton, NJ (1977): Carbon-13 in Uvigerina: Tropical rain forest history and the equatorial Pacific carbonate dissolution cycle. In: Andersen, N R & Malahoff, A (eds.), The Fate of Fossil Fuel in the Oceans. New York (Plenum), 401-427, https://doi.org/10.1594/PANGAEA.692091, 1977.

Shackleton, N. J. and Hall, M. A.: Stable Isotope Record of DSDP Hole 81-552A in the Northeastern Atlantic Ocean, Supplement to: Shackleton, NJ; Hall, MA (1984): Oxygen and carbon isotope stratigraphy of Deep Sea Drilling Project Hole 552A: Plio-Pleistocene glacial history. In: Roberts, DG; Schnittker, D; et al. (eds.), Initial Reports of the Deep Sea Drilling Project, Washington (U.S. Govt. Printing Office), 81, 599-609, https://doi.org/10.2973/dsdp.proc.81.116.1984, https://doi.org/10.1594/PANGAEA.698993, 1984.

Shackleton, N. J., Berger, A., and Peltier, W. R.: An Alternative Astronomical Calibration of the Lower Pleistocene Timescale Based on ODP Site 677, Earth and Environmental Science Transactions of The Royal Society of Edinburgh, 81, 251–261, https://doi.org/10.1017/S0263593300020782, 1990.

Shackleton, N. J., Hall, M. A., and Vincent, E.: Phase Relationships between Millennial-Scale Events 64,000–24,000 Years Ago, Paleoceanography, 15, 565–569, https://doi.org/10.1029/2000PA000513, 2000.

Shackleton, S., Baggenstos, D., Menking, J. A., Dyonisius, M. N., Bereiter, B., Bauska, T. K., Rhodes, R. H., Brook, E. J., Petrenko, V. V., McConnell, J. R., Kellerhals, T., Häberli, M., Schmitt, J., Fischer, H., and Severinghaus, J. P.: Global Ocean Heat Content in the Last Interglacial, Nature Geoscience, 13, 77–81, https://doi.org/10.1038/s41561-019-0498-0, 2020.

Sikes, E. L., Howard, W. R., Samson, C. R., Mahan, T. S., Robertson, L. G., and Volkman, J. K.: Southern Ocean Seasonal Temperature and Subtropical Front Movement on the South Tasman Rise in the Late Quaternary, Paleoceanography, 24, https://doi.org/10.1029/2008PA001659, 2009.

Sirocko, F., Garbe-Schönberg, D., and Devey, C.: Processes Controlling Trace Element Geochemistry of Arabian Sea Sediments during the Last 25,000 Years, Global and Planetary Change, 26, 217–303, https://doi.org/10.1016/S0921-8181(00)00046-1, 2000.

Skinner, L. C. and Shackleton, N. J.: Rapid Transient Changes in Northeast Atlantic Deep Water Ventilation Age across Termination I, Paleoceanography, 19, https://doi.org/10.1029/2003PA000983, 2004.

Skinner, L. C. and Shackleton, N. J.: An Atlantic Lead over Pacific Deep-Water Change across Termination I: Implications for the Application of the Marine Isotope Stage Stratigraphy., Quaternary Science Reviews, 24, 571–580, https://doi.org/Skinner, L. C. and Shackleton, N. J. (2005) An Atlantic lead over Pacific deep-water change across Termination I: implications for the application of the marine isotope stage stratigraphy. Quaternary Science Reviews, 24. pp. 571-580. DOI https://doi.org/10.1016/j.quascirev.2004.11.008 <https://doi.org/10.1016/j.quascirev.2004.11.008>, 2005.

Skinner, L. C., Shackleton, N. J., and Elderfield, H.: Millennial-Scale Variability of Deep-Water Temperature and $\Delta^{18}O_{dw}$ Indicating Deep-Water Source Variations in the Northeast Atlantic, 0–34 Cal. Ka BP, Geochemistry, Geophysics, Geosystems, 4, https://doi.org/10.1029/2003GC000585, 2003.

Sowers, T., Bender, M., Labeyrie, L., Martinson, D., Jouzel, J., Raynaud, D., Pichon, J. J., and Korotkevich, Y. S.: A 135,000-Year Vostok-Specmap Common Temporal Framework, Paleoceanography, 8, 737–766, https://doi.org/10.1029/93PA02328, 1993.

Spahni, R., Chappellaz, J., Stocker, T. F., Loulergue, L., Hausammann, G., Kawamura, K., Flückiger, J., Schwander, J., Raynaud, D., Masson-Delmotte, V., and Jouzel, J.: Atmospheric Methane and Nitrous Oxide of the Late Pleistocene from Antarctic Ice Cores, Science, 310, 1317–1321, https://doi.org/10.1126/science.1120132, 2005.

Stapel, J. G., Schwamborn, G., Schirrmeister, L., Horsfield, B., and Mangelsdorf, K.: Substrate Potential of Last Interglacial to Holocene Permafrost Organic Matter for Future Microbial Greenhouse Gas Production, Biogeosciences, 15, 1969–1985, https://doi.org/10.5194/bg-15-1969-2018, 2018.

Stein, R., Fahl, K., Gierz, P., Niessen, F., and Lohmann, G.: Arctic Ocean Sea Ice Cover during the Penultimate Glacial and the Last Interglacial, Nature Communications, 8, 373, https://doi.org/10.1038/s41467-017-00552-1, 2017.

Stern, J. V. and Lisiecki, L. E.: Termination 1 Timing in Radiocarbon-Dated Regional Benthic Δ^{18}O Stacks, Paleoceanography, 29, 1127–1142, https://doi.org/10.1002/2014PA002700, 2014.

Stott, L. D., Neumann, M., and Hammond, D.: Intermediate Water Ventilation on the Northeastern Pacific Margin during the Late Pleistocene Inferred from Benthic Foraminiferal Δ^{13}C, Paleoceanography, 15, 161–169, https://doi.org/10.1029/1999PA000375, 2000.

Tarasov, P., Granoszewski, W., Bezrukova, E., Brewer, S., Nita, M., Abzaeva, A., and Oberhänsli, H.: Quantitative Reconstruction of the Last Interglacial Vegetation and Climate Based on the Pollen Record from Lake Baikal, Russia, Climate Dynamics, 25, 625–637, https://doi.org/10.1007/s00382-005-0045-0, 2005.

Thomas, E. R., Wolff, E. W., Mulvaney, R., Steffensen, J. P., Johnsen, S. J., Arrowsmith, C., White, J. W. C., Vaughn, B., and Popp, T.: The 8.2ka Event from Greenland Ice Cores, Quaternary Science Reviews, 26, 70–81, https://doi.org/10.1016/j.quascirev.2006.07.017, 2007.

Tjallingii, R., Claussen, M., Stuut, J.-B. W., Fohlmeister, J., Jahn, A., Bickert, T., Lamy, F., and Röhl, U.: Coherent High- and Low-Latitude Control of the Northwest African Hydrological Balance, Nature Geoscience, 1, 670–675, https://doi.org/10.1038/ngeo289, 2008.

Tschumi, T., Joos, F., Gehlen, M., and Heinze, C.: Deep Ocean Ventilation, Carbon Isotopes, Marine Sedimentation and the Deglacial CO_2 Rise, Climate of the Past, 7, 771–800, https://doi.org/10.5194/cp-7-771-2011, 2011.

Turetsky, M. R., Abbott, B. W., Jones, M. C., Anthony, K. W., Olefeldt, D., Schuur, E. A. G., Grosse, G., Kuhry, P., Hugelius, G., Koven, C., Lawrence, D. M., Gibson, C., Sannel, A. B. K., and McGuire, A. D.: Carbon Release through Abrupt Permafrost Thaw, Nature Geoscience, 13, 138–143, https://doi.org/10.1038/s41561-019-0526-0, 2020.

Tzedakis, P. C., Drysdale, R. N., Margari, V., Skinner, L. C., Menviel, L., Rhodes, R. H., Taschetto, A. S., Hodell, D. A., Crowhurst, S. J., Hellstrom, J. C., Fallick, A. E., Grimalt, J. O., McManus, J. F., Martrat, B., Mokeddem, Z., Parrenin, F., Regattieri, E., Roe, K., and Zanchetta, G.: Enhanced Climate Instability in the North Atlantic and Southern Europe during the Last Interglacial, Nature Communications, 9, 1–14, https://doi.org/10.1038/s41467-018-06683-3, 2018.

Venz, K. A. and Hodell, D. A.: New Evidence for Changes in Plio–Pleistocene Deep Water Circulation from Southern Ocean ODP Leg 177 Site 1090, Palaeogeography, Palaeoclimatology, Palaeoecology, 182, 197–220, https://doi.org/10.1016/S0031-0182(01)00496-5, 2002.

Venz, K. A., Hodell, D. A., Stanton, C., and Warnke, D. A.: A 1.0 Myr Record of Glacial North Atlantic Intermediate Water Variability from ODP Site 982 in the Northeast Atlantic, Paleoceanography, 14, 42–52, https://doi.org/10.1029/1998PA900013, 1999.

Vidal, L., Schneider, R., Marchal, O., Bickert, T., Stocker, T., and Wefer, G.: Link between the North and South Atlantic during the Heinrich Events of the Last Glacial Period, Climate Dynamics, 15, 909–919, https://doi.org/10.1007/s003820050321, 1999.

Waelbroeck, C., Duplessy, J.-C., Michel, E., Labeyrie, L., Paillard, D., and Duprat, J.: The Timing of the Last Deglaciation in North Atlantic Climate Records, Nature, 412, 724–727, https://doi.org/10.1038/35089060, 2001.

Waelbroeck, C., Skinner, L. C., Labeyrie, L., Duplessy, J.-C., Michel, E., Riveiros, N. V., Gherardi, J.-M., and Dewilde, F.: The Timing of Deglacial Circulation Changes in the Atlantic, Paleoceanography, 26, https://doi.org/10.1029/2010PA002007, 2011.

Wang, L., Sarnthein, M., Erlenkeuser, H., Grimalt, J., Grootes, P., Heilig, S., Ivanova, E., Kienast, M., Pelejero, C., and Pflaumann, U.: East Asian Monsoon Climate during the Late Pleistocene: High-Resolution Sediment Records from the South China Sea, Marine Geology, 156, 245–284, https://doi.org/10.1016/S0025-3227(98)00182-0, 1999.

Wei, G.-J., Huang, C.-Y., Wang, C.-C., Lee, M.-Y., and Wei, K.-Y.: High-Resolution Benthic Foraminifer $\Delta^{13}C$ Records in the South China Sea during the Last 150 Ka, Marine Geology, 232, 227–235, https://doi.org/10.1016/j.margeo.2006.08.005, 2006.

Yu, Z., Loisel, J., Brosseau, D. P., Beilman, D. W., and Hunt, S. J.: Global Peatland Dynamics since the Last Glacial Maximum, Geophysical Research Letters, 37, https://doi.org/10.1029/2010GL043584, 2010.

Zahn, R. and Stüber, A.: Suborbital Intermediate Water Variability Inferred from Paired Benthic Foraminiferal Cd/Ca and $\Delta^{13}C$ in the Tropical West Atlantic and Linking with North Atlantic Climates, Earth and Planetary Science Letters, 200, 191–205, https://doi.org/10.1016/S0012-821X(02)00613-1, 2002.

Zahn, R., Winn, K., and Sarnthein, M.: Benthic Foraminiferal $\Delta^{13}C$ and Accumulation Rates of Organic Carbon: Uvigerina Peregrina Group and Cibicidoides Wuellerstorfi, Paleoceanography, 1, 27–42, https://doi.org/10.1029/PA001i001p00027, 1986.

Zarriess, M. and Mackensen, A.: The Tropical Rainbelt and Productivity Changes off Northwest Africa: A 31,000-Year High-Resolution Record, Marine Micropaleontology, 76, 76–91, https://doi.org/10.1016/j.marmicro.2010.06.001, 2010.

Zarriess, M. and Mackensen, A.: Testing the Impact of Seasonal Phytodetritus Deposition on $\Delta^{13}C$ of Epibenthic Foraminifer Cibicidoides Wuellerstorfi: A 31,000 Year High-Resolution Record from the Northwest African Continental Slope, Paleoceanography, 26, https://doi.org/10.1029/2010PA001944, 2011.

Zarriess, M., Johnstone, H., Prange, M., Steph, S., Groeneveld, J., Mulitza, S., and Mackensen, A.: Bipolar Seesaw in the Northeastern Tropical Atlantic during Heinrich Stadials, Geophysical Research Letters, 38, https://doi.org/10.1029/2010GL046070, 2011.

Zhang, J., Quay, P. D., and Wilbur, D. O.: Carbon Isotope Fractionation during Gas-Water Exchange and Dissolution of CO_2, Geochimica et Cosmochimica Acta, 59, 107–114, https://doi.org/10.1016/0016-7037(95)91550-D, 1995.

Zhang, J., Wang, P., Li, Q., Cheng, X., Jin, H., and Zhang, S.: Western Equatorial Pacific Productivity and Carbonate Dissolution over the Last 550 Kyr: Foraminiferal and Nannofossil Evidence from ODP Hole 807A, Marine Micropaleontology, 64, 121–140, https://doi.org/10.1016/j.marmicro.2007.03.003, 2007.